I. A CHEMICAL APPLICATION OF ELECTRON-NUCLEAR DOUBLE RESONANCE

II. AUXILIARY EQUIPMENT

Thesis by

Alvin L. Kwiram

In Partial Fulfillment of the Requirements

For the Degree of

Doctor of Philosophy

California Institute of Technology

Pasadena, California

1963

ACKNOWLEDGEMENTS

For the sake of brevity acknowledgement of those not directly connected with my scientific education shall not be made here. Nonetheless, their contributions to the enrichment of my life have been extensive.

I am indebted immeasurably to Professor H. M. McConnell, my scientific advisor. Not only was he willing to present me with a challenging problem, but he also exercised considerable patience during the course of its solution. Robert Frost in What Fifty Said unhappily states

> When I was young my teachers were the old
> I gave up fire for form till I was cold.
> I suffered like a metal being cast
> I went to school to age to learn the past.
> --Robert Frost

Happily, I can say exactly the opposite regarding the relationship that has existed between me and Professor McConnell.

Dr. A. F. Hildebrandt's advice during the developmental phase of the ENDOR experiment is certainly appreciated. That his contributions were not insignificant can easily be seen by a perusal of Sections E and F.

In a similar vein Professor C. A. Mead contributed not only to my understanding of electronic technicalities but also to my non-technical enlightenment through the many stimulating conversations on non-material subjects.

Bill Schuelke of the Chemistry Instrument Shop gave very generously of his time. His experience and quick insight simplified scores of design and construction problems.

Thanks are also directed to Professor J. H. Sturdivant for his ready help and his advice on crystallography problems; to Professor G. W. Robinson for repeatedly fulfilling last minute requests for low temperature materiel as well as for the stimulating association in Chem 21; and to the faculty from whom formal knowledge has been derived.

Informal disputation and discussion with fellow graduate students often elucidated points left unclear after the formal instruction. My collaboration with O. Hayes Griffith on various research projects will not soon be forgotten.

My graduate studies were made possible financially by a Woodrow Wilson Foundation Fellowship, a General Electric Foundation Fellowship, summer scholarships from the Sloan Foundation and from the E. I. du Pont de Nemours Company, and tuition scholarships from the Institute.

Finally the Eastman Kodak Scientific Award, apart from its attendant stipend and measure of honor, reiterates for me the uniqueness of the American way of life in both encouraging and allowing the unrestricted development of intellectual interests.

Meiner Mutter gewidmet;

für ihr Verständnis,

für ihre Gebete,

und für ihre Liebe.

ABSTRACT

Part I

The technique of electron-nuclear double resonance (ENDOR) is applied to the study of the hyperfine interactions in one (A) of the two radicals formed by x-irradiating single crystals of glutaric acid. It is shown that the other radical (B) can be destroyed with u.v. irradiation. Complete hyperfine tensors based on the EMR data are calculated for the A radical using an iterative procedure which is also prescribed. Comparing this data with the ENDOR measurements reveals an appreciable orientational disorder of the radicals as well as temperature dependent splittings. Small hyperfine interactions not resolvable in EMR spectra are observable via ENDOR. The experimental development is described in some detail.

Part II

A low temperature EMR system which permits in situ u.v. irradiation is described. The TE_{011} microwave cavity, which operates at room temperature, accommodates the helium cold finger along the cavities' axis of symmetry.

TABLE OF CONTENTS

PART I

A CHEMICAL APPLICATION OF ELECTRON-NUCLEAR DOUBLE RESONANCE

A. INTRODUCTION

For the past fifteen years the electron magnetic resonance (EMR) technique has been used to study the interactions between unpaired electrons and their environment. There is hardly an area in the physical sciences in which this technique has not been applied. Such studies have added greatly to our understanding of electron-electron and electron-nuclear interactions.

The energy level diagram drawn schematically in Figure 1 (not to scale) illustrates the various contributions to the energy of a single electron having spin quantum number $S = \frac{1}{2}$.* For simplicity only interactions with a nucleus having spin quantum number $I = \frac{1}{2}$ are considered. Consider the Zeeman interaction of the electron with the external field, H_o, only. The two resulting energy levels are shown in column b. The nuclear Zeeman contribution to the energy levels is shown in column c. The $S_z = \pm \frac{1}{2}$ levels are split equally by this interaction. In the notation (+-) the signs represent the S_z and I_z values of the electron and nucleus respectively—i.e. $S_z = + \frac{1}{2}$, $I_z = - \frac{1}{2}$ for (+-).

The direct interaction between the nucleus and the electron is referred to as the hyperfine interaction and is usually written $\vec{S} \cdot \underset{\sim}{A} \cdot \vec{I}$ where $\underset{\sim}{A}$ is the hyperfine coupling tensor. The hyperfine contribution is shown in column d.** Column d represents the final energy level distribu-

---

*Familiarity with the commonly used symbols of the EMR method will often be assumed throughout the text. Nevertheless, a glossary of symbols is given in Appendix 1.

**In going from column c to d the dependence of the hyperfine contribution on the S_z value has been shown explicitly.

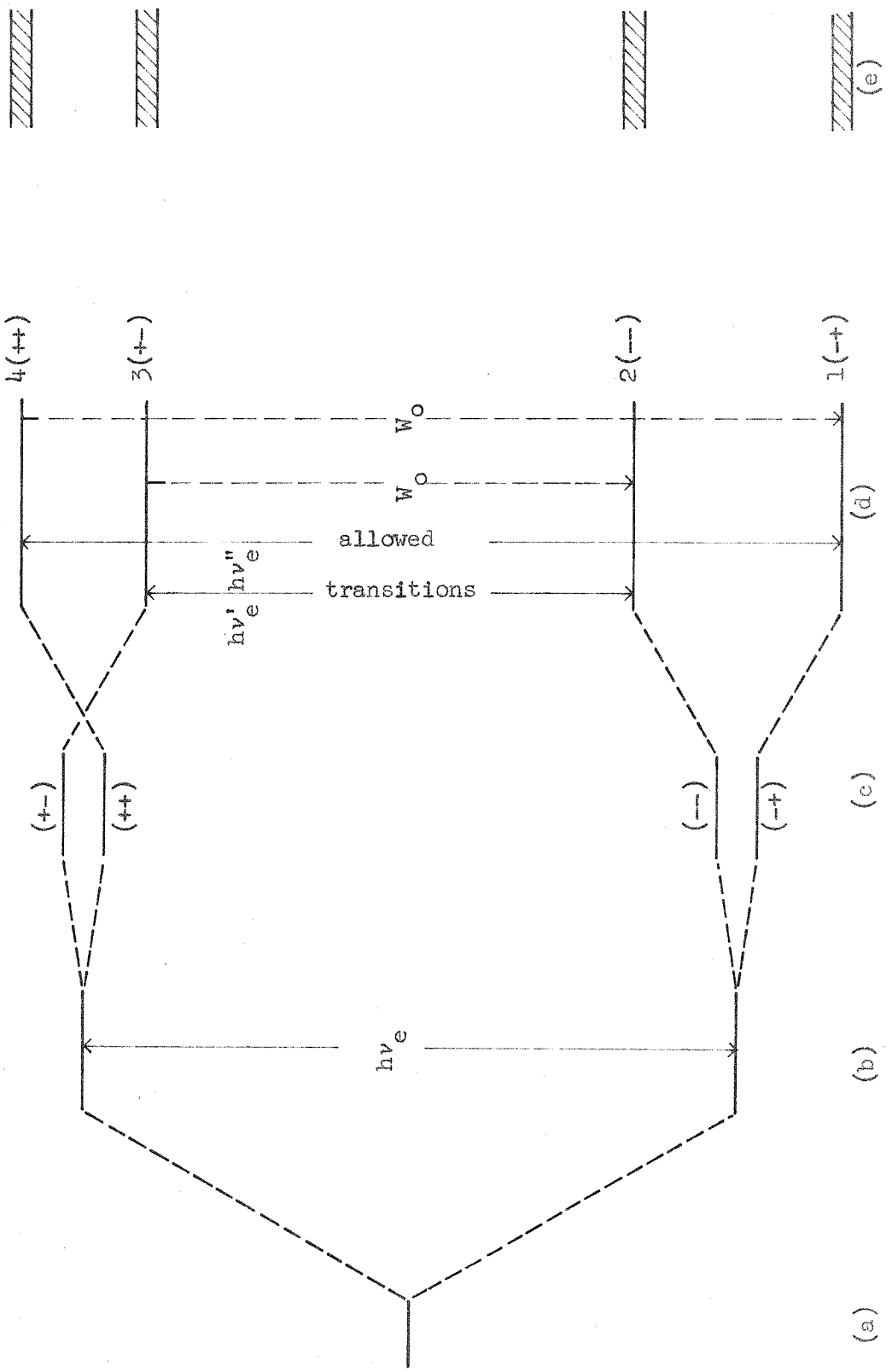

Figure 1

tion in high field for a single electron interacting with one nucleus having $I = \frac{1}{2}$. Consider now an ensemble of such electron-nucleus pairs.

The high frequency (10^{10} cps) magnetic field interacting with the electrons can induce transitions between the energy levels. When the resonance condition $h\nu_e = g|\beta|H_o$ is fulfilled, energy is absorbed from the radiation field. The magnitude of the resulting signal is proportional to the difference in the populations of the two levels involved. The transitions $\Delta m_S = \pm 1$, $\Delta m_I = 0$ are allowed; the transitions $\Delta m_S = \pm 1$, $\Delta m_I = \pm 1$ are "forbidden." ($m_S \equiv S_z$, $m_I \equiv I_z$.) The allowed nuclear transitions are those for which $\Delta m_S = 0$, $\Delta m_I = \pm 1$. The EMR technique measures directly the <u>differences</u> between the electronic transition energies.

If the relaxation time, $\frac{1}{W_o}$, has a finite value there can be a continuous absorption of energy. If $\frac{1}{W_o}$ is sufficiently long (say 10^{-5} sec) and one applies an intense radiation field (say 100 mW) at the resonant frequency, one will soon reach a steady state in which the populations of the two levels become equal and there is no net absorption of energy. This situation is referred to as saturation.

In column d the energy levels are represented as being sharply defined. Apart from the natural width of the levels due to the finite lifetime of the state ($\Delta E \, \Delta t \geq \hbar$), there may also be line-width contributions due to the local environment of the electron in the macroscopic sample. "Local environment" describes the fact that there may be slightly different effective magnetic fields at the positions of the various electrons in the sample.

This broadening of the energy levels (shown in column e) is directly reflected in the width of the resonance lines. When this broadening becomes of the order of the hyperfine level separation the hyperfine splittings cannot be resolved. Line broadening is especially troublesome when several nearly equivalent nuclei are present. This loss of resolution imposes a serious limitation on the information available from EMR.

An important modification of the standard EMR technique allows one quite often to regain some of the information lost in the unresolved EMR line. This modification, known as electron-nuclear double resonance, and abbreviated to ENDOR* was first conceived and experimentally verified by Feher in 1956. He described the ENDOR mechanism for the case shown in Figure 1, column d. Those energy levels are again drawn in the diagram below.

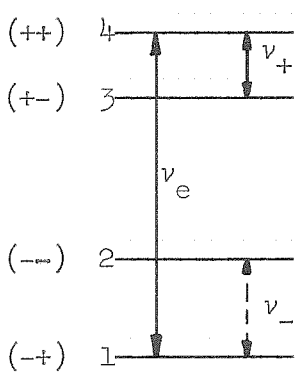

	(1)	(2)	(3)
(++) 4	$\frac{N}{4}(1-\Delta)$	$\frac{N}{4}$	$\frac{N}{4}(1-\frac{\Delta}{2})$
(+-) 3	$\frac{N}{4}(1-\Delta)$	$\frac{N}{4}(1-\Delta)$	$\frac{N}{4}(1-\frac{\Delta}{2})$
(-+) 2	$\frac{N}{4}(1+\Delta)$	$\frac{N}{4}(1+\Delta)$	$\frac{N}{4}(1+\Delta)$
(--) 1	$\frac{N}{4}(1+\Delta)$	$\frac{N}{4}$	$\frac{N}{4}$

The relative electronic population of the levels at thermal equilibrium is given in column 1. (Only the linear term in the expansion

---

*See 1 Sam. 28:7.

of the exponential $\exp[-g|\beta|H_o/kT] \equiv \exp[-\Delta]$ has been included and the nuclear Boltzmann factor being 10^3 times smaller than the electronic Boltzmann factor has been neglected.) If the allowed $1 \rightarrow 4$ transition is now saturated the level population will be that given in column 2. (We assume that the only important relaxation paths are $4 \rightarrow 1$ and $3 \rightarrow 2$.) The population of level four is greater than that of level three by about Δ. If the nuclear transition ν_+ is saturated then the level population is that given in column 3. (Imagine that the electronic transition does not follow this change instantaneously.) A difference in populations between levels one and four exists again, therefore there will be a change in the EMR signal level. In other words, ENDOR consists simply in observing the NMR transitions via the EMR signal. The allowed NMR transitions $\nu_{\pm}$ are the ENDOR frequencies.

The ENDOR line is usually narrower than the EMR line (sometimes by as much as four orders of magnitude). As a result, much of the information hidden under the EMR line can in principle be regained by the ENDOR technique. However, this is not its only utility. In Section B it will be shown that

$$\frac{2\, g_N \beta_N H_o}{h} = \nu_+ - \nu_-$$

and

$$\not{\delta} = \nu_+ + \nu_- \, .$$

The former relationship allows one to deduce the nuclear g-factor, g_N, directly from the measured ENDOR frequencies without a knowledge of the electronic wave function. The latter relationship gives $\not{\delta}$ which in turn is used to find $\underset{\sim}{A}$. In practice (partly because of the decreased line

width) one can measure $\nu_{\pm}$ by ENDOR more precisely than δ can be measured by EMR, and as a result $\underset{\sim}{A}$ can be found to greater precision from the ENDOR data.

The above reasons seemed of sufficient importance to prompt us to apply the ENDOR technique to the study of organic free radicals in the solid state. Although ENDOR had been applied to various inorganic systems when we began our work, nothing had been done on organic systems.

In the sections that follow, the ENDOR mechanisms are first described. Then a detailed procedure for calculating $\underset{\sim}{A}$ from EMR measurements is outlined and is subsequently used to calculate $\underset{\sim}{A}$ for the various protons in x-irradiated single crystals of glutaric acid. The solutions of the experimental problems encountered in the development of the ENDOR technique are described in detail. Finally, the ENDOR results obtained from x-irradiated single crystals of glutaric acid are presented.

B. ENDOR MECHANISMS AND SPIN HAMILTONIAN

ENDOR Mechanisms

As a prelude to the discussion of the ENDOR mechanism, consideration will first be given to certain historical developments which stimulated the development of the ENDOR technique.

Just before 1926 the lowest temperature attainable was about 0.7°K. This was achieved by high speed pumping on liquid helium, the liquified gas which could in principle provide the lowest temperatures. However the inherent properties of liquid helium made 0.7°K essentially its ultimate low temperature limit.

In 1926 Debye (1) and Giauque (2) independently proposed adiabatic demagnetization of paramagnetic salts as a method of reaching lower temperatures. Experimental verification soon followed in the work of Giauque and McDougall (3) and of Kurti and Simon (4) and of de Haas and Wiersma (5). The temperatures attained by these methods were in the range of 10^{-2} to 10^{-3}°K.

In 1934 Gorter (6) and Kurti and Simon (7) suggested that this low temperature limit might be extended if one also demagnetized the nuclei. This meant beginning the nuclear demagnetization at ultra-low temperatures (10^{-2}°K) and with very high fields (10^{5} gauss). This method now known as the "brute force method" involved formidable technical difficulties.

Not until 1948 did Gorter (8) and Rose (9) independently suggest the possibility of using the electron-nuclear interaction itself to polarize the nuclei and thus eliminate the experimental problems inherent in

the brute-force method. This suggestion is now known as the Rose-Gorter method. Variations on this theme were subsequently introduced by Bleaney (10) who eliminated the need of an external magnetic field and by Pound (11) who made use of the quadrupolar interaction. These methods all involved static nuclear alignment.

Kastler was the first, contrary to popular opinion, to propose methods for dynamic nuclear polarization. His initial suggestion (12) (1950) involved optically pumping atoms in a gas. His second method (13) (1951) invoked the use of electron-nuclear double resonance. His arguments were essentially equivalent to those involved in our discussion of Feher's first model (see introduction). Two years later Overhauser's paper (14) appeared on the polarization of nuclei in metals. His proposal was confirmed experimentally in the same year by Carver and Slichter (15). "Overhauser's" suggestion was quickly extended to non-metals by Abragam (16). Apart from Kastler's suggestion, these methods all depended directly on the relaxation processes to bring about the nuclear polarization. Since then a flurry of papers has appeared suggesting other means which do not rest solely on the relaxation mechanisms. All these methods for dynamic nuclear polarization can be divided into two broad classes depending on whether the electron-nuclear coupling is isotropic (scalar) or dipolar (tensor).

Most of the variations* normally referred to as the Overhauser effect fall in the former category. The true Overhauser effect (i.e.--- that occurring in metals) is one of these. Following Abragam's treatment

---

*The Underhauser effect (17) which occurs in liquids has to do with tensor coupling.

(16,18) the isotropic electron-nuclear interaction can be written as $a\vec{I}\cdot\vec{S}$. If one denotes by $W_{(+-) \rightleftharpoons (-+)}$ the probability of the flip-flop transitions (those in which an electron goes from (+) to (-) while a nucleus goes from (-) to (+)) and by $N_{\pm}$ and $n_{\pm}$ the number of spins $\vec{S}$ and $\vec{I}$ in the states $S_z = \pm \frac{1}{2}$ and $I_z = \pm \frac{1}{2}$ respectively, then under steady state conditions one can write (requiring that the nuclei relax only through their coupling with the electron),

$$N_+ n_- W_{(+-) \rightarrow (-+)} = N_- n_+ W_{(-+) \rightarrow (+-)} . \qquad \text{(B-1)}$$

Therefore,

$$\frac{W_{(+-) \rightarrow (-+)}}{W_{(-+) \rightarrow (+-)}} = \frac{N_-}{N_+} \frac{n_+}{n_-} . \qquad \text{(B-1)}$$

and since thermal equilibrium is assumed (no applied radio frequency (rf) fields) we obtain by Boltzmann's relation

$$\frac{W_{(+-) \rightarrow (-+)}}{W_{(-+) \rightarrow (+-)}} = \exp - \frac{\hbar(\omega_S - \omega_I)}{kT} . \qquad \text{(B-2)}$$

The electronic and nuclear resonance frequencies are referred to as ω_S and ω_I respectively. $\gamma \equiv \frac{\omega}{H_o}$. Saturating the <u>allowed</u> electronic transition ($\Delta m_S = \pm 1$, $\Delta m_I = 0$) makes $N_+ = N_-$ and therefore

$$\frac{n_+}{n_-} = \exp - \frac{\hbar (\omega_S - \omega_I)}{kT} . \qquad \text{(B-3)}$$

Clearly the enhancement in nuclear polarization is a function of $(\omega_S - \omega_I) \equiv H_o(\gamma_S - \gamma_I)$. Equation B-3 describes the case of scalar coupling in which

allowed electronic transitions are saturated. The Jeffries effect (19) is also a scalar effect occurring, however, when the forbidden transitions ($\Delta m_S = \pm 1$, $\Delta m_I = \pm 1$) are irradiated. It is important to notice that the polarization in these cases depends on the lattice induced forbidden transitions.

To treat the tensor case the wave function for the (--) state, $|-->$, can be represented by $|--> = |-->' + \alpha\, |-+>^*$ (where $\alpha < 1$) because of the dipolar (tensor) coupling. If ${}^{I}T_1 \ll W \ll {}^{S}T_1$ where ${}^{I}T_1$ and ${}^{S}T_1$, refer to the nuclear and electronic spin-lattice relaxation times respectively and W is the forbidden transition probability then one can induce the forbidden transitions directly and by equation B-1 a straightforward consideration of population dynamics will show that

$$\frac{n_+}{n_-} = \left(\frac{N_+}{N_-}\right)_o \qquad \text{for flip-flop transition}$$

$$\frac{n_+}{n_-} = \left(\frac{N_-}{N_+}\right)_o \qquad \text{for flip-flip transition.}$$

This is clarified in Figure 2. Subscript zero refers to equilibrium values. Notice that the polarization reverses depending on which forbidden transition is induced. Such effects are usually referred to as Solid effects. In each case, the dynamic nuclear polarization is observed via NMR. We

---

*$\alpha^2 \approx (H_{SI}/H_o)$, where H_{SI} is the local field at the nucleus I produced by the electron S. If W_o and W represent the probability for the allowed and forbidden electronic transitions respectively then $(W/W_o) \sim \alpha^2$. In the scalar coupling case W is much smaller than in this case.

Relative Populations for:	Thermal Equilibrium	Transition a Saturated	Transition b Saturated
(++)	$1 - \Delta$	1	$1 - \Delta$
(+−)	$1 - \Delta$	$1 - \Delta$	1
(−−)	$1 + \Delta$	1	$1 + \Delta$
(−+)	$1 + \Delta$	$1 + \Delta$	1

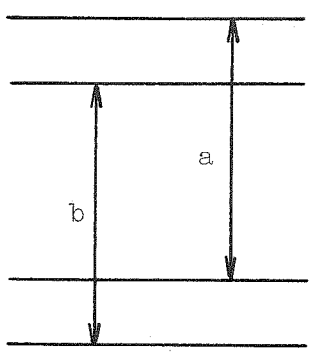

Thermal Equilibrium (no applied rf): $\frac{n_+}{n_-} = 1$

$$\frac{N_+}{N_-}_{o} = \frac{1 - \Delta}{1 + \Delta} = (1 - \Delta)(1 - \Delta + \cdots) \approx 1 - 2\Delta$$

$$\frac{N_-}{N_+}_{o} = \frac{1 + \Delta}{1 - \Delta} = (1 + \Delta)(1 + \Delta + \cdots) \approx 1 + 2\Delta$$

Transition a saturated:

$$\frac{n_+}{n_-} = \frac{1 + \frac{\Delta}{2}}{1 - \frac{\Delta}{2}} = (1 + \tfrac{\Delta}{2})(1 + \tfrac{\Delta}{2} + \cdots) \approx 1 + \Delta$$

Transition b saturated:

$$\frac{n_+}{n_-} = \frac{1 - \frac{\Delta}{2}}{1 + \frac{\Delta}{2}} = (1 - \tfrac{\Delta}{2})(1 - \tfrac{\Delta}{2} + \cdots) \approx 1 - \Delta$$

Figure 2

shall not discuss further the various modifications and special cases of these dynamic polarization methods but shall simply refer to several recent review articles (20,21,22).

It should be pointed out that the major utility of these effects is to enhance the normal NMR sensitivity. On the other hand, the major advantage of the ENDOR method, which observes these NMR transitions via EMR, lies in the increased resolution made possible. Suffice it to say that a consideration of dynamic nuclear polarization methods and experimental results can contribute to an understanding of ENDOR effects.

The first experiment in which the EMR line itself was used to monitor dynamic nuclear polarization was that proposed by Feher (23) and verified by Feher and Gere (24) using a sample of phosphorus-doped silicon at 1.25°K. At this temperature the electronic relaxation time is on the order of a minute and they were able to observe under adiabatic fast passage conditions (25) a definite nuclear polarization.

At this point (1956) the ENDOR experiment became self-evident. By simply using his same sample of phosphorus-doped silicon and monitoring the EMR line while inducing the NMR transition, Feher observed the first ENDOR signal (26). Shortly thereafter he observed (27) the ENDOR transitions for F-centers in KCl.

The normal EMR of F-centers in KCl reveals a single structureless line having a width of about 150Mc. On the other hand the ENDOR lines in KCl have a width of about 15kc—a resultant reduction by four orders of magnitude. From these lines one can deduce $|\Psi_i(0)|^2$, the spin density of the delocalized electron on nucleus i. In the phosphorus-doped silicon experiment Feher was able to observe ENDOR lines due to nuclei five

lattice sites removed from the donor center (28). As a result he was able to plot the "wave function" versus distance from the donor site.* In more recent work on F-centers investigators have been able to study the interaction of the electron with nuclei as far away as the tenth (29) shell around the color center.

To explain his observations Feher modified his first model (see introduction) to deal with inhomogeneously broadened lines. An inhomogeneously broadened line (30) is the resulting envelope of a large number of homogeneously broadened lines which are referred to as spin packets. (See Fig. 3a.) Within each spin packet thermal equilibrium of the spin system is always preserved. Therefore the effect of rf energy which flips spins at a particular frequency within the spin packet, is quickly communicated to the rest of the spins within the spin packet. However, there is very little communication between different spin packets. As a result the application of microwave power at one frequency will saturate (ideally) only that one spin packet. This gives rise to the so-called hole burning experiments (27) in which a rapid passage through the inhomogeneously broadened line immediately after such saturation reveals a line shape such as shown in Figure 3b where the "hole" is at the frequency at which the saturation was effected.

One can think of the spin packets (and their intensity) as being determined by the probabilities of the various possible nuclear configurations about the paramagnetic sites. Therefore, Feher proposed, when one

---

*It does not fall off monatonically. The probability plot looks like the plot of the amplitude versus time of a damped oscillator.

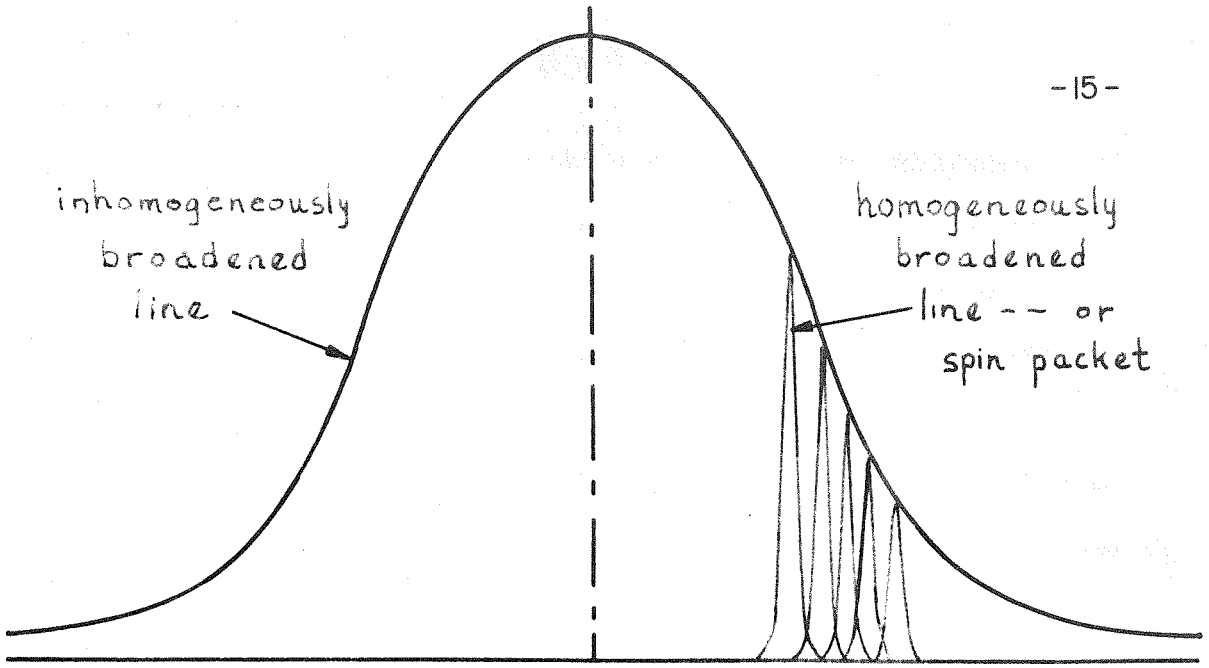
inhomogeneously
broadened
line
homogeneously
broadened
line -- or
spin packet

(a)

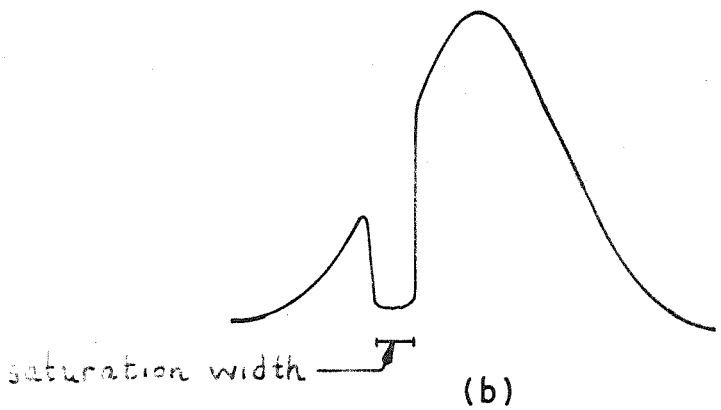
saturation width
T

(b)

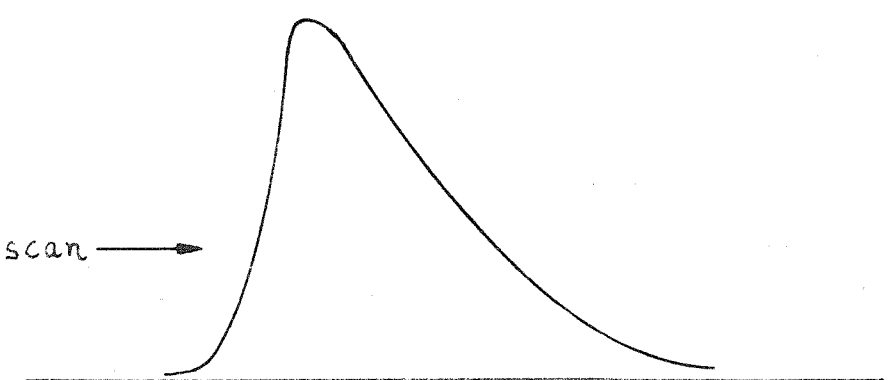
scan

(c)

Figure 3

induces a nuclear transition which changes the nuclear configuration of some spin packet to the nuclear configuration obtaining in the spin packet being saturated, the EMR is suddenly no longer saturated and consequently there will be a resulting change in the level of microwave power absorbed. This gives rise to the ENDOR signal.

This model explains the width of the ENDOR lines which are now seen to be of the order of the width of the spin packet. The important features of Feher's packet shifting model are

1) the ENDOR signal is seen when one shifts, via an NMR transition, the spin packets comprising the inhomogeneously broadened line;
2) the ENDOR signal decays at a rate dependent on $^{S}T_1$ (see Fig. 3c).

and 3) the ENDOR signal is positive and is a maximum near the center of the EMR line.

Although the Feher model qualitatively described the effects in the ENDOR systems discussed thus far, the same is not true in ruby,* in which ENDOR was first observed by Terhune, Lambe, Makhov, and Cross (33). Seemingly in direct contrast to Feher's model they observed

1) that the ENDOR signal decayed at a rate dependent on $^{I}T_1$;
2) that the ENDOR signal is negative and is a minimum near the center of the EMR line;

and 3) that an added ENDOR signal is seen when <u>distant</u> nuclei are flipped.

---

*Ruby consists of a dilute doping of Cr^{+3} in Al_2O_3. Dynamic nuclear polarization was first seen in ruby by Cowen, Schafer, and Spence (31) and by Abraham, McCausland, and Robinson (32).

By distant nuclei we mean those host aluminum nuclei whose direct interaction with the paramagnetic center is vanishingly small. The inversion of these distant nuclei can then have little effect on the spin packet distribution within the inhomogeneously broadened lines.

More detailed investigations by Lambe, Laurence, McIrvine and Terhune (34) (LLMT) revealed that when the EMR line is observed under conditions of absorption, χ'', the ENDOR transition causes a slight increase, but when the EMR line is observed under conditions of dispersion, χ', the ENDOR transition causes a large decrease. Another important feature is that the Cr^{53} nuclei are not necessary for the distant ENDOR effect.

The model proposed by LLMT to explain <u>their</u> results in ruby has applications in organic systems. We essentially reproduce their arguments, following rather closely their notation. Consider an inhomogeneously broadened line (see Fig. 3a) with a normalized line shape function $h(\omega'-\omega_o)$ having line width $1/T_2^*$. The inhomogeneous line is composed of homogeneously broadened lines having a normalized line shape function $g(\omega-\omega')$ and the width of the spin packet is given by $1/T_2$. Λ represents the nuclear Zeeman splitting. We assume firstly that

$$1/T_2 \ll \Lambda \ll 1/T_2^* \qquad \text{(B-4)}$$

and secondly that the application of microwave power at a frequency ω also induces forbidden transitions at $(\omega'' + \Lambda)$ and $(\omega''' - \Lambda)$ such that $\omega'' + \Lambda = \omega''' - \Lambda = \omega$. Since $\omega \approx \omega'' \approx \omega'' \gg \Lambda$ we can write $\omega'' + \Lambda \approx \omega + \Lambda$ and $\omega''' - \Lambda \approx \omega - \Lambda$. The flip-flip and flip-flop transitions have a reduced probability and a shape factor $g'(\omega \pm \Lambda - \omega')$ with normalization g',

the ratio of the forbidden to the allowed transition probability. The following symbols are also defined.

$N(\omega') = h(\omega'-\omega_o)$: the distribution function of electrons in local fields. $N(\omega')d\omega'$ gives the fraction of electrons which are in a local field such that their resonance lies between ω' and $\omega'+d\omega'$

$N^-(\omega')$: that part of $N(\omega')$ which has spin down

$N^+(\omega')$: that part of $N(\omega')$ which has spin up

$n(\omega') \equiv N^-(\omega') - N^+(\omega')$

M^- : the fraction of distant nuclei with spin down

M^+ : the fraction of distant nuclei with spin up

$m \equiv M^- - M^+$

It follows from these definitions that

$$M^-N^- - M^+N^+ = \tfrac{1}{2}(n + mN). \tag{B-5}$$

$$M^+N^- - M^-N^+ = \tfrac{1}{2}(n - mN). \tag{B-6}$$

Equilibrium values will be denoted with a zero subscript. To determine the effect of dynamic nuclear polarization on the EMR signal one must consider the time dependence of $n(\omega')$. One can write

$$\frac{dn}{dt} = \left(\frac{dn}{dt}\right)_{SL} + \left(\frac{dn}{dt}\right)_{\mu w} \tag{B-7}$$

where the subscripts refer to spin-lattice and microwave induced transitions respectively. Under steady state conditions $\frac{dn}{dt} = 0$. Then in the relaxation time approximation

$$\left(\frac{dn}{dt}\right)_{SL} = \frac{n-n_o}{T_1} \tag{B-8}$$

and also

$$\left(\frac{dn}{dt}\right)_{\mu w} = - \left(\frac{dn}{dt}\right)_{SL} . \tag{B-7a}$$

Therefore

$$\frac{n_o - n}{T_1} = \frac{\pi}{4} \gamma^2 H_1^2 \left[g(\omega-\omega')n(\omega') + g'(\omega+\Lambda-\omega')(M^+N^- - M^-N^+) + g'(\omega-\Lambda-\omega')(M^-N^- - M^+N^+) \right]. \tag{B-9}$$

Similarly

$$\frac{m_o - m}{T_N} = \frac{\pi}{4} \gamma^2 H_1^2 \left[\int g'(\omega-\Lambda-\omega')(M^-N^- - M^+N^+) d\omega' - \int g'(\omega+\Lambda-\omega')(M^+N^- - M^-N^+) d\omega' \right] . \tag{B-10}$$

Using equations B-5 and B-6 and the definition of the saturation parameter $S \equiv (\frac{1}{2}\gamma H_1)^2 T_1 T_2$ one can write

$$n(\omega') = \frac{n_o + \frac{\pi S}{2T_2} N(\omega')[g'(\omega+\Lambda-\omega') - g'(\omega-\Lambda-\omega')] m}{1 + \frac{\pi S}{2T_2} [2g(\omega-\omega') + g'(\omega+\Lambda-\omega') + g'(\omega-\Lambda-\omega')]} . \tag{B-11}$$

Similarly by taking advantage of the approximation B-4, $1/T_2 \ll \Lambda \ll 1/T_2^*$, one obtains

$$\frac{m}{m_o} = \frac{1 + (2T_N/T_1T_2)[\frac{1}{2}g'S/(1 + \frac{1}{2} g'S)] h(\omega'-\omega_o) \left[1 + \frac{4}{\pi} T_2^{*2} \omega(\omega_o-\omega)\right]}{1 + (2T_N/T_1T_2)[\frac{1}{2}g'S/(1 + \frac{1}{2} g'S)] h(\omega'-\omega_o)(1 + \frac{1}{4} g'S)} . \tag{B-12}$$

The plot of $n(\omega')$ versus ω' (eq. B-11) is shown below:

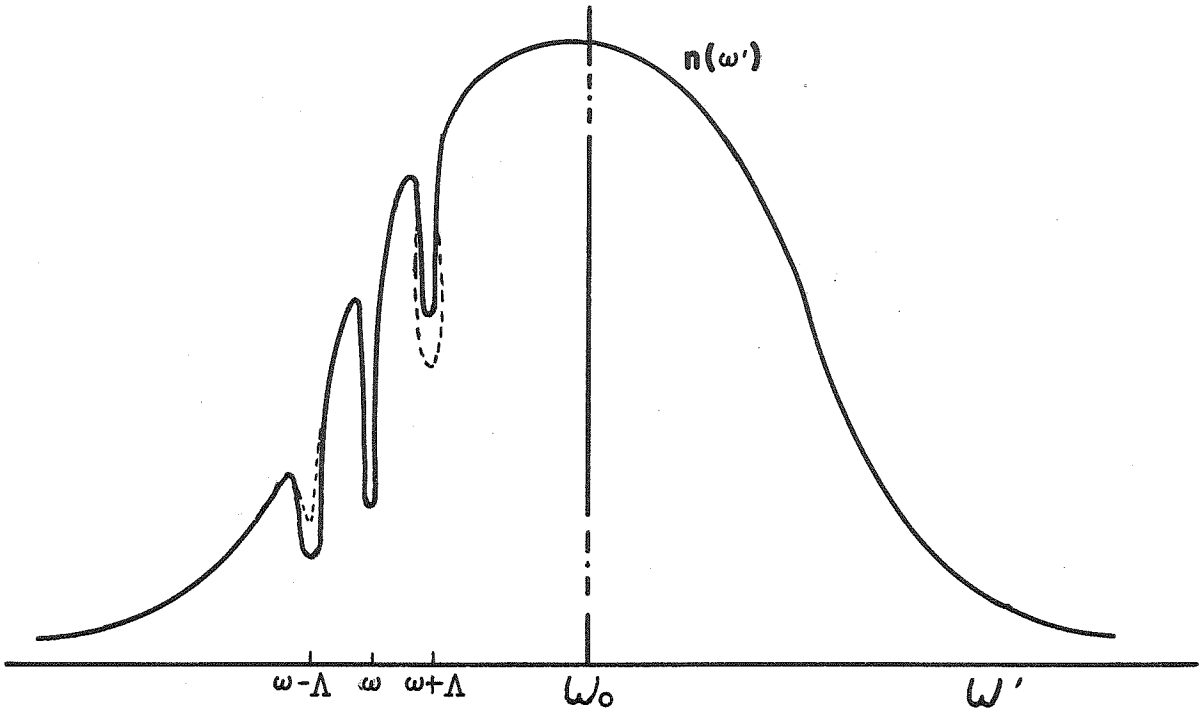

Electron-spin population changes upon application of the ENDOR frequencies.

(a) —— $m \neq 0$: Steady-state nuclear polarization (no rf).

(b) --- $m = 0$: ENDOR signal applied (rf at nuclear Zeeman frequency).

In equation B-11 the factor $(\pi S/2T_2) \gtrsim 10^4$ for the typical experiment. Roughly speaking then, one can neglect the first term in the denominator whenever $g \sim g' \sim 1$ and conversely the second term can be neglected whenever $g \approx g' \approx 0$. The first term in the numerator just gives the line shape of $n(\omega')$ in the absence of any rf and it looks essentially like an absorption curve. Equation B-11 can obviously be rewritten as

$$n(\omega') = \frac{n_o(\omega')}{1 + \frac{\pi S}{2T_2}[2g(\omega-\omega')+g'(\omega+\Lambda-\omega')+g'(\omega-\Lambda-\omega')]} + \frac{\frac{\pi S}{2T_2}N(\omega')[g'(\omega+\Lambda-\omega') - g'(\omega-\Lambda-\omega')]m}{1 + \frac{\pi S}{2T_2}[2g(\omega-\omega')+g'(\omega+\Lambda-\omega')+g'(\omega-\Lambda-\omega')]} . \quad \text{(B-13)}$$

Clearly the first term will be reduced each time ω' is in the region of the lines given by g and the (g')'s. The second term will also contribute to this modulation. In particular from $m > 0$ the dip in $n(\omega')$ will be shallower for $\omega' = \omega - \Lambda$ and deeper for $\omega' = \omega + \Lambda$ as compared with the case when $m = 0$. When an rf field is applied $m \to 0$ and in that case the distribution shown by the dotted lines is obtained.

Expressions for χ'' and χ' the spin susceptibility for absorption and dispersion respectively can now be found. Based on the analysis of Portis (30) on inhomogeneously broadened lines LLMT obtain the expressions

$$\chi''(\omega) = \tfrac{1}{2}\chi_o \omega_o h(\omega-\omega_o)\left[\int_o^\infty \frac{\pi g(\omega-\omega')d\omega'}{1+(\pi S/T_2)g(\omega-\omega')} + \text{const} - m(\omega_o-\omega)[\text{positive definite term}]\right] \tag{B-14}$$

$$\chi'(\omega) = \tfrac{1}{2}\chi_o\left[\int_o^\infty \frac{2\omega'^2 h(\omega'-\omega_o)d\omega'}{\omega'^2-\omega^2} + \frac{m}{m_o}\frac{\frac{1}{2}g'S}{1-\frac{1}{2}g'S}\frac{2\pi}{T_2}h(\omega-\omega_o)\right] \tag{B-15}$$

It is easy to see from equation B-14 that the absorption effect for $m \to 0$ will always be an increase. However, note that the change occurring in $n(\omega')$ (eq. B-13 or B-11) when the rf is turned off or on is in opposite directions in the two sidebands. As a result absorption effects tend to cancel whereas dispersion effects add.

On the other hand the two terms in equation B-15 always have the same sign. This can be seen if it is first noticed from equation B-12 that $m \gtrless 0$ for $\omega_o \gtrless \omega$. (Recall the Abragam model for dynamic nuclear polarization.) Second, the weighting of those contributions to the integral for $\omega' < \omega$ and for $\omega' > \omega$ is such that the resulting sign depends on

whether $\omega < \omega_o$ or $\omega > \omega_o$--and the sign turns out to be the same as that for m. Therefore when $m \rightarrow 0$, χ' always decreases. These effects are in qualitative agreement with the results of LLMT.

They further showed that the response of the EMR signal when either Al^{27} (distant) or Cr^{53} (local) transitions were induced was essentially identical. In both cases χ' decreases significantly and χ'' increases moderately.* Furthermore, the decay of the ENDOR signal in either local or distant ENDOR goes at the rate of the spin lattice relaxation time for the Al^{27} nuclei. All indications point to the fact that the mechanism for both distant and local ENDOR in ruby is the same. Therefore, the mechanism, based on the forbidden transition analysis of Abragam, would be one in which the nuclear polarization of distant nuclei is removed in both cases. For distant ENDOR this is done by directly inducing the distant nuclear Zeeman frequencies. For local ENDOR the local nuclei after being depolarized must communicate this depolarization to the distant nuclei for the observation of the ENDOR effect. Spin diffusion may be the mechanism for this communication. A schematic representation of this model as given by LLMT is shown below.

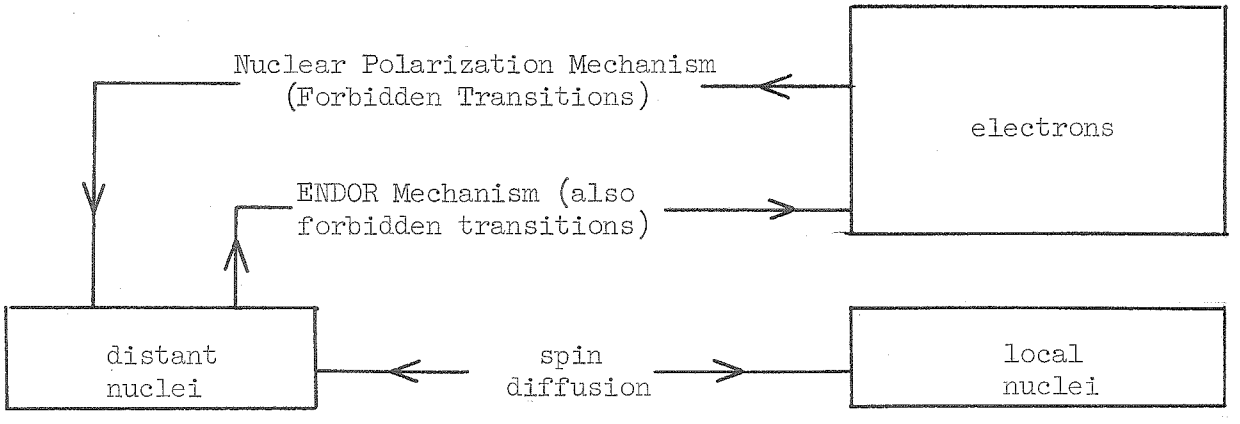

*It can also be shown (34) that the packet shifting model of Feher predicts a decrease in χ'.

At the time we began our work on ENDOR it was very difficult to plan an optimized experiment. The only ENDOR experiments that had been done were those of Feher and thus the only proposed mechanism was the packet-shifting mechanism. But this applied to inhomogeneously broadened lines. It is probably true that the EMR lines of solid state free-radicals are to some extent inhomogeneously broadened. However, the characteristics of these lines are considerably different from those of the inorganic systems considered so far, and consequently one could not with confidence plan an experiment based on the packet-shifting mechanism.

Furthermore, a considerable amount of work has been done on the measurement of relaxation times, line broadening processes, and line widths in inorganic materials. Even today the exact opposite can be said for solid state free-radicals, and yet these properties can have a profound effect on both the mechanism and feasibility of ENDOR.

As a matter of fact, ENDOR has still not been observed in malonic acid* and the reason for this is not at all understood. Our first ENDOR experiment was performed on malonic acid at room temperature. Recently it has been shown that at least in ruby the ENDOR signal disappears above 20°K (31,35). Even under favorable circumstances the ENDOR signal can be very elusive.

However, assuming that one can see ENDOR in solid state free-radicals one must consider how the data can be used in calculating the hyperfine tensors. This can involve some difficulties and so we shall describe a procedure by which the calculations can be made in a rather straightforward way.

---

*Distant ENDOR has been observed in malonic acid (35).

Spin Hamiltonian

There are many publications (36-41) dealing with organic free radicals in the solid state. The spin Hamiltonian for a radical having $\vec{S} = \frac{1}{2}$ in which nucleus i has spin $\vec{I}^i$ can be written

$$\mathcal{H} = - \vec{\mu}_e \cdot \vec{H}_o - \sum_i \vec{\mu}_N^i \cdot \vec{H}_o + h \sum_i \vec{S} \cdot \underset{\sim}{A}^i \cdot \vec{I}^i \quad . \tag{B-16}$$

The first and second terms refer to the Zeeman energies of the electron and nucleus respectively. The third term includes the contact and dipolar interactions. Actually $\underset{\sim}{A}$ can be written as the sum of two tensors,

$$\underset{\sim}{A} = \underset{\sim}{a} + \underset{\sim}{b} \qquad \text{where } \underset{\sim}{a} = a \, \underset{\sim}{1} \qquad \text{and}$$

$$\underset{\sim}{b} = \begin{pmatrix} b_{xx} & b_{xy} & b_{xz} \\ b_{xy} & b_{yy} & b_{yz} \\ b_{xz} & b_{yz} & b_{zz} \end{pmatrix} .$$

The isotropic coupling constant, a, is given by $a = \frac{1}{3}$ trace $\underset{\sim}{A} = \frac{1}{3}$ trace $\underset{\sim}{a}$, and this implies that trace $\underset{\sim}{b} = 0$. The tensor $\underset{\sim}{b}$ represents the dipolar contribution. $\underset{\sim}{A}$ is a symmetric tensor and can be written

$$\underset{\sim}{A} = A_{11}\vec{i}\vec{i} + A_{22}\vec{j}\vec{j} + A_{33}\vec{k}\vec{k} + A_{12}(\vec{i}\vec{j} + \vec{j}\vec{i}) + A_{13}(\vec{i}\vec{k} + \vec{k}\vec{i}) + A_{23}(\vec{j}\vec{k} + \vec{k}\vec{j}) \quad . \tag{B-17}$$

Equation B-16 can be written in a more useful form by using the relations

$$\begin{aligned} \vec{\mu}_e &= - |\beta| \vec{S} \cdot \underset{\sim}{g} \\ \vec{\mu}_N &= g_N \beta_N \vec{I} \end{aligned} \quad . \tag{B-18}$$

One obtains

$$\mathcal{H} = |\beta|\vec{S}\cdot\underset{\sim}{g}\cdot\vec{H}_o + \sum_{i=1}^{n}\left[h\vec{S}\cdot\underset{\sim}{A}^i\cdot\vec{I}^i - g_N^i\beta_N^i\vec{H}_o\cdot\vec{I}^i\right]. \tag{B-19}$$

In analogy to the hyperfine tensor one can write the g-factor tensor as

$$\underset{\sim}{g} = g_o\underset{\sim}{1} + \underset{\sim}{g}' \ . \tag{B-20}$$

In most organic free-radicals in the solid state the elements of $\underset{\sim}{g}'$, $g'_{ij} \approx 10^{-3}\, g_o$. Therefore, for the calculation of energy levels $\underset{\sim}{g} \approx g_o\,\underset{\sim}{1}$.* Furthermore in the systems we shall study with $|\vec{H}_o| \approx 3000$ gauss, S_H is approximately a good quantum number. So we will make the further approximation that $\vec{S} = S_H\vec{u}_H$. If one also defines $\vec{H}_o \equiv H_o\vec{u}$ one can rewrite equation B-19 as

$$\mathcal{H} = S_H g_o|\beta|H_o + \Sigma\left[hS_H\vec{u}_H\cdot\underset{\sim}{A}^i\cdot\vec{I}^i - g_N^i\beta_N^i H_o\vec{u}_H\cdot\vec{I}^i\right]. \tag{B-21}$$

When dealing with protons one can define

$$\nu_p \equiv h^{-1}g_N\beta_N H_o \tag{B-22}$$

$$\text{and } |\nu_e| \equiv h^{-1}g_o|\beta|H_o \ .$$

Then

$$\mathcal{H} = S_H h|\nu_e| - h\,\Sigma\left[\nu_p\vec{u}_H - S_H\vec{u}_H\cdot\underset{\sim}{A}^i\right]\cdot\vec{I}^i \ . \tag{B-23}$$

The quantity in square brackets can be defined as

$$\nu^{i\to i}_u \equiv \nu_p\vec{u}_H - S_H\vec{u}_H\cdot\underset{\sim}{A}^i \tag{B-24}$$

which then allows one to write

$$\mathcal{H} = S_H h|\nu_e| - h\sum_i \nu^{i\to i}_u\cdot\vec{I}^i \equiv S_H h|\nu_e| - h\,\Sigma\,\nu^i I_u i \ . \tag{B-25}$$

---

*For some purposes it is valuable to actually determine $\underset{\sim}{g}'$. For example, the minimum diagonal value of $\underset{\sim}{g}$ is related to the axis of the π-orbital in a R_2CH radical (42).

In equation B-25 ν^i represents the ENDOR transition frequencies for the i^{th} nucleus. Consider just one nucleus. For that case

$$\mathcal{H} = S_H h|\nu_e| - h\nu I_u \ . \tag{B-26}$$

If one has eigenfunctions for this $\mathcal{H}$ then the energy levels for the system can be calculated directly. If $\nu_{\pm}$ represents the magnitude of the vector in the $\vec{u}_{\pm}$ direction (i.e. for $S_H = \pm \frac{1}{2}$) and furthermore if I_u represents the eigenvalues $\pm \frac{1}{2}$ of the operator $\vec{I}$ for the component of the nuclear spin angular momentum in the direction of the unit vector $\vec{u}$, then the <u>energy levels</u> will be given by

$$E^1 = \tfrac{1}{2}h|\nu_e| + \tfrac{1}{2}h\nu_+$$

$$E^2 = \tfrac{1}{2}h|\nu_e| - \tfrac{1}{2}h\nu_+$$

$$E^3 = -\tfrac{1}{2}h|\nu_e| + \tfrac{1}{2}h\nu_-$$

$$E^4 = -\tfrac{1}{2}h|\nu_e| - \tfrac{1}{2}h\nu_- .$$

Consider only the allowed transitions ($\Delta m_S = \pm 1$). The energy of each <u>transition</u> will be

$$\begin{aligned} E^1 - E^4 &= h|\nu_e| + \tfrac{1}{2}h(\nu_+ + \nu_-) \\ E^2 - E^3 &= h|\nu_e| - \tfrac{1}{2}h(\nu_+ + \nu_-). \end{aligned} \tag{B-27}$$

We are interested only in the <u>splitting</u> $\mathcal{S}'$ between the transition frequencies so we write

$$\mathcal{S}' \equiv (E^1 - E^4) - (E^2 - E^3) = h(\nu_+ + \nu_-) \ . \tag{B-28}$$

The splitting in terms of frequency is just $\not{\delta}$

$$\not{\delta} \equiv \frac{\not{\delta}'}{h} = \nu_+ + \nu_- \qquad \text{(B-29)}$$

Under certain restricted conditions it can also be shown that

$$\frac{2g_N\beta_N H_o}{h} = \nu_+ - \nu_- \ .$$

A typical energy level diagram in high field as a function of H_o is shown below.

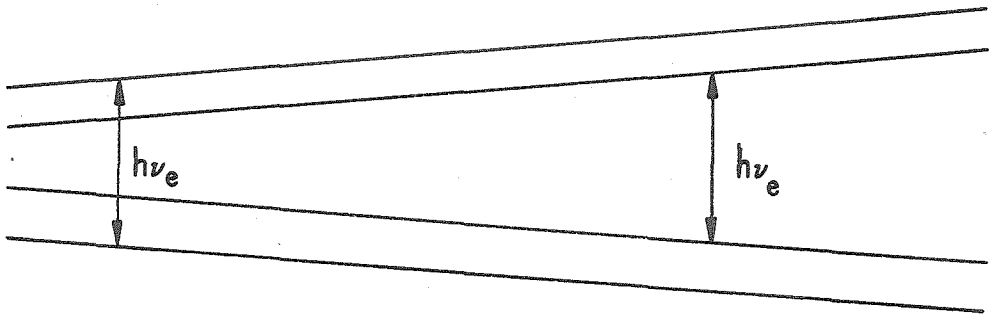

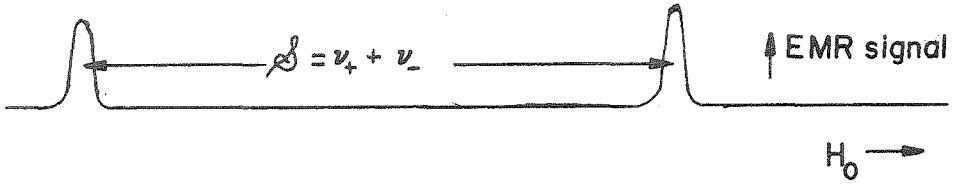

Since the Hamiltonian was written as a sum of n terms, the energies for n nuclei will just be a sum of terms for individual nuclei. So, for a radical having several magnetic nuclei one can consider each nucleus individually and construct the energy level diagram by superposition.

The general problem in EMR is to calculate $\underset{\sim}{A}$ from the measured splittings $\not{\delta}$. The ENDOR technique determines $\nu_{\pm}$ directly and usually with greater precision and so this provides a way of getting better values

for $\underset{\sim}{A}$. The method described here for doing this requires only that the ENDOR transition frequencies $\nu_{\pm}$ be measured along the three coordinate axes.

In Section C it is shown that in general

$$4\left(\nu_{\pm}\right)^2 = \sum_{i=1}^{3} (2\nu_p \pm A_{ii})^2 u_i^2 \pm 2 \sum_{i=1}^{3} \sum_{j=1}^{3} (2\nu_p \pm A_{ii}) A_{ij} u_i u_j \Delta_{ij}$$

$$+ \sum_{i=1}^{3} \sum_{j=1}^{3} \sum_{k=1}^{3} A_{ik} A_{jk} u_i u_j \Delta_{ik} \Delta_{jk} \qquad \text{(C-15)}$$

Here u_{ij} are direction cosines and

$$\Delta_{mn} \equiv \left\{ \begin{array}{l} 0 \text{ for } m = n \\ \\ 1 \text{ for } m \neq n \end{array} \right\}$$

From this one can derive directly

$$(\nu_-)^2 - (\nu_+)^2 = 2\nu_p (A_{11}u_1^2 + A_{22}u_2^2 + A_{33}u_3^2) + 4\nu_p (A_{12}u_1u_2 + A_{23}u_2u_3 + A_{13}u_1u_3). \qquad \text{(B-30)}$$

Then clearly the difference of the squares of the ENDOR transition frequencies along the coordinate axes gives in turn A_{11}, A_{22}, and A_{33}. By going back to equation C-15 one can write (for $u_i=1$, $u_j=u_k=0$)

$$4\left(\nu_{\pm}\right)^2 = (2\nu_p \pm A_{ii})^2 u_i^2 + A_{ij}^2 u_i^2 + A_{ik}^2 u_i^2$$

$$\left\{ \begin{array}{c} i \\ j \\ k \end{array} \right\} = 1,2,3 \qquad i \neq j \neq k \,.$$

Since A_{ii} is known one has two equations in two unknowns for each of the three orientations and therefore one can solve for the off-diagonal elements. This then gives $\underset{\sim}{A}$ directly from $\underline{\nu}_{\pm}$. There is only one problem. When more than one nucleus interacts with the electron it is not clear how one should assign the ENDOR lines. Furthermore, since only square terms appear in the equations for calculating the off-diagonal elements of the tensor from $\underline{\nu}_{\pm}$, the absolute signs remain unknown.

To reduce these problems it is imperative that one first calculate $\underset{\sim}{A}$ from the standard EMR data. One then calculates the ENDOR frequencies $\underline{\nu}_{\pm}$. These calculated frequencies are compared with the observed frequencies and then after assignment of $\underline{\nu}_{\pm}$ to a particular nucleus, $\underset{\sim}{A}$ for that nucleus can be calculated.

Therefore, the first step in making use of ENDOR data is to calculate the hyperfine tensors from the splittings $\not{\delta}$ measured in the standard EMR experiment. This will be done in subsequent sections.

In this section it has been indicated that

1. Dynamic nuclear polarization (DNP) is the basis of ENDOR.
2. The general Overhauser effect is one case of DNP in which one has scalar coupling of $\vec{I}$ and $\vec{S}$ and in which one normally induces allowed transitions.
3. The Abragam scheme is another case of DNP in which one normally induces the forbidden transition. We indicated how this gives rise to reversed polarization.
4. Feher's model for packet shifting ENDOR was discussed and its salient features listed.

5. We developed in some detail the arguments for the LLMT model listing its salient features and pointed out the differences between this model and Feher's packet-shifting model.
6. The paucity of experimental and theoretical information on relaxation and line broadening effects in organic free-radicals in the solid state was pointed out.
7. Finally, the spin Hamiltonian for organic free-radicals was introduced and a method for finding the hyperfine tensor from the ENDOR data was described.

C. METHOD FOR OBTAINING NUCLEAR HYPERFINE AND ELECTRON g-FACTOR TENSORS

In the preceding sections it was indicated that ENDOR is intimately tied up with the conventional EMR method. It goes almost without saying that the EMR spectrum should, therefore, be rather well understood before one proceeds with an ENDOR experiment. More specifically, to calculate the ENDOR transition frequencies, one needs to know the hyperfine tensors for the interacting protons. To this end, a straightforward procedure for obtaining the nuclear hyperfine and electron g-factor tensors from the usual EMR data has been developed.

The object, then, is simply to take the measured values of the EMR splittings, $\delta = \nu_+ + \nu_-$, and from these find ν_+ and ν_- and thus $\underset{\sim}{A}$. However, since

$$\nu_{\pm} \vec{u}_{\pm} = \nu_p \vec{u}_H \mp \vec{u}_H \cdot \underset{\sim}{A}$$

one needs to square $\nu_{\pm} \vec{u}_{\pm}$ and then take the square root to get $\nu_{\pm}$. This leaves our unknowns, namely the elements of $\underset{\sim}{A}$, A_{ij}, under the radical sign. What is worse, one must take the sum of two such quantities, ν_+ and ν_-, and this makes the task of solving for the tensor elements formidable. We therefore introduce the procedure which follows.*

Step 1 Using a very crude Hamiltonian one obtains the orders of magnitude and signs of the tensor elements.

Step 2 Using an approximate Hamiltonian one improves the above elements.

---

*This procedure based on McConnell's work (36,43) is similar to a method used by Pooley (44).

Step 3 Using the "exact" Hamiltonian the final elements are calculated.

For Step 1 the following assumptions are made:

a) ν_p is negligible

b) $\vec{I} = \vec{u}_H I_H$ --i.e., the nuclear spin is quantized along the external field direction.

These are by no means valid assumptions, but they give a set of initial values for the tensor elements which will then be improved by an iterative procedure in Steps 2 and 3.

Using a) and b) the Hamiltonian equation B-26

$$\mathcal{H} = h|\nu_e|S_H - h\nu I_u$$

then becomes

$$\mathcal{H} = h|\nu_e|S_H + S_H I_H \vec{u}_H \cdot \underset{\sim}{A} \cdot \vec{u}_H \ . \qquad \text{(C-1)}$$

One can show that the splitting, $\mathcal{S}$, will be given by $\mathcal{S} = \vec{u}_H \cdot \underset{\sim}{A} \cdot \vec{u}_H$. Having chosen a rectangular coordinate system with a triple of unit vectors $\vec{i}$, $\vec{j}$, and $\vec{k}$, one can then write

$$\vec{u}_H \equiv u_1\vec{i} + u_2\vec{j} + u_3\vec{k} \qquad \text{(C-2)}$$

where the (u_i)'s are the usual direction cosines. Recall equation B-17

$$\underset{\sim}{A} = A_{11}\vec{i}\vec{i} + A_{22}\vec{j}\vec{j} + A_{33}\vec{k}\vec{k} + A_{12}(\vec{i}\vec{j} + \vec{j}\vec{i}) + A_{23}(\vec{j}\vec{k} + \vec{k}\vec{j}) + A_{13}(\vec{i}\vec{k} + \vec{k}\vec{i}). \qquad \text{(B-17)}$$

Using this equation and equation C-2 one obtains

$$\vec{u}_H \cdot \underset{\sim}{A} = (u_1A_{11}+u_2A_{12}+u_3A_{13})\vec{i} + (u_2A_{22}+u_1A_{12}+u_3A_{23})\vec{j} + (u_3A_{33}+u_2A_{23}+u_1A_{13})\vec{k}$$

$$\text{or } \vec{u}_H \cdot \underset{\sim}{A} = \sum_{i,j=1}^{3} u_i A_{ij} \vec{e}_j \qquad \text{(C-3)}$$

where

$$\vec{e}_1 = \vec{i}$$
$$\vec{e}_2 = \vec{j}$$
$$\vec{e}_3 = \vec{k} \ .$$

Therefore,

$$\vec{u}_H \cdot \underset{\sim}{A} \cdot \vec{u}_H = u_1(u_1A_{11}+u_2A_{12}+u_3A_{13})+u_2(u_1A_{12}+u_2A_{22}+u_3A_{23})+u_3(u_1A_{13}+u_2A_{23}+u_3A_{33}) \tag{C-4}$$

It is most convenient to use the splittings which one obtains when the field lies along the three orthogonal axes of the coordinate system. For these cases

$$u_H = u_i \vec{e}_i \qquad i = 1,2,3 \qquad \text{and } u_i = 1 \ .$$

For this case

$$\mathscr{S}(\vec{i}) = A_{11}$$
$$\mathscr{S}(\vec{j}) = A_{22}$$
$$\mathscr{S}(\vec{k}) = A_{33} \tag{C-5}$$

or

$$A_{ii} = \mathscr{S}(\vec{e}_i).$$

which give rather approximate diagonal elements.

For the off diagonal elements one proceeds as follows. The splittings, $\mathscr{S}$, are usually measured at least every 10° in the three mutually perpendicular planes formed by the triple $(\vec{i}\vec{j}\vec{k})$. For those measurements one writes

$$\vec{u}_H = u_i \vec{e}_i + u_j \vec{e}_j$$

$$\begin{pmatrix} i \\ j \end{pmatrix} = 1,2,3 \qquad i \neq j \tag{C-6}$$

Then

$$\vec{u}_H \cdot \underset{\sim}{A} \cdot \vec{u}_H = \tfrac{1}{2}(A_{jj} + A_{ii}) - \tfrac{1}{2}(A_{jj} - A_{ii})\cos 2\theta + A_{ij}\sin 2\theta$$

$$\not{\phi} = \tfrac{1}{2}(A_{ii} + A_{jj}) + \left[\tfrac{1}{4}(A_{ii} - A_{jj})^2 + A_{ij}^2\right]^{\frac{1}{2}} \sin 2(\theta + \phi). \qquad \text{(C-7)}$$

where θ is the angle measured from $\vec{e}_i$ to $\vec{u}_H$ (not from $\vec{e}_j$ to $\vec{u}_H$).

Equation C-7 is obtained by using the identity

$$A\sin\xi + B\cos\xi \equiv (A^2 + B^2)^{\frac{1}{2}} \sin(\xi + \varphi).$$

This identity clearly holds on the condition that

$$\cos\varphi = A(A^2 + B^2)^{-\frac{1}{2}}$$

$$\sin\varphi = B(A^2 + B^2)^{-\frac{1}{2}} .$$

From equation C-7 and the conditions on the values for $\cos 2\phi$ and $\sin 2\phi$ one finds

$$A_{ij} = \frac{A_{ii} - A_{jj}}{2 \tan 2\phi} . \qquad \text{(C-8)}$$

The values of A_{ii} and A_{jj} have already been found. The angle ϕ is found by matching curves of the form $R + P \sin 2(\theta + \phi)$ versus θ against the plot of $\not{\phi}$ (or $\not{\phi}^2$) versus θ. (Since ϕ is just a phase-angle it is easier to measure it when compared with the plot of $\not{\phi}^2$ versus θ). The result of these calculations gives crude values for the elements A_{ij}. It will be shown in Section D that simpler methods can sometimes be used to find at least one of the off-diagonal elements. Using the values obtained from equations C-5 and C-8 we proceed to Step 2.

For Step 2 the only approximation made is that the term in ν_p is negligible. Equations B-24 and B-26 then give

$$\vec{\nu u} = -S_H \vec{u}_H \cdot \underset{\sim}{A} \; . \tag{C-9}$$

As before $\not{\nu} = \nu_+ + \nu_-$ and since

$$\not{\nu}^2 = \nu_-^2 + 2\nu_-\nu_+ + \nu_+^2 = \frac{1}{4}(\vec{u}_H \cdot \underset{\sim}{A})^2 + \frac{1}{2}(\vec{u}_H \cdot \underset{\sim}{A})^2 + \frac{1}{4}(\vec{u}_H \cdot \underset{\sim}{A})^2$$

$$\not{\nu}^2 = \vec{u}_H \cdot \underset{\sim}{A}^2 \cdot \vec{u}_H \; . \tag{C-10}$$

Writing out the general case in component form one has (writing it in a particularly convenient form)

$$\not{\nu}^2 = \sum_{i,j} u_i^2 A_{ij}^2 + 2 \sum_{i<j} \left[u_i u_j \, A_{ij}(A_{ii} + A_{jj}) + \sum_k A_{ik} A_{jk} \Delta_{ik} \Delta_{jk} \right] \tag{C-11}$$

where

$$\left\{ \begin{matrix} i \\ j \\ k \end{matrix} \right\} = 1,2,3$$

and

$$\Delta_{mn} \equiv \left\{ \begin{matrix} 0 \text{ when } m = n \\ \\ 1 \text{ when } m \neq n \end{matrix} \right\} .$$

The second term on the right includes only cross-terms $u_i u_j$. Therefore, measuring splittings along the coordinate axes gives (since then $u_i = 1$)

$$A_{ii}^2 = \not{\nu}^2(\vec{e}_i) - A_{ij}^2 - A_{ik}^2$$

$$i = 1,2,3 \tag{C-12}$$

$$i \neq j \neq k \; .$$

Using A_{ij} and A_{ik} calculated from equation C-8, A_{ii} can be found immediately.

For the off-diagonal elements it is least cumbersome algebraically if one measures the other three splittings in those directions which have direction cosines $\left(\frac{1}{\sqrt{2}}\ \frac{1}{\sqrt{2}}\ 0\right)$, $\left(\frac{1}{\sqrt{2}}\ 0\ \frac{1}{\sqrt{2}}\right)$, and $\left(0\ \frac{1}{\sqrt{2}}\ \frac{1}{\sqrt{2}}\right)$. In other words, one of the field vectors for these intermediate directions would be

$$\vec{u}_H = \frac{1}{\sqrt{2}}\vec{i} + \frac{1}{\sqrt{2}}\vec{j} \qquad \text{(C-13)}$$

or in general

$$\vec{u}_H = u_i\vec{e}_i + u_j\vec{e}_j$$

where

$$u_i = u_j = \frac{1}{\sqrt{2}}$$

$$\left\{\begin{matrix} i \\ j \\ k \end{matrix}\right\} = 1,2,3 \ .$$

Using equations C-11 and C-13 one then obtains

$$\mathcal{S}^2(\vec{e}_i\vec{e}_j) = \tfrac{1}{2}\ (\vec{e}_i + \vec{e}_j)\cdot\underset{\sim}{A^2}\cdot(\vec{e}_i + \vec{e}_j)$$

$$= \tfrac{1}{2}\ (A_{ii}^2 + A_{jj}^2) + A_{ij}^2 + \tfrac{1}{2}\ (A_{ik}^2 + A_{jk}^2) + A_{ij}(A_{ii}+A_{jj})$$

$$+ A_{ik}A_{jk} \ .$$

Completing the square with respect to A_{ij} gives

$$\mathcal{S}^2(\vec{e}_i\vec{e}_j) = \left[A_{ij} + \frac{A_{ii}+A_{jj}}{2}\right]^2 - \left(\frac{A_{ii}+A_{jj}}{2}\right)^2 + \frac{A_{ii}^2+A_{jj}^2}{2} + \frac{A_{ik}^2+A_{jk}^2}{2} + A_{ik}A_{jk} \ .$$

Solving for A_{ij} gives

$$A_{ij} = \left[\mathcal{S}^2(\vec{e}_i\vec{e}_j) - \tfrac{1}{2}(A_{ii}^2+A_{jj}^2) - A_{ik}A_{jk} - \tfrac{1}{2}(A_{ik}^2+A_{jk}^2) + \left(\frac{A_{ii}+A_{jj}}{2}\right)^2\right]^{\frac{1}{2}} - \frac{A_{ii}+A_{jj}}{2} \ . \qquad \text{(C-14)}$$

$$\left\{ \begin{matrix} i \\ j \\ k \end{matrix} \right\} = 1,2,3 \qquad i \neq j \neq k \ .$$

In calculating the diagonal elements in Step 2 off-diagonal elements from Step 1 were used. After new off-diagonal elements are found in Step 2 using equation C-14 one can go back and calculate new diagonal elements using equation C-12. This iterative procedure is continued until the values for the tensor elements stabilize. We take the values thus obtained and proceed to Step 3. (The tensors obtained to this point may be sufficiently accurate for many purposes. Compare the tensors obtained by various steps in Section D. However, for prediction of ENDOR frequencies one wants the most accurate values obtainable.)

For Step 3 the "exact" Hamiltonian is used. The problem is to get $\mathcal{S} = \nu_+ + \nu_-$ in a form useful for calculations. Starting again from

$$\nu_{\mp} \vec{u}_{\mp} = \nu_p \vec{u}_H \pm \tfrac{1}{2} \vec{u}_H \cdot \underset{\sim}{A}$$

it is straightforward to show that

$$4(\nu_{\mp})^2 = \sum_{i=1}^{3} (2\nu_p \pm A_{ii})^2 u_i^2 \pm 2 \sum_{i=1}^{3} \sum_{j=1}^{3} (2\nu_p \pm A_{ii}) A_{ij} u_i u_j \Delta_{ij}$$

$$+ \sum_{i=1}^{3} \sum_{j=1}^{3} \sum_{k=1}^{3} A_{ik} A_{jk} u_i u_j \Delta_{ik} \Delta_{jk} . \qquad \text{(C-15)}$$

Where

$$\Delta_{mn} \equiv \left\{ \begin{matrix} 0 \text{ when } m = n \\ \\ 1 \text{ when } m \neq n \end{matrix} \right\} .$$

A little thought quickly reveals that to find $(\nu_+ + \nu_-)$ for the general case could be almost impossible. It is therefore advisable to choose special cases immediately. In fact, as was done in Step 2, one considers first the diagonal elements which will be related to measurements along the $(\vec{e}_i)$'s and then one finds the off-diagonal elements which will be related to measurements along the intermediate directions.

Choosing $\vec{u}_H = u_i\vec{e}_i = \vec{e}_i$ one can immediately write

$$4\,\nu_{\mp}(e_i)^2 = \left(2\nu_p \pm A_{ii}\right)^2 + A_{ij}^2 + A_{ik}^2$$

$$i = 1,2,3 \quad ; \quad i \neq j \neq k$$

$$\mathcal{S}^2(\vec{e}_i) = \left[\nu_+(\vec{e}_i)+\nu_-(\vec{e}_i)\right]^2 = \tfrac{1}{2}(A_{ii}^2+A_{ij}^2+A_{ik}^2+4\nu_p^2) + 2\nu_-(\vec{e}_i)\nu_+(\vec{e}_i)\ . \qquad (C\text{-}16)$$

By appropriate grouping and factoring and writing $\nu_{\mp}(\vec{e}_i) = \nu_{\mp}$ it can be shown that

$$\nu_-\nu_+ = \frac{1}{4}\left\{A_{ii}^2 + A_{ij}^2 + A_{ik}^2 + 4\nu_p^2\right\}\left\{1 - \left[\frac{4\nu_p A_{ii}}{A_{ii}^2 + A_{ij}^2 + A_{ik}^2 + 4\nu_p^2}\right]^2\right\}^{\frac{1}{2}}. \qquad (C\text{-}17)$$

In order to expand the term under the square root sign one must show that the term in the square brackets, which shall be denoted by f_{ii}, lies in the range $-1 \leq f_{ii} \leq +1$ which is equivalent to $0 \leq f_{ii}^2 \leq 1$. By completing the square in the denominator the term can be written

$$f_{ii}^2 = \left[\frac{4\nu_p A_{ii}}{A_{ij}^2 + A_{ik}^2 + (A_{ii} - 2\nu_p)^2 + 4\nu_p A_{ii}}\right]^2 .$$

Therefore expanding the factor under the square root sign gives

$$(1 - f_{ii}^2)^{\frac{1}{2}} = 1 - \frac{1}{2} f_{ii}^2 - \frac{1}{8} f_{ii}^4 - \frac{1}{16} f_{ii}^6 \cdots$$

Substituting this back into equation C-17 gives

$$2\nu_-\nu_+ = \frac{1}{2}\frac{4\nu_p A_{ii}}{f_{ii}}\left(1 - \frac{1}{2}f_{ii}^2 - \frac{1}{8}f_{ii}^4 - \frac{1}{16}f_{ii}^6 - \cdots\right)$$

$$2\nu_-\nu_+ = \frac{1}{2}\left(A_{ii}^2 + A_{ij}^2 + A_{ik}^2 + 4\nu_p^2\right) - 4\nu_p A_{ii}\left(\frac{f_{ii}}{4} + \frac{f_{ii}^3}{16} + \frac{f_{ii}^5}{32} + \cdots\right) \quad \text{(C-18)}$$

If one defines

$$F_{ii} \equiv \frac{f_{ii}}{4} + \frac{f_{ii}^3}{16} + \frac{f_{ii}^5}{32} + \cdots \quad \text{(C-19)}$$

then combining equations C-16, C-18, and C-19 one obtains

$$\mathcal{J}^2 = A_{ii}^2 + A_{ij}^2 + A_{ik}^2 + 4\nu_p^2 - 4\nu_p A_{ii} F_{ii} .$$

Completing the square with respect to A_{ii} and solving for A_{ii} one finally gets

$$A_{ii} = \left[\mathcal{J}^2(\vec{e}_i) - (4\nu_p^2 + A_{ij}^2 + A_{ik}^2) + (2\nu_p F_{ii})^2\right]^{\frac{1}{2}} + 2\nu_p F_{ii}. \quad \text{(C-20)}$$

Now we wish to obtain expressions for the off-diagonal elements. One chooses $\vec{u}_H$ as in equation C-13 and derives expressions for A_{ij} in a manner similar to that employed in solving for A_{ii} in Step 3. The main problem again arises with the cross terms. One finds that

$$\nu_{\mp} = \frac{1}{8}\left[2\left[A_{ij} \pm \tfrac{1}{2}(4\nu_p \pm A_{ii} \pm A_{jj})\right]^2 + \tfrac{1}{2}(A_{ii} - A_{jj})^2 + (A_{ik} + A_{jk})^2\right]^{\frac{1}{2}} . \quad \text{(C-21)}$$

Defining

$$a \equiv a_{ij} \equiv A_{ij} + \tfrac{1}{2}(A_{ii} + A_{jj})$$

$$b \equiv 2\nu_p$$

and

$$c \equiv c_{ij} \equiv \tfrac{1}{2}(A_{ii} - A_{jj})^2 + (A_{jk} + A_{ik})^2$$

one obtains after some considerable algebraic manipulation

$$2\nu_-\nu_+ = \tfrac{1}{2}(a^2-b^2)\left\{1 + \left[\frac{[c + 2(a^2+b^2)]\left[1 - \dfrac{2(a^2+b^2)}{c + 2(a^2+b^2)}\right]}{4(a^2-b^2)^2}\right]^2\right\}^{\frac{1}{2}} . \qquad \text{(C-22)}$$

Defining $$G_{ij}^2 \equiv 1 + \left\{\frac{[c + 2(a^2+b^2)]\left[1 - \dfrac{2(a^2+b^2)}{c + 2(a^2+b^2)}\right]}{4(a^2-b^2)^2}\right\}^2 .$$

equation C-22 can then be written as

$$2\nu_-\nu_+ = \tfrac{1}{2}\, a^2\, G_{ij} - \tfrac{1}{2}\, b^2\, G_{ij} . \qquad \text{(C-23)}$$

The off-diagonal element of interest, A_{ij}, appears only in a_{ij}. So in writing $2\nu_-\nu_+$ we have obtained A_{ij} explicitly---except that A_{ij} also appears in G_{ij}. However, G_{ij} is fairly insensitive to variations in A_{ij}. Furthermore, one uses the value of A_{ij} obtained in Step 2 to find G_{ij} and again employs an iterative procedure to improve all the tensor elements. Using $\mathcal{S}^2 = \nu_-^2 + 2\nu_-\nu_+ + \nu_+^2$ and equations C-21 and C-23 and regrouping terms one can solve for A_{ij} to get

$$A_{ij} = \left[\frac{2\mathcal{S}^2(\vec{e}_i\vec{e}_j) - 2\nu_p^2\,(1-G_{ij}) - \frac{1}{4}\,(A_{ii}-A_{jj})^2 - \frac{1}{2}\,(A_{ik}+A_{jk})^2}{1 + G_{ij}}\right]^{\frac{1}{2}} - \tfrac{1}{2}(A_{ii}+A_{jj}) . \qquad \text{(C-24)}$$

This completes the procedure for calculating hyperfine tensors. For the sake of convenience we shall summarize the equations obtained in the three steps. In all cases

$$\begin{matrix} i \\ j \\ k \end{matrix} = 1,2,3 \qquad i \neq j \neq k .$$

For Step 1

$$A_{ii} = \mathcal{A}(\vec{e}_i) \tag{C-5}$$

$$A_{ij} = (A_{ii}-A_{jj})/2\tan 2\phi \ . \tag{C-8}$$

For Step 2

$$A_{ii} = \left[\mathcal{A}^2(\vec{e}_i) - A_{ij}^2 - A_{ik}^2\right]^{\frac{1}{2}} \tag{C-12}$$

$$A_{ij} = \left[\mathcal{A}^2(\vec{e}_i\vec{e}_j) - \tfrac{1}{2}(A_{ii}^2+A_{jj}^2) - A_{ik}A_{jk} - \tfrac{1}{2}(A_{ik}^2+A_{jk}^2) + \left(\frac{A_{ii}+A_{jj}}{2}\right)^2\right]^{\frac{1}{2}} - \frac{A_{ii}+A_{jj}}{2} \ . \tag{C-14}$$

For Step 3

$$A_{ii} = \left[\mathcal{A}^2(\vec{e}_i\vec{e}_j) - (4\nu_p^2+A_{ij}^2+A_{ik}^2) + (2\nu_p F_{ii})^2\right]^{\frac{1}{2}} + 2\nu_p F_{ii} \tag{C-20}$$

$$A_{ij} = \left[\frac{2\mathcal{A}^2(\vec{e}_i\vec{e}_j)-(2\nu_p)^2(1-G_{ij})-\frac{1}{4}(A_{ii}-A_{jj})^2 - \frac{1}{2}(A_{ik}+A_{jk})^2}{1+G_{ij}}\right]^{\frac{1}{2}} - \tfrac{1}{2}(A_{ii}+A_{jj}). \tag{C-24}$$

The hyperfine tensor thus obtained can be diagonalized and in turn the eigenvectors and the appropriate similarity transformation (45) can be found. This gives the direction cosines of the principal axes of the tensor in terms of the arbitrarily chosen triple $(\vec{i}\vec{j}\vec{k})$. To obtain the g-factor tensor one can see by looking at the terms of interest in the Hamiltonian that $\vec{S}\cdot\underset{\sim}{g}\cdot\vec{H}_o$ can be written $H_o S_H \vec{u}_H \cdot \underset{\sim}{g}\cdot\vec{u}_H$ and that the form of this expression is identical to that used in Step 1 for deriving the hyperfine tensor. So the equations and methods used there can be applied directly in order to find the g-factor tensor. For convenience we shall summarize the equations explicitly in terms of the (g_{ij})'s. We define the measured g-value for the $\vec{e}_i$ directions as $\mathcal{G}(\vec{e}_i)$.

Then one can write

$$g_{ii} = \mathcal{G}(\vec{e}_i) \tag{C-25}$$

$$g_{ij} = \frac{g_{ii} - g_{jj}}{2\tan 2\phi} \tag{C-26}$$

Here again ϕ is a phase angle and can be obtained from a comparison of plots of the form

$$R + P \sin(\theta+\phi) \text{ versus } \theta \text{ against a plot of } \mathcal{G}(\theta) \text{ versus } \theta \ .$$

We shall now proceed to Section D where the procedures described in this section will be employed to calculate the hyperfine and g-factor tensors in glutaric acid.

D. CALCULATION OF HYPERFINE TENSORS IN IRRADIATED GLUTARIC ACID

The EMR of the radicals formed in single crystals of glutaric acid had been investigated by Horsfield, Morton and Whiffen (46) (hereafter referred to as HMW). Their stated purpose was that of measuring the hyperfine interactions due to the γ-protons (see structure of radical below). This was of basic importance in the development of the theory of electron-nuclear interactions in solid state free-radicals. However, their preliminary studies revealed the presence of two non-identical radicals. It had been shown that annealing sometimes destroys one radical preferentially but their efforts in this direction failed. They therefore proceeded with their interpretation (of the composite system) assuming that the two radicals were distortion isomers of the form (A,B)

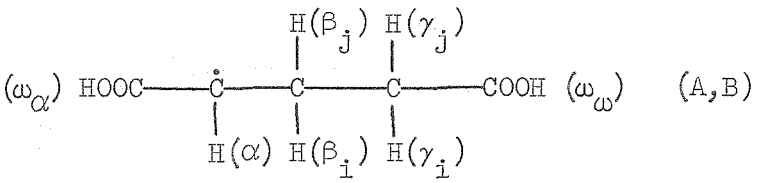

(A,B)

By distortion isomers we mean radicals having non-identical electronic structure but arising from identical physical structures by distortions. They designated the two radicals by A and B, where A refers to the radical having the larger isotropic contribution to the hyperfine interaction. They calculated the hyperfine tensors for the α-proton for both the A and B radicals. However, because the superposition of the spectra due to radicals A and B causes poor resolution for many orientations they did not calculate the β-proton tensors but only listed their general characteristics. Furthermore, this same problem permitted them to place only an upper limit of about 10 Mc on the γ-proton interaction. As was

seen in Sections A and B the ENDOR technique is well suited for determining the magnitude of such an interaction. However, the complexity of the glutaric acid spectrum promoted the search for a simpler system to which one could apply the ENDOR technique and still obtain information on the γ-proton coupling constant.

At about this time certain investigations (47) in these laboratories indicated that u.v.-irradiation of x-irradiated crystals gave results similar to those obtained by annealing. Consequently, a single crystal of glutaric acid was x-irradiated and the EMR spectrum taken before and after u.v.-treatment. There was a marked change. It appeared as though the signal intensity due to one radical had been considerably reduced while that of the other seemed neither to have increased nor decreased. In Figure 4 and Figure 4 (overlay) we show two spectra illustrating this rather nice change.

Subsequently accurate measurements were made, in three mutually perpendicular planes, of the splittings for the remaining radical. Figure 5 and Figure 5 (overlay) are plots of $\delta^2(\theta)$ versus θ for the α-proton for rotations in one of these planes (xz). Figure 5 represents the data of HMW whereas Figure 5 (overlay) refers to our data. It is quite apparent (since similar results also obtained for the two β-protons) that the radical which remained after u.v.-treatment is, within the limits of accuracy of our measurements, identical to radical A of HMW. However, concerning the γ-proton interaction, we were only able to reduce the upper limit from 10 Mc to 5 Mc. Nevertheless, the resultant simplified spectrum of the glutaric acid radical (A) now made this system useable for the application of the ENDOR technique.

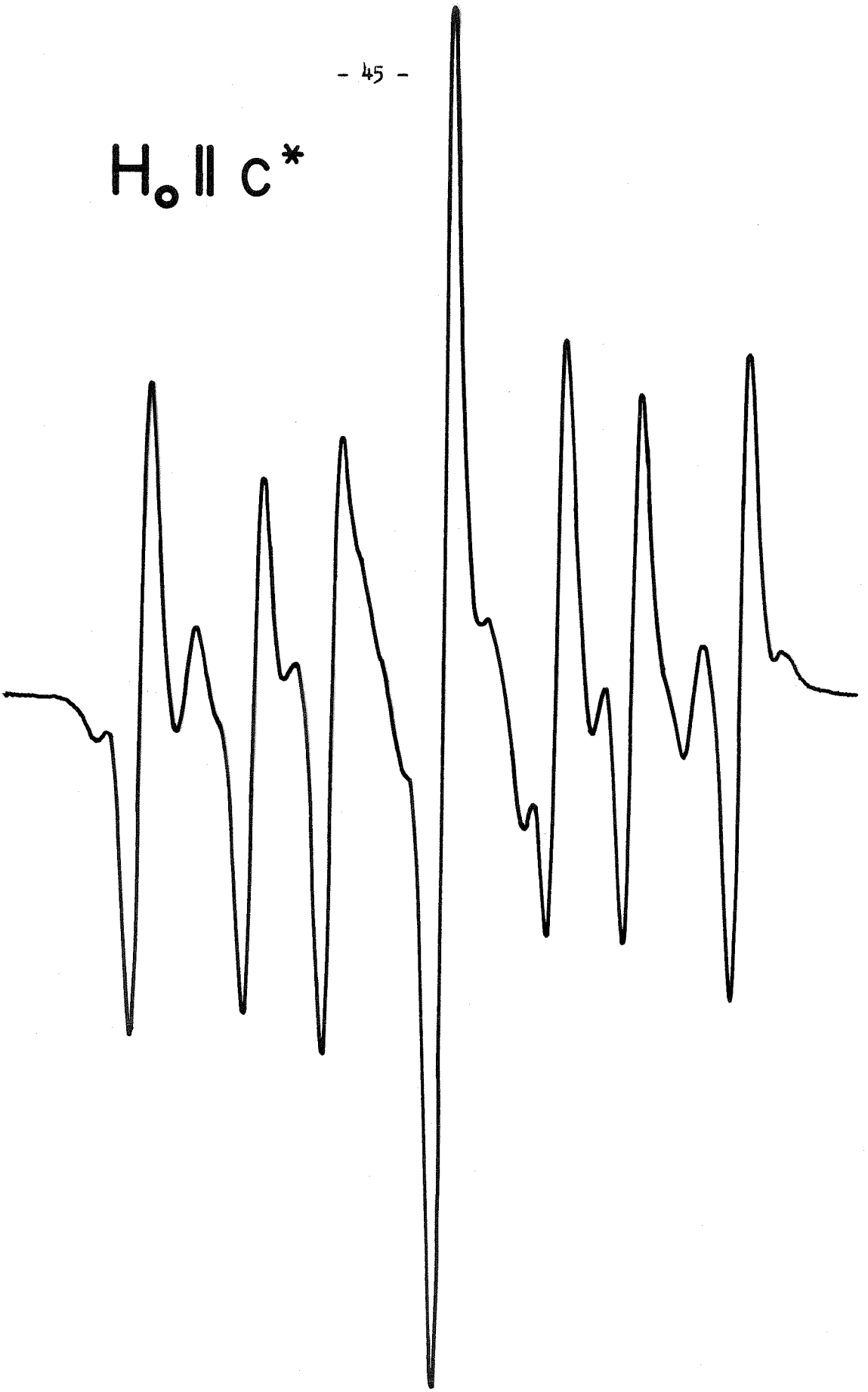

Figure 4 (Overlay) EMR spectrum of x- and uv-irradiated single crystal of glutaric acid

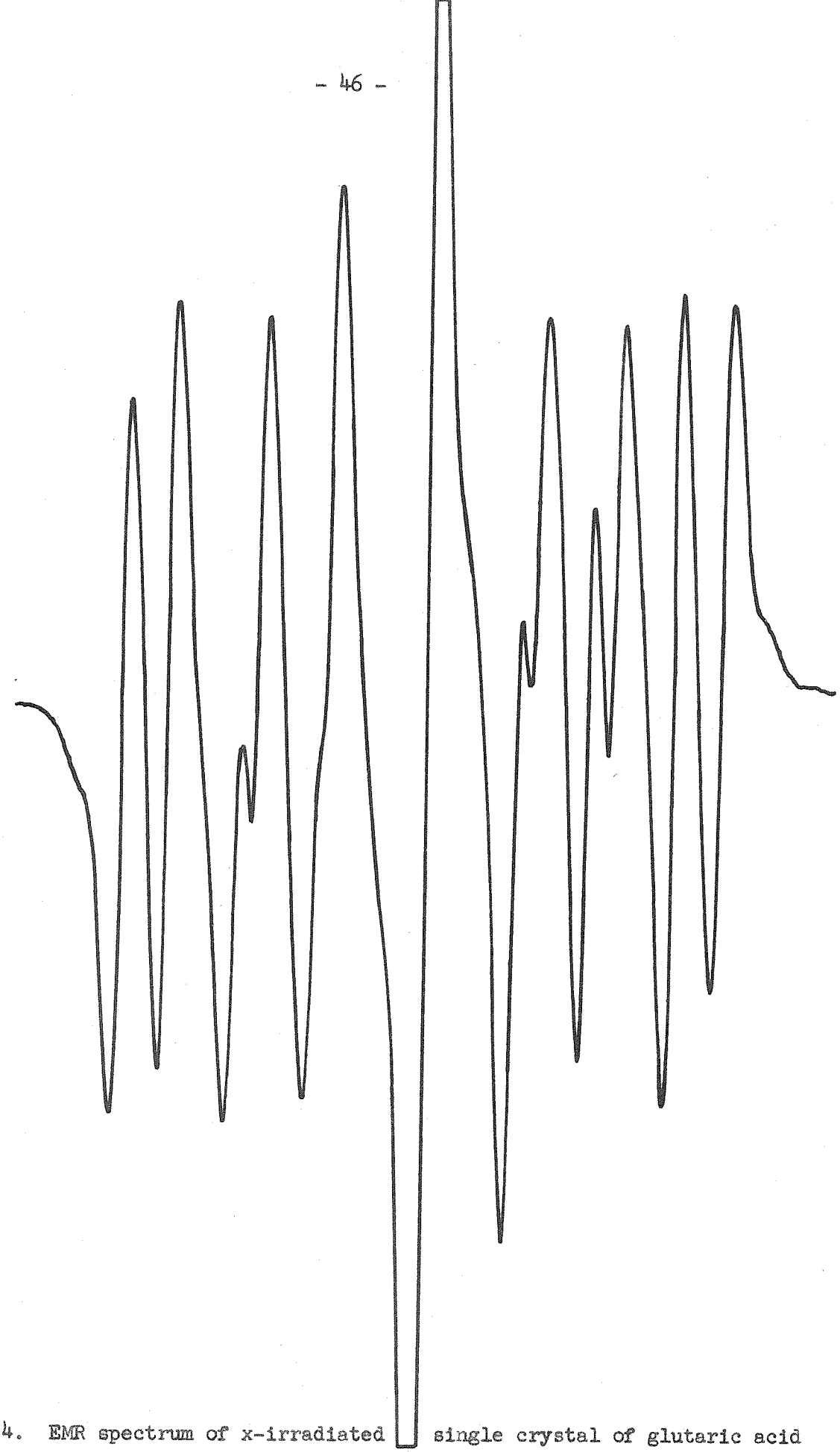

Figure 4. EMR spectrum of x-irradiated single crystal of glutaric acid

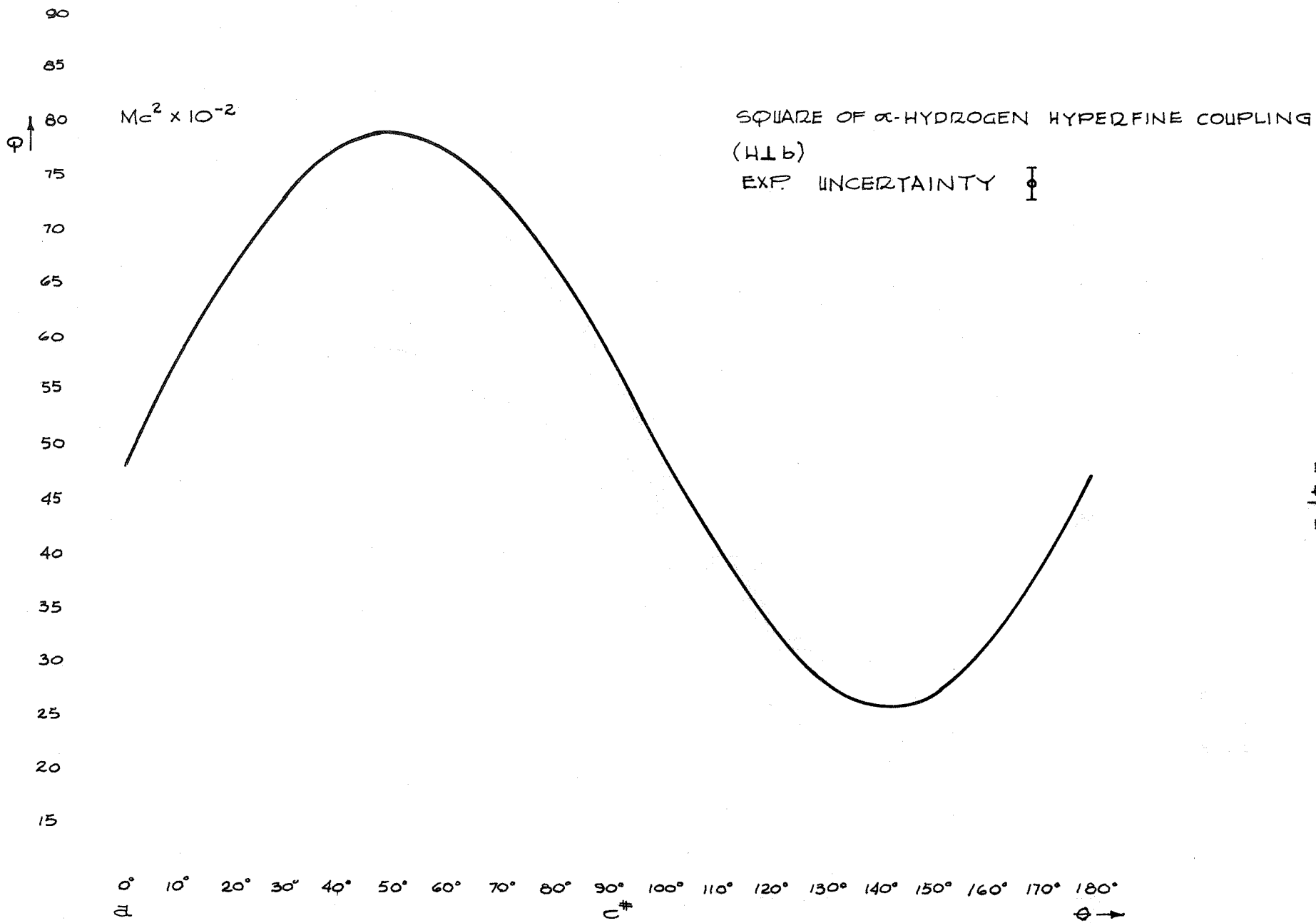

Figure 5 (Overlay) Glutaric acid data

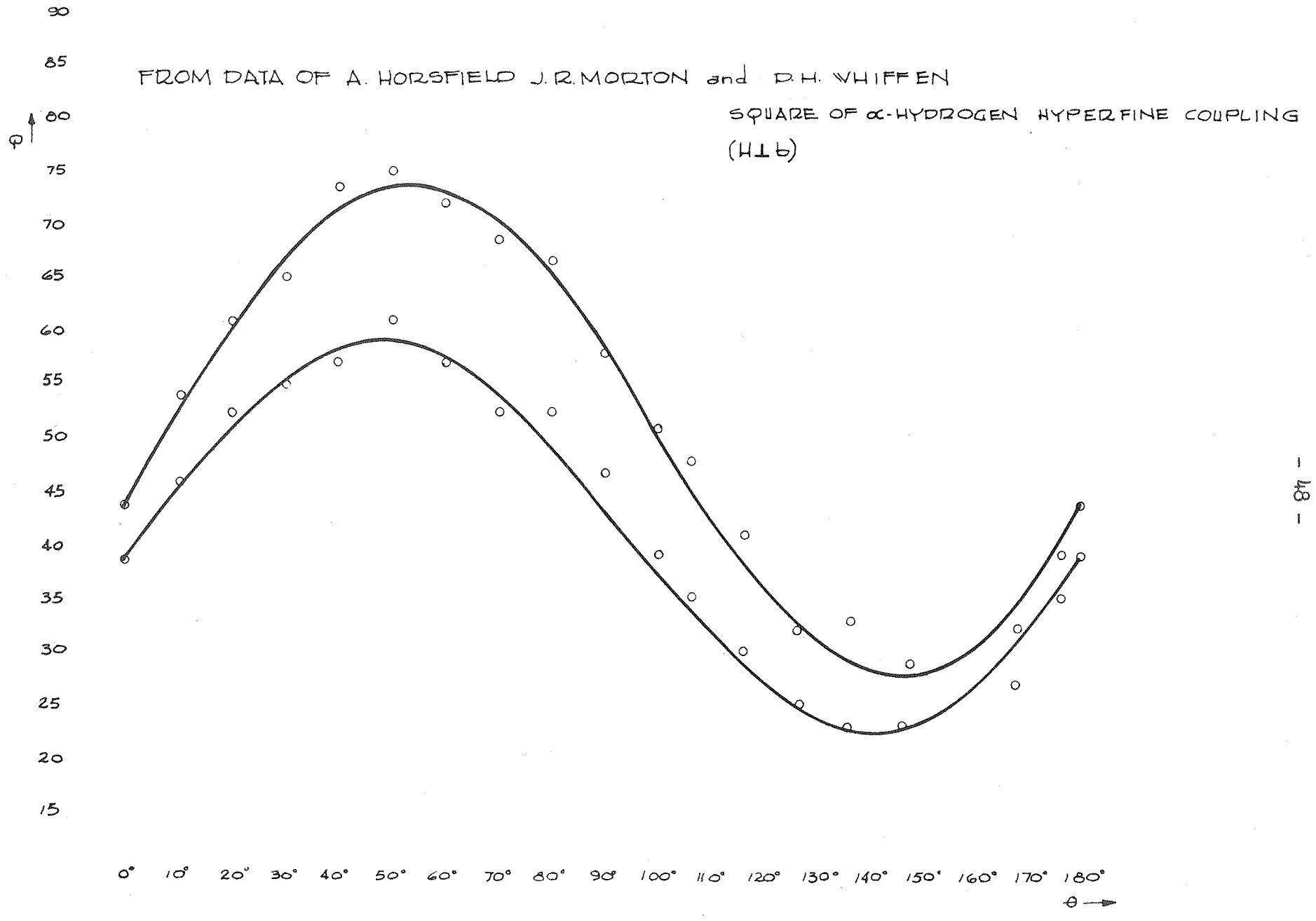

Figure 5. Glutaric acid data

In this section then, we discuss some general principles involved in obtaining EMR data from single crystals and then, using our data for radical A we calculate the hyperfine and g-factor tensors employing the methods outlined in Section C. Toward the end of the section the nature of the A and B radicals are discussed.

Single crystals of glutaric acid were grown. Large well-formed crystals simply fell out of water solution the first time, and since then I have been unable to repeat this feat. The crystals were placed about two inches in front of a General Electric model CA-7 x-ray tube and irradiated for about four hours (at 30 ma) at 45 KV. They were then exposed to u.v.-irradiation from an 85 watt General Electric Mercury Lamp model number H85A3/UV from which the glass envelope had been removed. The crystal was placed approximately at the focal point of a quartz lens (f = 10 cm). The spectra were observed using a standard x-band EMR spectrometer as described in Section F.

Before taking spectra useful for hyperfine tensor calculations one must decide on a relationship between the coordinate system used in the calculation of the hyperfine tensor, and the crystal morphology. In particular, the coordinate system should be chosen so that two conditions are satisfied:

1. the number of spectrally different radicals is a minimum for measurements made along the coordinate axes and in associated planes;

and 2. the coordinate system is simply related to the external features of the crystal. (This is important only because it makes the mechanics of crystal mounting and orientation easier.)

When these two requirements are incompatible, one must decide on the basis of the particular system, which one should be given priority. Consider the problem for glutaric acid.

Glutaric acid crystallizes in the monoclinic space group C_{2h}^{6} (I2/a) with four molecules per unit cell (48). Pairs of these molecules are related by a center of inversion and are therefore spectrally equivalent for any arbitrary $\vec{H}_o$. As a result one needs to consider only the two molecules in the unit cell which are always differently oriented with respect to any arbitrary $\vec{H}_o$. However, their orientations are related by the symmetry operations of the space group. In particular, for monoclinic systems these two molecules are related by a two-fold screw axis which, for EMR purposes, is equivalent to a two-fold rotation axis. This axis is normally designated the $\vec{b}$ axis.

In general, one assumes (as far as EMR spectra are concerned), that the radicals produced in these crystals still exhibit the symmetry of the parent space group. This is usually found to be true to within experimental accuracy. Consequently, if the tensor for one radical in the unit cell is known, the tensor for the other(s) can be obtained by the appropriate transformation.

In particular, in the case of monoclinic systems it was stated that the two spectrally different radicals in the unit cell are related by a

rotation of π about the $\vec{b}$ axis. Later, we shall choose the y axis to be coincident with the $\vec{b}$ axis; so we now consider the general rotation matrix (49) for a rotation by π about the y axis.

$$R_{y(\phi)} = \begin{pmatrix} \cos\phi & 0 & \sin\phi \\ 0 & 1 & 0 \\ -\sin\phi & 0 & \cos\phi \end{pmatrix} \qquad \text{(D-1)}$$

$$\text{and } R_{y(\pi)} = \begin{pmatrix} -1 & 0 & 0 \\ 0 & 1 & 0 \\ 0 & 0 & -1 \end{pmatrix}. \qquad \text{(D-2)}$$

If the tensor for one of the radicals is

$$\underset{\sim}{A} = \begin{pmatrix} A_{11} & A_{12} & A_{13} \\ A_{12} & A_{22} & A_{23} \\ A_{13} & A_{23} & A_{33} \end{pmatrix}, \qquad \text{(D-3)}$$

then the tensor, $\underset{\sim}{A}'$, for the other radical, obtained by the usual techniques, is $\underset{\sim}{A}' = R\,\underset{\sim}{A}\,R^{-1}$.

$$\underset{\sim}{A}' = \begin{pmatrix} A_{11} & -A_{12} & A_{13} \\ -A_{12} & A_{22} & -A_{23} \\ A_{13} & -A_{23} & A_{33} \end{pmatrix}. \qquad \text{(D-4)}$$

Note that the only difference between $\underset{\sim}{A}$ and $\underset{\sim}{A}'$ is in the signs of the elements A_{12} and A_{23}.

Probably the most important feature of monoclinic symmetry is the spectral equivalence of all identical radicals when $\vec{H}_o$ is perpendicular or parallel to the symmetry axis. One way in which this can be seen is the following.

Consider the magnetic field fixed in some arbitrary orientation relative to one of the molecules in the unit cell. See Figure 6a. (Clearly no matter what we do to the orientation of the molecule the relative orientation of the magnetic field remains the same.) Now if one performs a rotation by π about $\vec{b}$ one obtains, in keeping with the properties of the monoclinic space group, the orientation of the other radical in the unit cell. See Figure 6b. There is no useful relationship between $\vec{H}_o$ before and after the rotation, except when $\vec{H}_o$ is perpendicular to the two-fold axis. In that case the direction of $\vec{H}_o$ after rotation is in exactly the opposite direction from that obtaining before rotation. See Figures 6c,d. The sign of $\vec{H}_o$ makes no difference in the spectra. Therefore the radicals are spectrally equivalent when $\vec{H}_o \cdot \vec{b} = 0$. (The one other case when the radicals are spectrally equivalent is clearly seen to occur for $\vec{H}_o \| \vec{b}$. See Figures 6e,f.)

In order to capitalize on this fact, we will choose one of the coordinate axes, y, to be coincident with the crystallographic $\vec{b}$ axis. Condition 1 is now satisfied (as far as is possible).

In order to satisfy condition 2 one has to look at the crystal morphology. Glutaric acid crystals obtained from water or alcohol solution usually grow in the form of thick tablets on (001). The faces forming the edges of these tablets are seldom well defined. However, (101) is a good cleavage plane and as a result one can unambiguously decide on the directions of $\vec{a}$, $\vec{b}$, and $\vec{c}$ relative to the morphology. To satisfy condition 2 then, we choose the x axis to be coincident with $\vec{a}$ and this fixes z which lies along $\vec{c}^*$. The latter is defined as the direction perpendicular to $\vec{b}$ and $\vec{a}$ and lying between $\vec{a}$ and $\vec{c}$. Spectra can now be taken in the xy, yz, and xz planes.

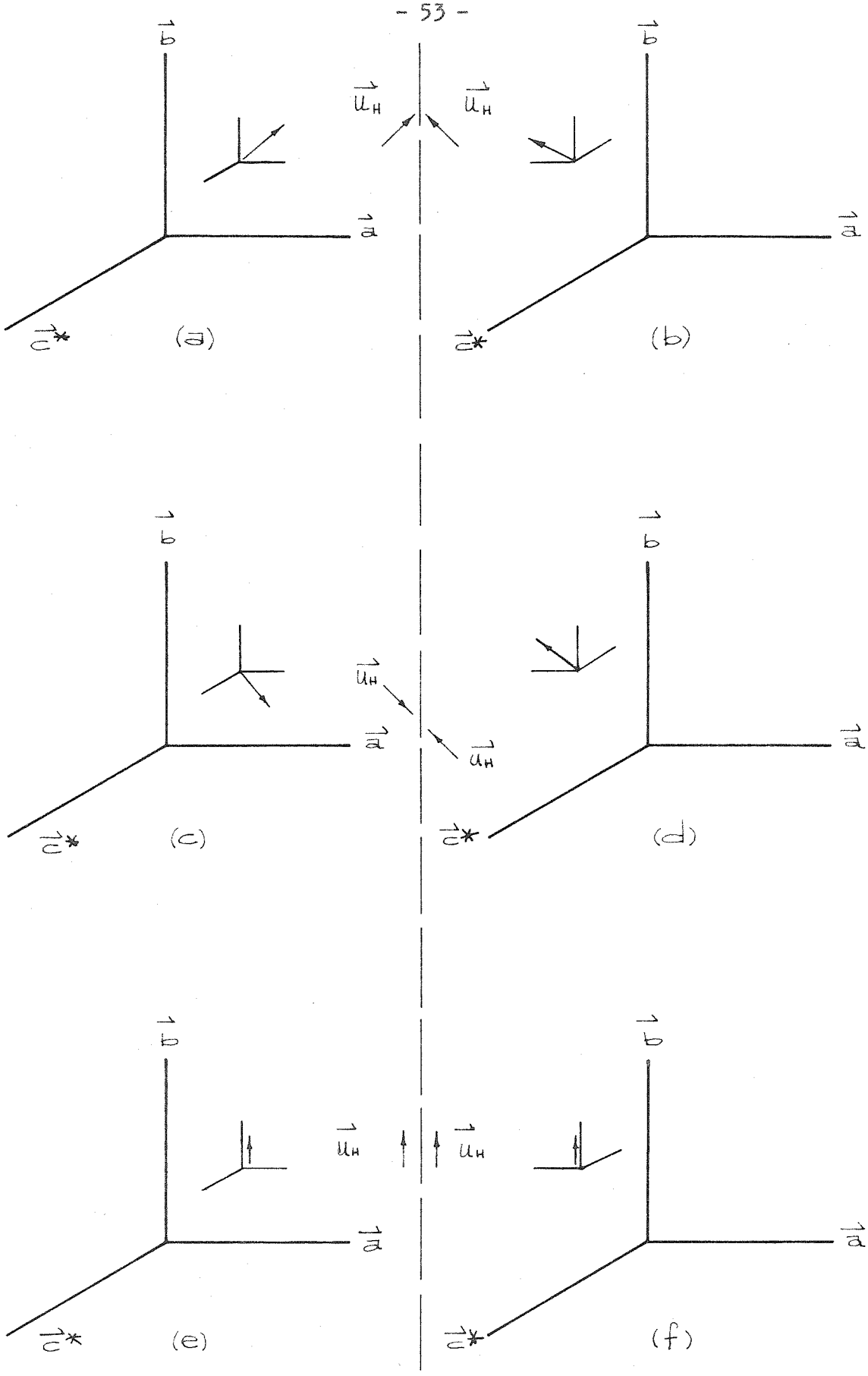

Figure 6

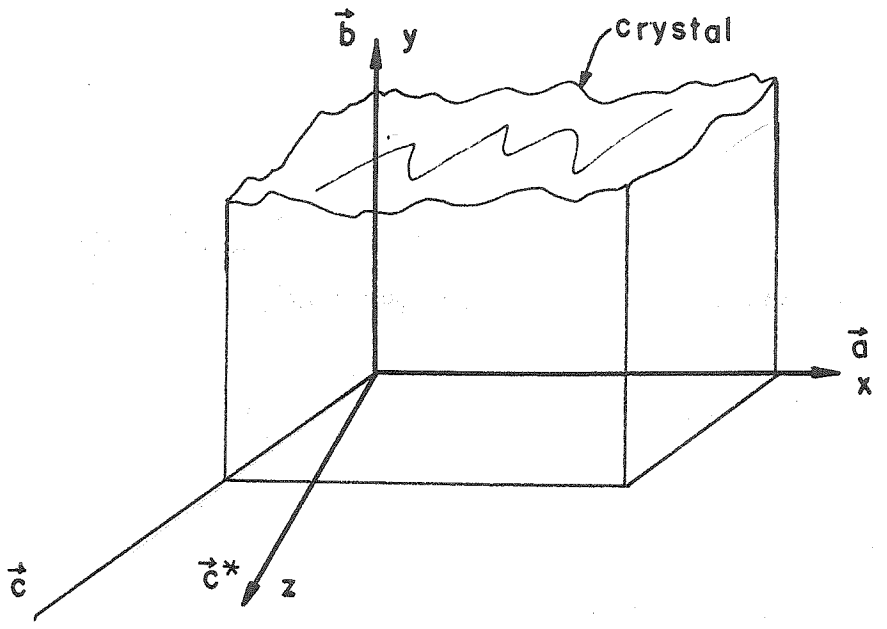

Spectra were taken every 5° in the xz plane ($\perp\vec{b}$) and every 10° in the xy and yz planes. Typical spectra for $\vec{H}_o \perp \vec{b}$ (xz plane) and for $\vec{H}_o$ not $\perp\vec{b}$ are shown in Figure 7. For the former case (Fig. 7a) (xz plane) splittings can be measured directly and rather accurately. For the latter case (Fig. 7b) one has the superposition of the spectra from two differently oriented but identical radicals and the measurement of the splittings becomes much more difficult and less accurate. We now proceed directly to the calculation of the hyperfine tensors.

As outlined in Section C one begins with Step 1. From equation C-5 we have

$$A_{ii} = \mathcal{A}(\vec{e}_i)$$

Actually, by looking at equation C-20 (or C-12) one can see that A_{ii} will be somewhat smaller than $\mathcal{A}(\vec{e}_i)$ so anticipating this one chooses a slightly smaller value for A_{ii} to begin with.

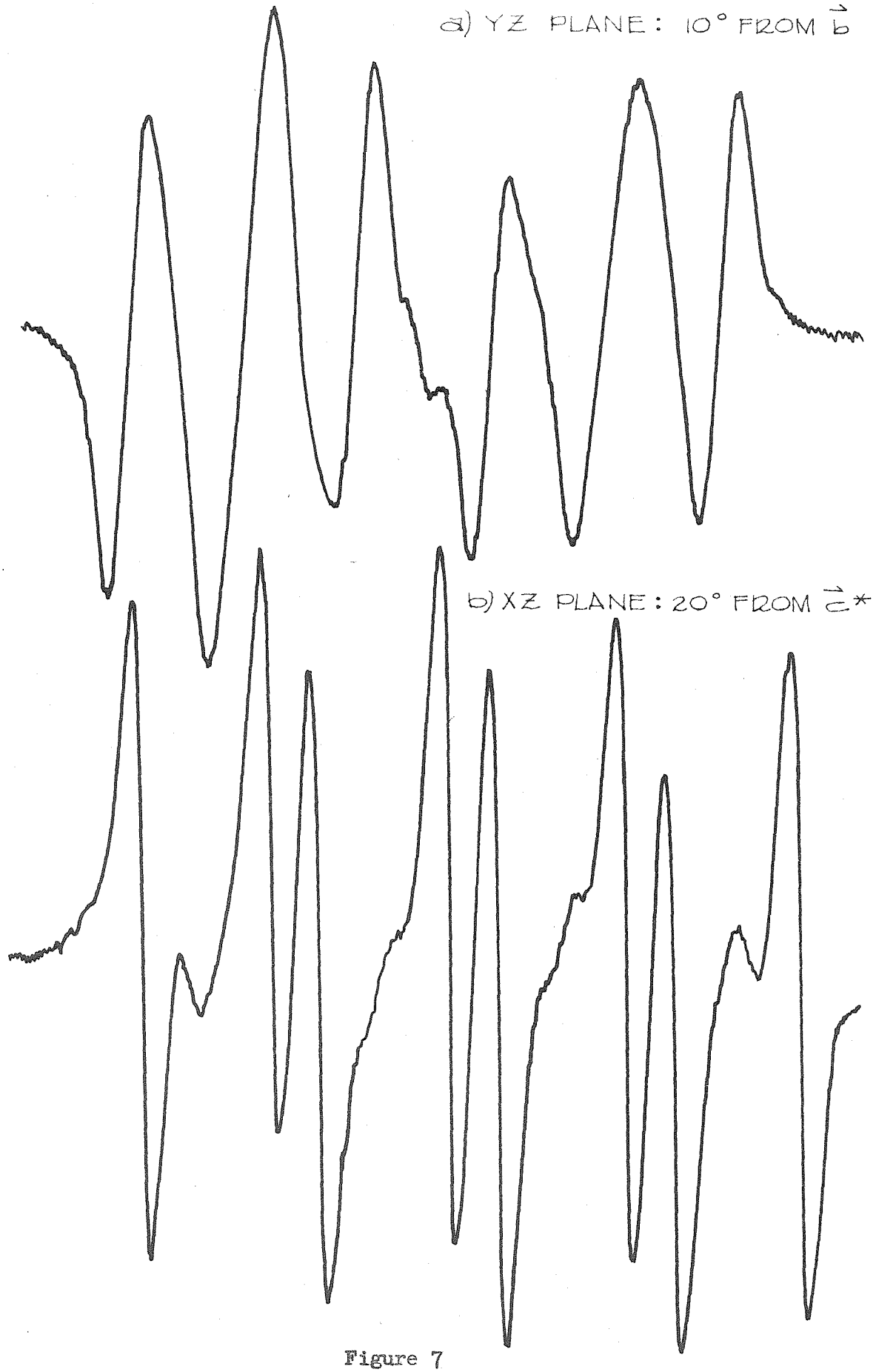

Figure 7

We measured (in Mc)

$$\mathcal{S}_{\beta_S}(\vec{e}_1) = 40.3 \qquad \mathcal{S}_{\alpha}(\vec{e}_1) = 68.5 \qquad \mathcal{S}_{\beta_L}(\vec{e}_1) = 129.0$$

$$\mathcal{S}_{\beta_S}(\vec{e}_2) = 42.0 \qquad \mathcal{S}_{\alpha}(\vec{e}_2) = 34.2 \qquad \mathcal{S}_{\beta_L}(\vec{e}_2) = 127.2$$

$$\mathcal{S}_{\beta_S}(\vec{e}_3) = 46.0 \qquad \mathcal{S}_{\alpha}(\vec{e}_3) = 77.5 \qquad \mathcal{S}_{\beta_L}(\vec{e}_3) = 126.5$$

So one can say that

$$A^{\alpha}_{11} \approx 64$$

$$A^{\alpha}_{22} \approx 32$$

$$A^{\alpha}_{33} \approx 72$$

where A^{α}_{ii} means the ii element for the α-proton.

(We show these values only for illustrative purpose and therefore omit detailed values for $\beta_{S,L}$-protons.) For the off-diagonal elements equation C-8 gives

$$A_{ij} = \frac{A_{ii}-A_{jj}}{2\tan 2\phi} \ .$$

Consider

$$A_{13} = \frac{A_{11}-A_{33}}{2\tan 2\phi} \ .$$

Figure 8 and Figure 8 (overlay) show a plot of $R + P \sin 2(\theta+\phi)$ versus θ matched to the plot of $\mathcal{S}^2(\theta)$ versus θ. Using $\phi \approx -5.5°$ one gets

$$A^{\alpha}_{13} \approx 21 \ .$$

In finding A_{12} and A_{23} a slightly different method was used. From equations D-3 and D-4 one can write

$$\underset{\sim}{A} = \begin{pmatrix} A_{11} & \pm A_{12} & A_{13} \\ \pm A_{12} & A_{22} & \pm A_{23} \\ A_{13} & \pm A_{23} & A_{33} \end{pmatrix}$$

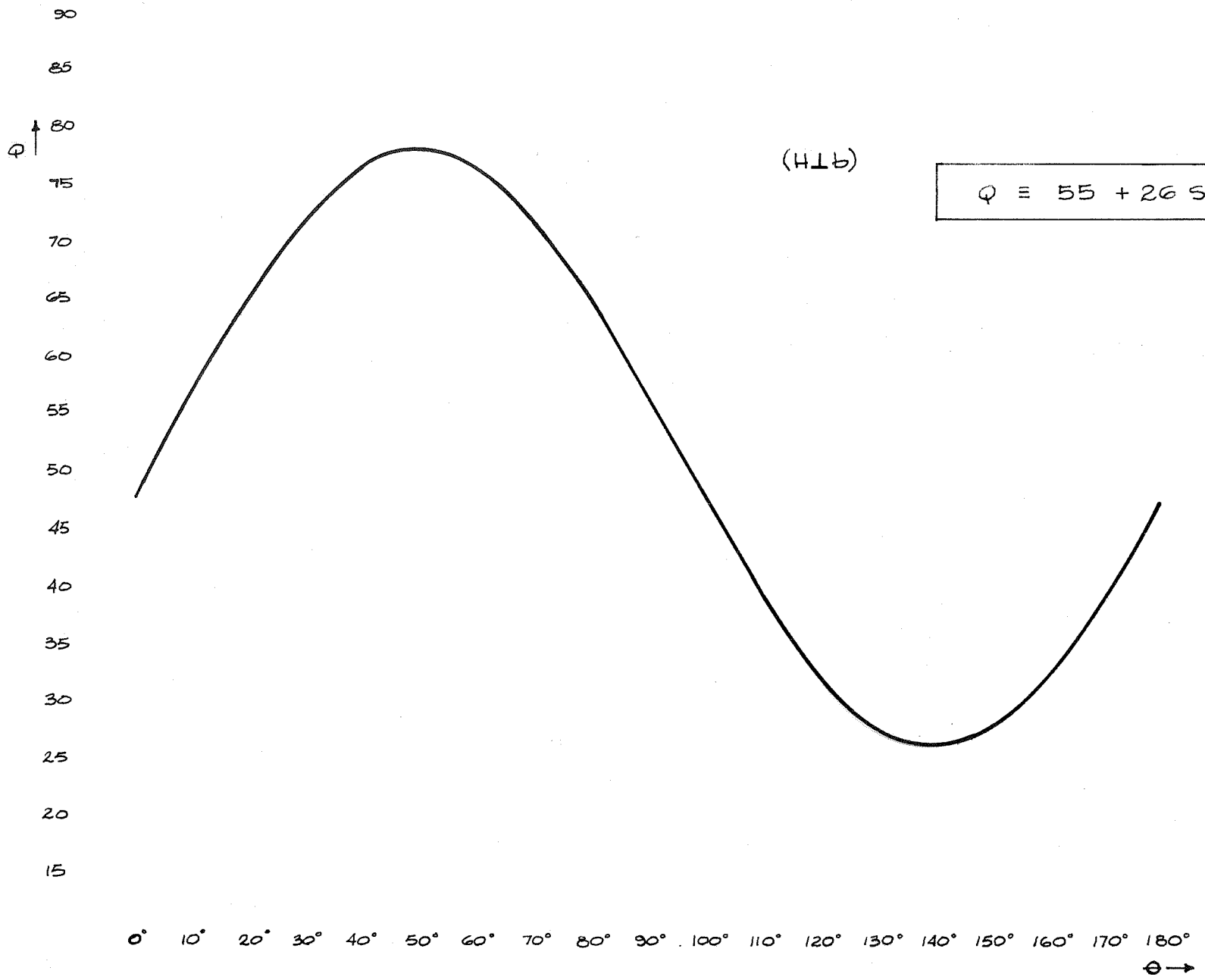

Figure 8 (Overlay) Glutaric acid data

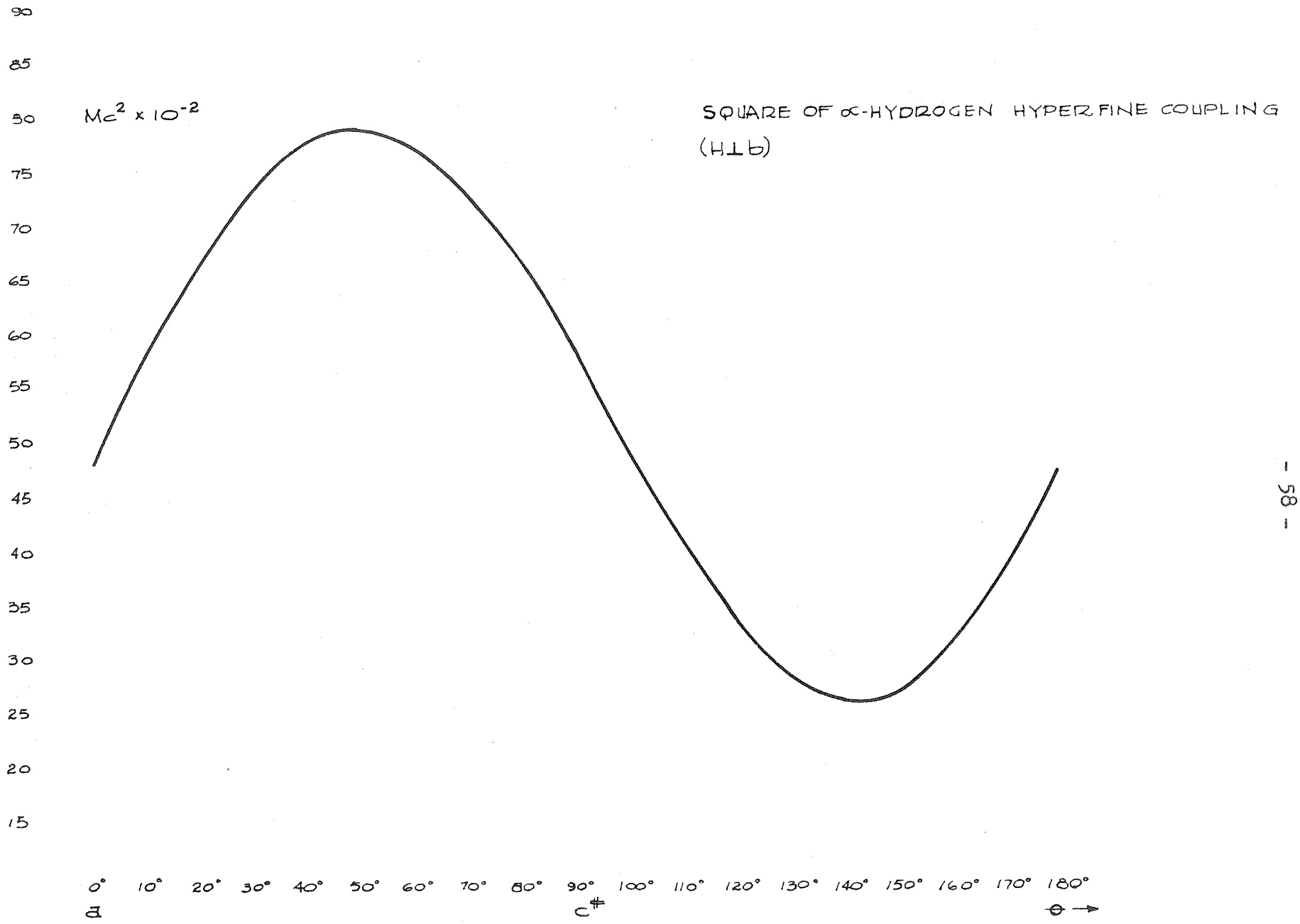

Figure 8. Glutaric acid data

and it is seen that the A_{12} and A_{23} elements for the two differently oriented radicals are related by a factor of (-1) in the tensor. If, as in equation C-13 the unit-field vector is designated as

$$\vec{u}_H = u_i \vec{e}_i + u_j \vec{e}_j \qquad \begin{pmatrix} i \\ j \end{pmatrix} = 1,2,3 \qquad i \neq j$$

then for rotations in the xy plane, for example, $\vec{u}_H = (\cos\phi)\,\vec{e}_1 + (\sin\phi)\,\vec{e}_2$.

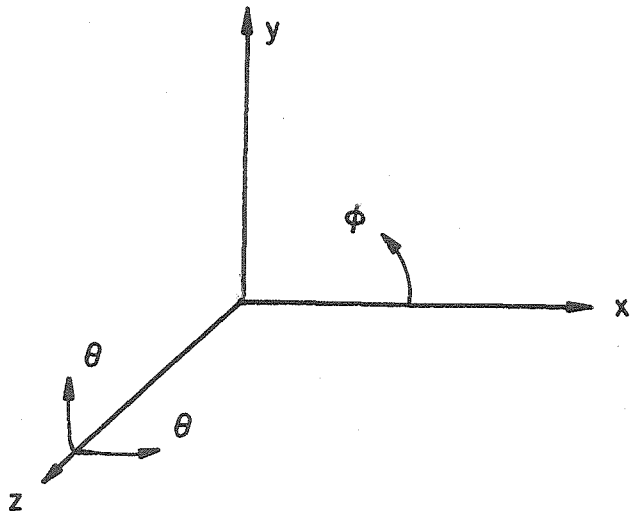

One can obtain an expression for $\mathcal{S}$ for this direction of $\vec{u}_H$.

$$\mathcal{S} = \vec{u}_H \cdot \underset{\sim}{A} \cdot \vec{u}_H = (\cos\phi \;\; \sin\phi \;\; 0) \begin{pmatrix} A_{11} & \pm A_{12} & A_{13} \\ \pm A_{12} & A_{22} & A_{23} \\ A_{13} & \pm A_{23} & A_{33} \end{pmatrix} \begin{vmatrix} \cos\phi \\ \sin\phi \\ 0 \end{vmatrix}$$

$$\mathcal{S} = A_{11}\cos^2\phi + A_{22}\sin^2\phi \pm A_{12}\sin 2\phi \qquad \text{(D-5)}$$

$$\text{and } \mathcal{S}_+ - \mathcal{S}_- = 2A_{12}\sin 2\phi \qquad \text{(D-6)}$$

$\mathcal{S}_\pm$ refers to the choice of the $\pm$ sign in the second equation for $\mathcal{S}$. We mentioned before that when $\vec{H}_o$ is not perpendicular to $\vec{b}$ the spectra are a

superposition of the spectrum due to each radical. So at any of these orientations one can measure both $\mathcal{S}_+$ and $\mathcal{S}_-$ (from the same spectrum) and thereby calculate A_{12}.

$$A_{12} = \frac{\mathcal{S}_+ - \mathcal{S}_-}{2\sin 2\phi} \qquad \text{(D-7)}$$

similarly

$$A_{23} = \frac{\mathcal{S}_+ - \mathcal{S}_-}{2\sin 2\theta} \; . \qquad \text{(D-7a)}$$

Using these formulae and the appropriate data one gets

$$A^{\alpha}_{12} \approx 10$$

$$A^{\alpha}_{23} \approx 0 \; .$$

As a very crude first approximation, then

$$\underset{\sim}{A}^{\beta S} = \begin{pmatrix} 40 & 0 & 1 \\ 0 & 42 & 0 \\ 1 & 0 & 46 \end{pmatrix}, \qquad \underset{\sim}{A}^{\beta L} = \begin{pmatrix} 128 & \pm 8 & 4 \\ \pm 8 & 126 & 0 \\ 4 & 0 & 125 \end{pmatrix}$$

$$\text{and } \underset{\sim}{A}^{\alpha} = \begin{pmatrix} 64 & \pm 10 & 21 \\ \pm 10 & 32 & 0 \\ 21 & 0 & 72 \end{pmatrix}$$

where the same methods have been applied to find $\underset{\sim}{A}^{\beta L,S}$. These values are now used in Step 2. Equation C-12 gives

$$A^2_{ii} = \mathcal{S}^2(\vec{e}_i) - A^2_{ij} - A^2_{ik} \; .$$

Here the values for A_{ij} and A_{ik} calculated in Step 1 are used to find the (A_{ii})'s. Employing equation C-14 to calculate the (A_{ij})'s using the new values of the (A_{ii})'s one obtains

$$\underset{\sim}{A}^{\beta S} = \begin{pmatrix} 40.3 & \pm 1.5 & -0.7 \\ \pm 1.5 & 42.0 & 0.2 \\ -0.7 & 0.2 & 46.0 \end{pmatrix} \qquad \underset{\sim}{A}^{\beta L} = \begin{pmatrix} 128 & \pm 7 & 6.5 \\ \pm 7 & 126 & \mp 1 \\ 6.5 & \mp 1 & 125 \end{pmatrix}$$

$$\underset{\sim}{A}^{\alpha} = \begin{pmatrix} 64.5 & \pm 12.5 & 18.0 \\ \pm 12.5 & 32.8 & \pm 0.5 \\ 18.0 & \pm 0.5 & 74.6 \end{pmatrix}$$

Using these values one iterates using equations C-12 and C-14 until the values stabilize, and the result of this is (after three iterations for the α-proton and one for the β-protons)

$\underset{\sim}{A}^{\beta S}$ = no change $\qquad$ $\underset{\sim}{A}^{\beta L}$ = no change

$$\underset{\sim}{A}^{\alpha} = \begin{pmatrix} 65.0 & \pm 12.0 & 17.7 \\ \pm 12.0 & 32.0 & \pm 0.4 \\ 17.7 & \pm 0.4 & 75.4 \end{pmatrix}$$

We now proceed to Step 3. Using equation C-20 and C-24 and needed values from Step 2 one obtains

$$\underset{\sim}{A}^{\beta S} = \begin{pmatrix} 39.5 & \pm 2.5 & 0 \\ \pm 2.5 & 41.0 & \pm 1 \\ 0 & \pm 1 & 45.5 \end{pmatrix} \qquad \underset{\sim}{A}^{\alpha} = \begin{pmatrix} 64.6 & \pm 12.8 & 17.9 \\ \pm 12.8 & 28.5 & \mp 2.5 \\ 17.9 & \mp 2.5 & 75.1 \end{pmatrix}$$

$$\underset{\sim}{A}^{\beta L} = \begin{pmatrix} 128.6 & \pm 6.5 & 5.8 \\ \pm 6.5 & 126.9 & \mp 2.0 \\ 5.8 & \mp 2.0 & 126.2 \end{pmatrix}$$

Again iterating one finally obtains (after three iterations for the α-proton and one for the β-protons)

$$\underset{\sim}{A}^{\beta S} = \text{no change} \qquad A^{\alpha} = \begin{pmatrix} 64.0 & \pm 12.7 & 18.4 \\ \pm 12.7 & 27.5 & 0.5 \\ 18.4 & 0.5 & 75.0 \end{pmatrix} \qquad \underset{\sim}{A}^{\beta L} = \text{no change}$$

The final values for the hyperfine tensors for the α- and β-protons of the A radical in glutaric acid are

$$\underset{\sim}{A}^{\beta S} = \begin{pmatrix} 39.5 & \pm 2.5 & 0 \\ \pm 2.5 & 41.0 & \pm 1 \\ 0 & \pm 1 & 45.5 \end{pmatrix} \qquad A^{\alpha} = \begin{pmatrix} 64.0 & \pm 12.7 & 18.4 \\ \pm 12.7 & 27.5 & 0.5 \\ 18.4 & 0.5 & 75.0 \end{pmatrix}$$

$$\underset{\sim}{A}^{\beta L} = \begin{pmatrix} 128.6 & \pm 6.5 & 5.8 \\ \pm 6.5 & 126.9 & \mp 2.0 \\ 5.8 & \mp 2.0 & 126.2 \end{pmatrix}$$

The same methods employed in obtaining the tensor elements for $\underset{\sim}{A}^{\alpha}$ in Step 1 were used in calculating the g-tensor. The standards for these measurements were 1,1-diphenyl 2-picryl hydrazyl (DPPH) as the field marker and the peroxylamine disulfonate ion, $(SO_3)_2NO^{=}$, (PDS) for field calibration. The result of these measurements is

$$\underset{\sim}{g} = \begin{pmatrix} 2.0030 & \mp 0.0007 & 0.0006 \\ \mp 0.0007 & 2.0034 & 0.0000 \\ 0.0006 & 0.0000 & 2.0028 \end{pmatrix}$$

The uncertainty in these values is about $\pm$ 0.0003.

A comment should be made on the calculation of the hyperfine tensors. The α-proton splittings exhibit the greatest anisotropy. This means that the off-diagonal elements of the tensor can be quite large. We also saw that the A^{α}_{22} element is approximately $2\nu_p$ and it is interesting to note that a considerable change occurred in the A^{α}_{22} element in going from Step 2 to Step 3 as one would expect from the approximation upon which Step 2 is based. All other elements seemed well behaved. However, it would probably be best to limit the use of the procedure to systems in which the coupling constants are $\geq 2\nu_p$. In general the procedure worked very well, requiring only about three iterations in both Steps 2 and 3 for the α-proton and one iteration in both Steps 2 and 3 for the β-protons. However, the calculations are quite tedious and it would be rather straightforward and advantageous to write a computer program for this procedure. In general, for free radicals of the type described in this section this procedure should be applicable to protons with coupling constants greater than about $2\nu_p$.

HMW discuss the general features of the radicals so we shall make only a few comments on the nature of the radicals. The proposal of HMW that the radicals are distortion isomers certainly seems to be the most plausible explanation. They suggest that possibly the two isomers are energetically equivalent and that as a result a dynamic equilibrium exists with a half-life of exchange of longer than 10^{-7} sec. If this were true it would be very difficult to explain why one radical should disappear almost entirely on u.v. treatment while the other remains at almost the same intensity. Another suggestion made by them is that a large activation energy for interconversion may exist. Again for the reason stated above this seems unlikely.

The final possibility HMW mention is that the space group is actually C_S^4 which means essentially that the two ends of the molecule are not quite equivalent. Such slight deviations in the carboxyl groups would not seem to be sufficient to give the pronounced effects observed. However, the possibility cannot be completely ruled out. In all fairness it should be noted that we have not shown HMW to be wrong but have simply eliminated some of the not unreasonable possibilities which they suggested.

In a sense, the result obtained with u.v. treatment makes the problem more puzzling than before. It would be interesting to pursue this problem somewhat more. One could possibly obtain some revealing information by finding the decay rate of radical B versus the energy of the light. The use of polarized light and the decay of radical B as a function of the angle of polarization relative to the crystal morphology might also add some pertinent information.

The production of radicals A and B is peculiar to the single crystal of glutaric acid. We irradiated glutaric acid included in urea* and obtained spectra arising from only one radical and found that the intensity did not seem to be affected by u.v. treatment. The proton coupling constants due to the radical in urea were (not unexpectedly) different from those for either the A or B radical.

Finally, one word of caution should be added. The hyperfine tensors calculated above are based on spectra taken at room temperature.

---

*Griffith and McConnell (50) have shown that many radical-forming compounds can be studied as guest molecules in a non radical-forming host.

It cannot be expected, a priori, that the same splittings will be measured at other temperatures. Actually, at one orientation it was observed that the splitting due to the β_L-proton increased on going to lower temperatures. In Figure 9 a high and a low temperature spectrum are shown. The only splitting that seems to change is that due to the β_L-proton and the change is about 10 Mc. This is a rather large and unusual change. As a result of this the ENDOR transitions for this proton will be about 5 Mc higher than what one would predict from the room temperature data. This will be dealt with further in Section G.

To summarize then, we would like to reiterate some of the main points of this section.

1. When single crystals of glutaric acid are irradiated with x-rays two non-identical radicals A and B are formed. These radicals are distortion isomers having the structure HOOC-$\dot{C}$H-CH_2-CH_2-COOH.
2. Irradiation of these crystals with u.v. light destroys radical B but does not seem to effect radical A.
3. The hyperfine tensors for protons α, β_S, and β_L and the g-tensor were calculated for radical A. The isotropic contributions were 55.8, 42.0 and 127.2 and 2.0031 respectively.
4. Several of the possible explanations tendered by HMW regarding the nature of the distortion isomers do not appear plausible in view of our experiments.
5. Single crystals of glutaric acid included in urea give only a single radical on x-irradiation and this seems not to be affected by the u.v.-irradiation.

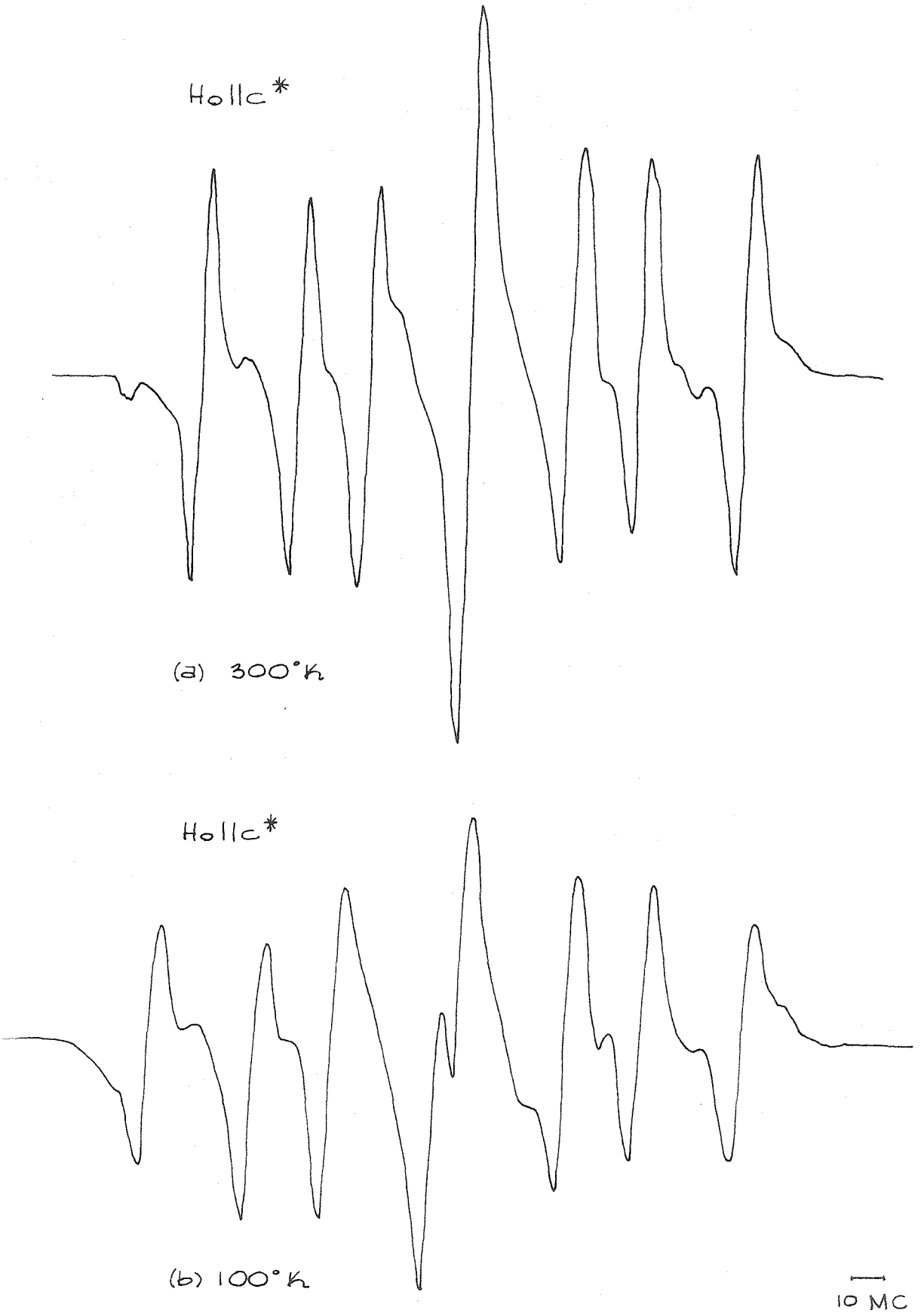

Figure 9. Glutaric acid spectra

6. β_L was found to be a function of temperature and the deviation over the range of interest was found to be about 10 Mc.

7. Even with the improved resolution obtained by bleaching radical B, splittings due to γ-protons were still not observed.

With the information presented in this section one can calculate the data important for the ENDOR experiments. The problems encountered in development of the ENDOR technique will now be considered.

E. THE ENDOR PROBLEM*

A formal introduction to this section is omitted since the entire section is essentially an introduction to Section F. In this section only the experimental problems encountered in the developmental phase are discussed.

In the summer of 1959 we decided to apply the ENDOR technique to the study of organic free radicals. R. W. Fessenden, during the last two months of his postdoctoral stay at the Institute, introduced me to the electronics problems and the first experiment was done under his direction.

Again we state that the technique is based on the standard EMR experiment. To a first approximation, the only new requirement is that of introducing a second rf field** at the sample position. The frequency range of interest for these experiments is 1-100 Mc, and one must be able to vary the frequency continually over this range. The introduction of such an rf field at low power levels is very simple and straightforward--and at high power levels becomes rather difficult. We shall simply state that high power levels were deemed necessary--levels sufficient to produce a 1 gauss field at the sample position.

The obvious way to get rf frequencies at this power level inside a microwave cavity is to place the rf coil <u>inside</u> the cavity. However,

---

*For a basic understanding of the various aspects of electronics one should consult references 51-53.

**Henceforth we shall refer to the x-band frequencies used in standard EMR experiments as microwave frequencies. The low frequencies used to induce the ENDOR transitions will be referred to as rf frequencies.

placing a conductor at an arbitrary position inside the cavity will not only reduce the cavity Q but in most cases will completely change the cavity's resonant characteristics. The conductor must be positioned so as to cause a minimum perturbation of the field distribution in the cavity. One has essentially two conditions.

(1) The coil should be placed in a plane where $E \approx 0$ since this causes the minimum perturbation to the system.

(2) One would like to maximize the sample filling factor for both the microwave and rf magnetic fields.

A cavity in which these conditions could be satisfied had already been built. A rectangular cavity resonating in the dominant TE_{10} mode has a field configuration (51) (for TE_{102}) as shown in Figure 10a. The magnetic field density is a maximum in the c/2 plane and the electric field density is a minimum. Therefore, placing the rf coil in the c/2 plane satisfied both conditions given above. A coil (made in the form of a watch spring) mounted in this plane resulted in a useable cavity.

The availability of a high-power sweep-frequency rf signal generator was another matter. Generators with high (and even very high) power output in these frequency ranges are available but they cannot be continuously varied in frequency. Furthermore, we knew of no commercial wide-band amplifier that could do the equivalent job. Consequently, we modified a war surplus generator and obtained very roughly the desired specifications. For (phase sensitive) detection purposes a reactance modulator was inserted in the plate circuit of the oscillator to allow

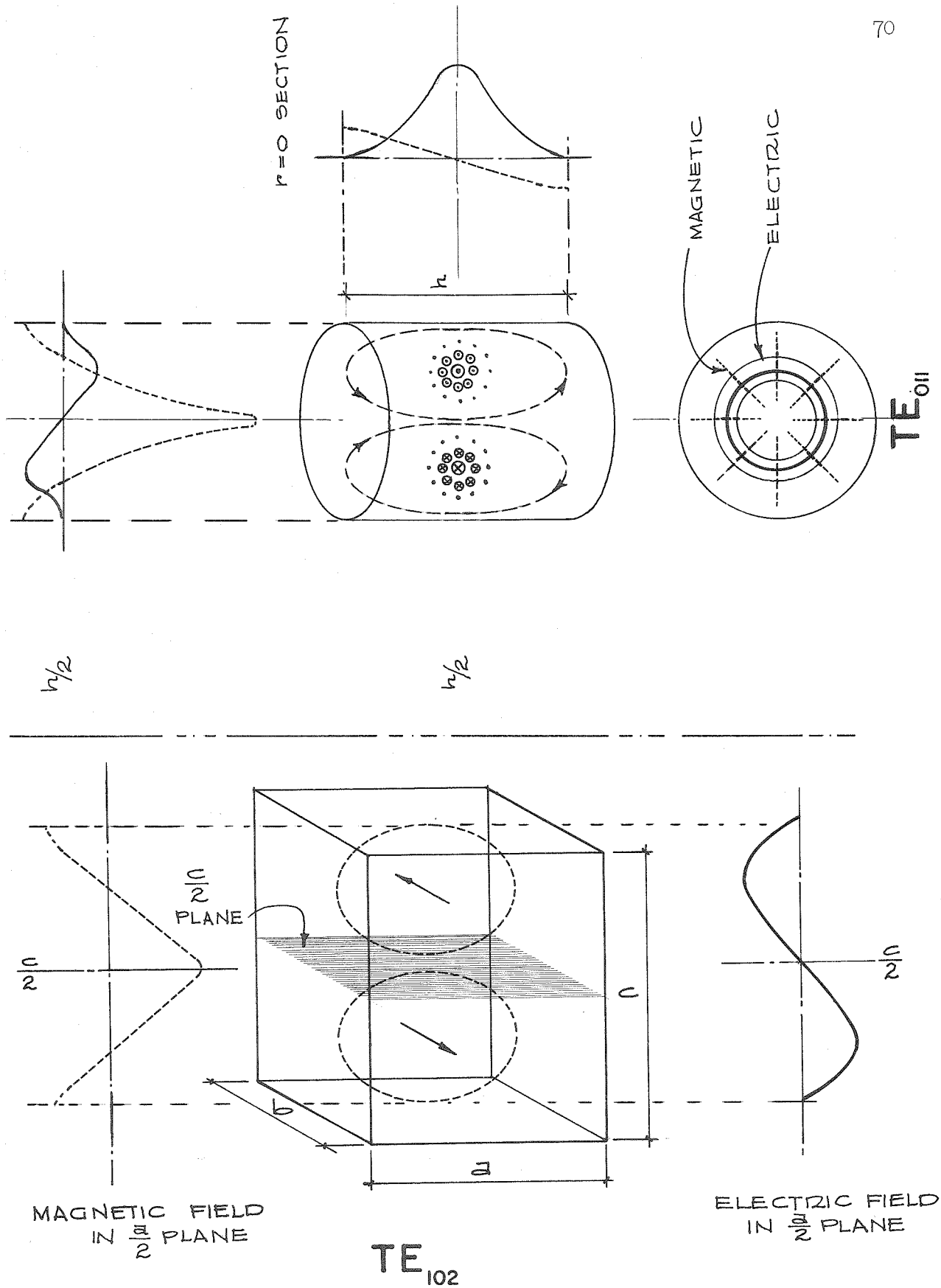
r=0 SECTION
h
MAGNETIC
ELECTRIC
TE011
h/2
h/2
c/2
PLANE
c/2
c
b
a
c/2
MAGNETIC FIELD
IN a/2 PLANE
ELECTRIC FIELD
IN a/2 PLANE
TE102

Figure 10

frequency modulation of the rf.* To reiterate--our first ENDOR system consisted of the standard EMR spectrometer, a special TE_{102} cavity, and a modified war surplus f.m. signal generator.

The sample for this experiment was a single crystal of malonic acid in which a high concentration of $(HOOC)_2\dot{C}-H$ had been produced. Up until that time very few radicals had been studied in the solid state. This radical had been investigated quite thoroughly in these laboratories and it was the obvious choice.

In our first try rf pick up prevented us from doing a definitive experiment. After eliminating this problem by appropriate shielding and grounding, several room temperature ENDOR experiments were done but without success. This concluded the association which Dr. Fessenden had with the problem.

The overall feeling one was left with after these early attempts was that sensitivity would probably constitute the major problem. There are two strongly coupled and rather apparent ways in which to increase sensitivity and/or signal to noise ratio (S/N).

1. Increase the Q** of the cavity.

2. Do the experiment at low temperatures.

The ability to saturate the EMR signal is of course of prime importance. For a given electron spin-lattice relaxation time $^{S}T_1$ this is a function of the magnetic field intensity in the cavity (H_1) which in turn is a

---

*Another generator built later is described in Part II. It employs essentially the same features as this one did.

**$Q \equiv \frac{\Delta\omega}{\omega} = 2\pi \frac{\text{energy stored in cavity}}{\text{energy lost in cavity per cycle}}$

function of the cavity Q and of the available microwave power. At room temperature with a 150 mW source one is barely able to begin saturating the EMR lines of the radicals produced in the dicarboxylic acid crystals. If one were to increase ${}^{S}T_1$ for these systems saturation would be feasible. Kronig (52) has shown that generally $T_1 \propto \frac{1}{T}$ for $T < 80°K$ and $T_1 \propto \frac{1}{T^7}$ for $T > 80°K$. In other words H_1 can be effectively increased by going to lower temperatures. (Reduced temperatures will also increase S/N simply because of the Boltzmann distribution). Increasing the power available from the source was not feasible, but improving the cavity Q was.

Q is inversely related to the resistivity of the cavity walls. Decreasing the temperature will therefore effectively increase the available power. Furthermore, the highest Q can be obtained with cylindrical cavities operating in the TE_{01} mode. (See Fig. 10b). It seemed reasonable therefore to employ a cylindrical cavity at low temperatures.

In proposing to use a cylindrical cavity one is confronted anew with the problem of introducing the rf. Several possibilities were considered:

(i) A coil on the outside of the cavity

(ii) A helix which simultaneously acts as a microwave and rf structure*

(iii) A coil on the inside of the cavity.

Possibilities (i) and (ii) were studied and rejected. Both resulted (with the techniques available then) in a reduction of either microwave

---

*Such a structure was designed, at the time of my candidacy exam, in connection with a proposal for a radio frequency maser employing the hyperfine levels in a free-radical. More recently (55) this method has been proposed and employed in similar double resonance experiments.

or rf fields at the sample position. The third possibility had two parts. One was that of cutting the silver plating on the cavity walls (made of some dielectric) in such a way as to effectively form an rf coil.* The other was to place a "conventional" coil in the cavity similar to the way in which it was done in the rectangular cavity. The former presented some practical problems. The latter we had already solved so we proceeded to develop it.

We designed and built a cylindrical cavity (out of brass) containing an elongated rf coil having its long dimension along the cylinder axis. (This is done so that $\vec{E}$ over the region of the coil is everywhere small and perpendicular to the coil wires.) The low temperature glass dewars which could accommodate our cavity in the 5" magnet gap were also built at this time. (See Section F, Fig. 20.) Using this system several experiments were done at 77°K using malonic acid crystals with negative results. It became clear that the cavity was not ideal (the coil in the cavity actually reduced the cavity Q considerably) and since it could not be used at liquid helium temperatures, it was abandoned.

The above experiments left us with the impression that a rectangular cavity, constructed with care, could have a Q comparable to that which our cylindrical cavity had. Therefore we set about to carefully design and build our third microwave cavity.

Since a good 100kc modulation and phase sensitive detection system had just been acquired we wanted to build the cavity so that this high

---

*See proposition number 3.

modulation frequency could be used. (The increase in sensitivity would be about $\sqrt{10^5/400} = 16$). However the skin depth, δ, of silver at 100kc is about 0.010 inches. Therefore, in order to field modulate at 100kc from outside the cavity one needed to find a dielectric material from which to build the cavity. This would allow one to put a sufficiently thin silver coating on the internal cavity walls permitting the 100kc fields to penetrate. The need for peculiar configurations having high tolerances and the necessity of thermal shock resistance eliminated the glasses. After a considerable search and some research a filled epoxy resin* was found which could be placed directly in liquid nitrogen without showing any ill effects.

The internal cavity walls were made very smooth by casting the epoxy around a highly polished nylon plug having the desired dimensions. The nylon plug was coated with an extremely thin layer of silicone grease which acted as a mold release. To obtain a continuous epoxy surface the resin was degassed before pouring. After prolonged and slow curing the nylon plug was removed by a thermal and mechanical shock method. A one-half inch hole was tapped two-thirds of the length of the nylon plug. The inserted lag bolt after being submerged in liquid nitrogen was forcibly jarred using a manual press. The subsequent removal of this tightly fitting plug left behind a highly burnished surface.

The resulting resin block was then machined to the prescribed dimensions (see Fig. 11). The tolerances in most cases were 0.0005"

---

*Furane Plastics Company, Los Angeles. Epoxy 10-F with D-40 catalyst.

TE_{102} ENDOR CAVITY

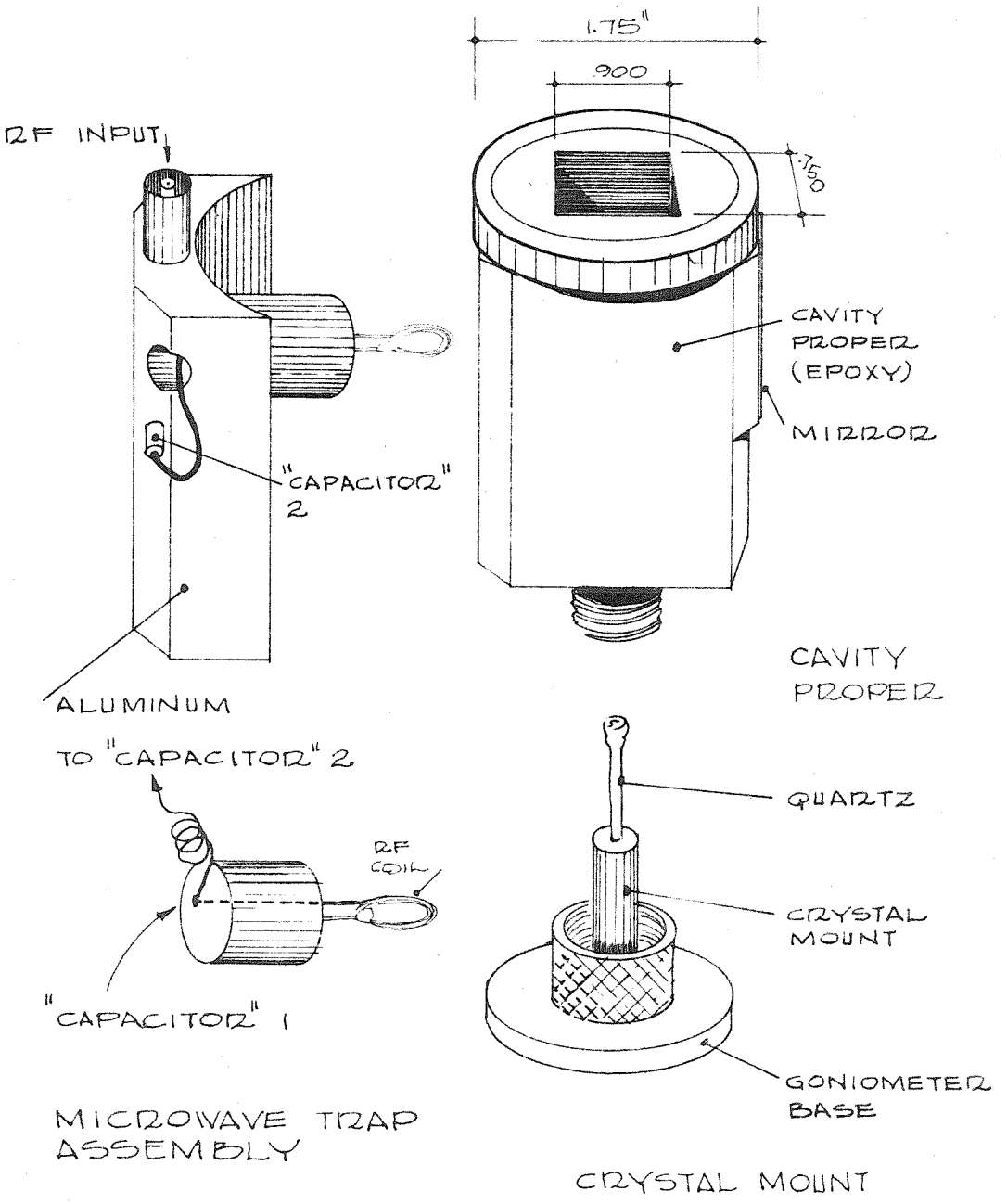

Figure 11

and 20' for critical angles. The object of these close tolerances was to allow final positioning of the rf coil in the cavity as nearly as possible in the E = 0 (c/2) plane. The cavity was then chemically silver plated (56) and buffed. The surface of the silver after plating is quite rough and is covered by a sediment. Carefully buffing the coating increased the unloaded Q by about a factor of 2. In Figure 11 the microwave trap assembly is shown. It was found that microwaves were coupled out of the cavity by the rf coil giving rise to microphonics and reduced Q. The trap was designed to have the electrical characteristics sketched below.

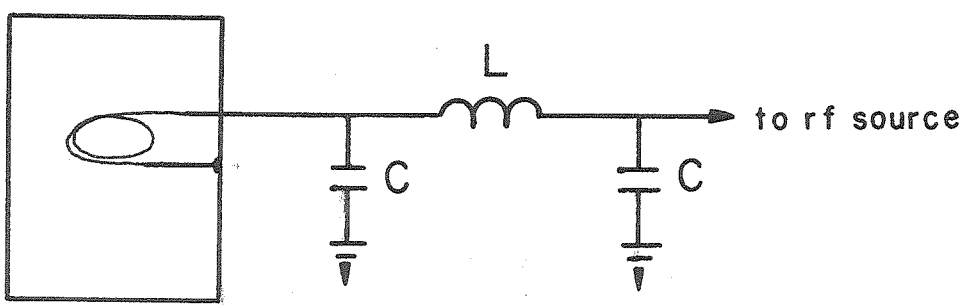

Physically each capacitor consisted of an insulated #22 wire passing through an aluminum block. The inductor consisted of three turns on a 1/8" diameter. This trap completely eliminated the microwave leakage problem.

The sample mount was rather unorthodox. A quartz rod was brought up through the bottom of the cavity directly through the maximum $\vec{E}$ field to the plane of the rf coil. This destroyed cavity resonance. The problem was solved by adding a dummy quartz rod in the upper half of the cavity so as to restore the symmetry. The quartz did not seem to affect the Q.

The rf coil consists of four turns of 0.010" × 0.015" 99.995% silver ribbon.* The plane of the coil was mounted perpendicular to the surface of the insert to within less than 1°. This unit was then inserted into the cavity and oriented so that the plane of the coil was within less than 1° of being parallel to the top surface of the cavity. A picture of the completed unit after it had yielded all the ENDOR data is shown in Figure 12.

After the completion of the ENDOR cavity in the fall of 1960, the only known deterrent to our doing a definitive ENDOR experiment was the rf source--its characteristics were simply not good enough. After canvassing all the major electronics distributors I learned of the existence of a wide-band amplifier, built by Instruments for Industry (IFI),** that could handle 100 watts of power in the 1-200 Mc range. The cost was $5,000! IFI also built one covering the same range having a 3 watt capability for 1/10 the price. The former was within the right power range but in the wrong price range. We felt that probably the reverse was true of the latter. Therefore we began to build the rf generator described in Part II. This generator had a 15 watt output over most of its range and this could be increased by using higher plate voltages.

In December of 1960 when we had almost completed this high-power generator we got word from T. Cole of the Ford Motor Company

---

*The coil was wound and mounted on the insert by Don Boyko of DB Products of Pasadena. I am very grateful for his generous and expert assistance.

**Instruments for Industry, Hicksville, New York.

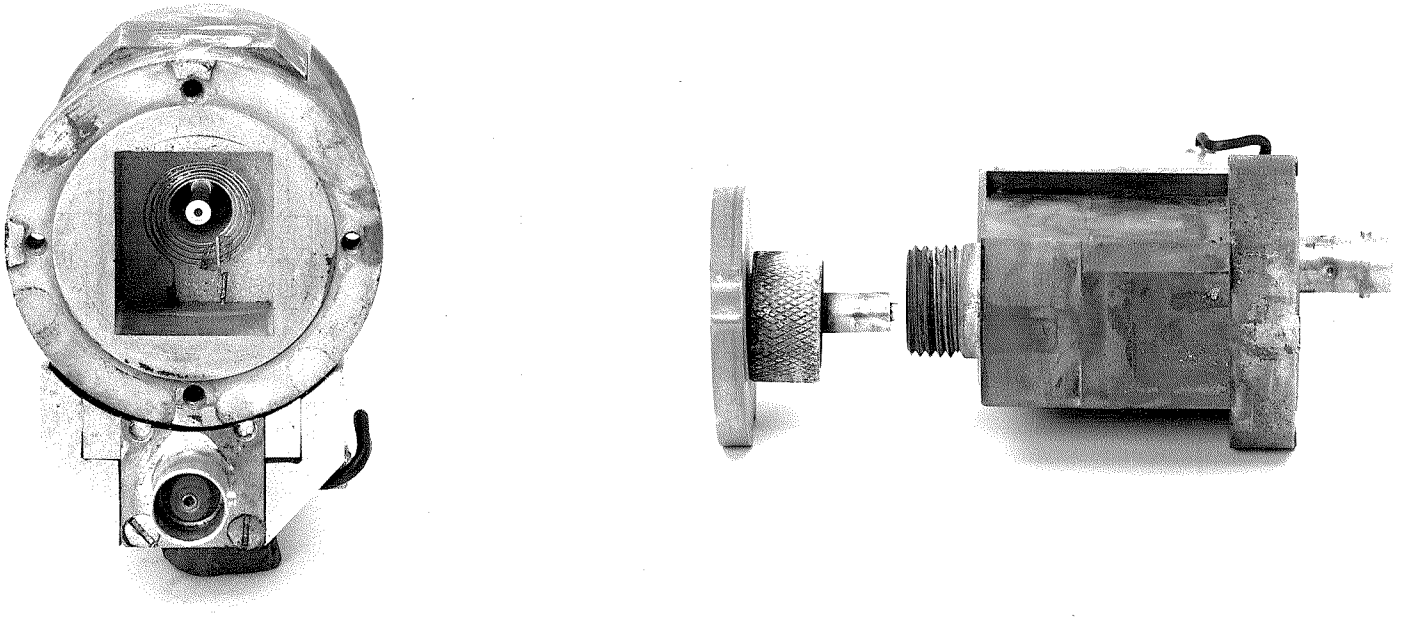

Figure 12. TE_{102} ENDOR cavity

Scientific Laboratories* that they had observed the ENDOR transition in succinic acid using the equipment employed in the ruby ENDOR experiment of LLMT. They had used the 3-watt IFI amplifier! Nevertheless, we continued building the rf unit and completed it in early 1961.

In order to test the equipment it was decided to first look for ENDOR in either KCl or ruby.** The ENDOR in KCl had been observed both at 4.2°K (26) and at room temperature (58). Therefore it was decided to do our first experiment on KCl at 77°K. We saw a signal--a spurious one. It appeared at the point where the KCl line was expected and it had the right line width. Dr. Hildebrandt suggested that the signal was probably due to resonant rf pickup in the cables leading to the microwave crystal detector. To check this he supplied me with a filter which was mounted next to the microwave crystal inside the Varian microwave bridge. This completely eliminated the "KCl" line. However, it had been observed that the F-centers in the KCl crystal bleached very rapidly and so it was decided to go directly to 4.2°K using a ruby crystal. A single crystal of ruby was cut to the appropriate dimensions and shape.†

Then we were suddenly stopped by a ridiculously simple problem--how to attach the sample. The waxes used at room temperature‡ and at

---

*The effect is reported by Cole, Heller and Lambe (CHL) in reference 57.

**The ruby crystal was supplied by A. F. Hildebrandt.

†This was done by Wm. Schuelke of the Chemistry Instrument Shop.

‡Cenco Universal Red Wax.

77°K* were not satisfactory for the helium temperature experiment. After several days of searching an adhesive was found (see reference 59) that seemed to be ideally suited to our problem. It is made from General Electric Insulating Varnish and Adhesive #7031 by mixing in a 1:1 ratio with toluene. If one does not exercise care in using this glue the bond will not be satisfactory. The glue forms a surface film very quickly which will not adhere properly at low temperatures. However, if one applies a very thin film to a clean surface and immediately presses the other surface to it a bond is formed which sets up quickly and is strong even at very low temperatures. In all the times I have used this glue I have never had a crystal fall off at low temperatures.**

Since liquid helium passes through even the smallest fissures with the greatest of ease, all efforts to seal out this refrigerant failed.† Subsequently when the rf was turned on the helium in the cavity would vaporize causing great instabilities in the electronics. A. F. Hildebrandt suggested that we pump on the helium to make it superfluid. This solved the problem since the thermal conductivity of liquid helium is so high that it boiled only at the surface. Also in the course of this experiment the signal generator gave a considerable amount of trouble. Therefore, it was decided to purchase the 3-watt

---

*Apiezon N or Silicone grease. These have worked at 4.2°K but their lack of rigidity at room temperature is undesirable.

**Difficulties are sometimes encountered in mounting samples such as certain organic crystals which are soluble in the glue. This is particularly so when a lot of glue is unnecessarily used.

†At 77°K we had very successfully used a rubber cement-kerosene mixture for this purpose.

IFI amplifier. When this finally arrived it was driven with the output from the General Radio signal generators and using field modulation we immediately observed the ENDOR transitions in ruby at 1.5°K. See Figure 13.

This was now the summer of 1961. Almost a year had been lost because of the rf source. However, the ENDOR system seemed to be working well, and we were now ready to study organic free-radicals.

CHL had seen the ENDOR transitions in succinic acid (57). They had been unable to see ENDOR in malonic acid. We therefore decided to look for the ENDOR transitions in a radical which also contained γ-protons. The first member of the saturated dicarboxylic acid series in which this could be done is glutaric acid. The EMR of the glutaric acid radicals had already been done but it did not seem advisable for our purposes to investigate it because of the problems mentioned in Section D. The next member of the series is adipic acid. Since this looked like a "clean" system we decided to study it. Once again this was the wrong decision.

After a month or so a single crystal of adipic acid was obtained from solution. A helium temperature experiment was done using this crystal. We saw no signal. When the system was dismantled it was found that the crystal had shattered. However, since a normal looking EMR spectrum had been obtained at helium temperatures we felt that the crystal had shattered on warm-up. (Actually the spectrum appeared normal because of the small anistropy of the proton splittings.) After the second lesson we took single crystals and dropped them into liquid nitrogen. They all shattered. It was felt that crystals grown from the melt might have fewer imperfections and therefore not shatter. After build-

Figure 13. ENDOR spectrum of Al^{27} in ruby

ing a crystal grower and obtaining an excellent single crystal the tests were repeated on a cleaved section. It did NOT shatter. We therefore spent some time using Laue and Supper precession methods to find the appropriate orientations. In order to avoid introducing strains the crystals were cut with an "acid" saw. Again the cooling tests were repeated. All adipic acid crystals shattered regardless of conditions. More careful experiments revealed that they did so in the range of 110°K to 150°K regardless of the rapidity with which that temperature range was reached. A low temperature powder picture could be taken to determine whether a phase transition is involved. It was felt that adipic acid could still be studied by

1) casting the crystal in an epoxy resin

or 2) doping some appropriate non-radical forming host with adipic acid.

However, at about this time (late 1961) we had begun to check into the glutaric acid situation more fully. (See Section D.) Since it began to look promising the work on adipic acid was abandoned.

Before going on to the next section to discuss the final experimental set up and its use in collecting the ENDOR data the high points of this section will be summarized.

1. ENDOR was initially tried on malonic acid at room temperature using a rectangular cavity containing a watch-spring-like coil. Result: negative
2. The next attempt was made on malonic acid at 77°K using a cylindrical cavity containing an elongated rectangular coil. Result: negative

3. A liquid helium temperature system was designed and constructed. A new rf source was also built. With this system F-centers in KCl were investigated at 77°K. Result: negative

4. The above system was applied to the study of ruby at 4.2°K. Problems encountered due to helium entering the cavity were eliminated by using superfluid helium. The rf source which had been used was replaced by a G.R. signal generator and an IFI wideband amplifier. Result: POSITIVE

5. We tried to observe the ENDOR transitions in adipic acid.
   Results: negative--adipic acid crystals shatter on being cooled.

F. THE ENDOR EXPERIMENT

In this section consideration is given to the complete ENDOR system and the basic steps followed in doing the experiment are described. The various pieces of equipment are listed by number.* These numbers may be compared with those in Figures 14–20.

The common unit in both ENDOR and EMR is the EMR Spectrometer. This is the standard x-band unit V4500(525)** made by Varian Associates. It consists of the following items:

(1) Low-High Power Microwave Bridge V4500-414(55E)

(2) EPR Control Unit V4500-10(51)

(3) Power Supply (Control Units) V4260B(59)

(4) Power Supply (Klystron) V4500-20(44)

(5) Precession Field Scanning Unit V4280A(77)

(6) Selector Panel V4295

(7) Oscilloscope Dumont 304AR(OF15)

(8) 100kc Field Modulation and Control Unit V4560(224)

This unit was modified with the Varian Kit to allow the use of lower reflector voltages.

(9) Mode Sweep Unit†

---

*The model number is followed by the serial number in parentheses.

**At some time or other during the course of our experiments almost every one of the more than 30 pieces of equipment decided to quit functioning properly!

†Originally built by R. W. Fessenden and later modified.

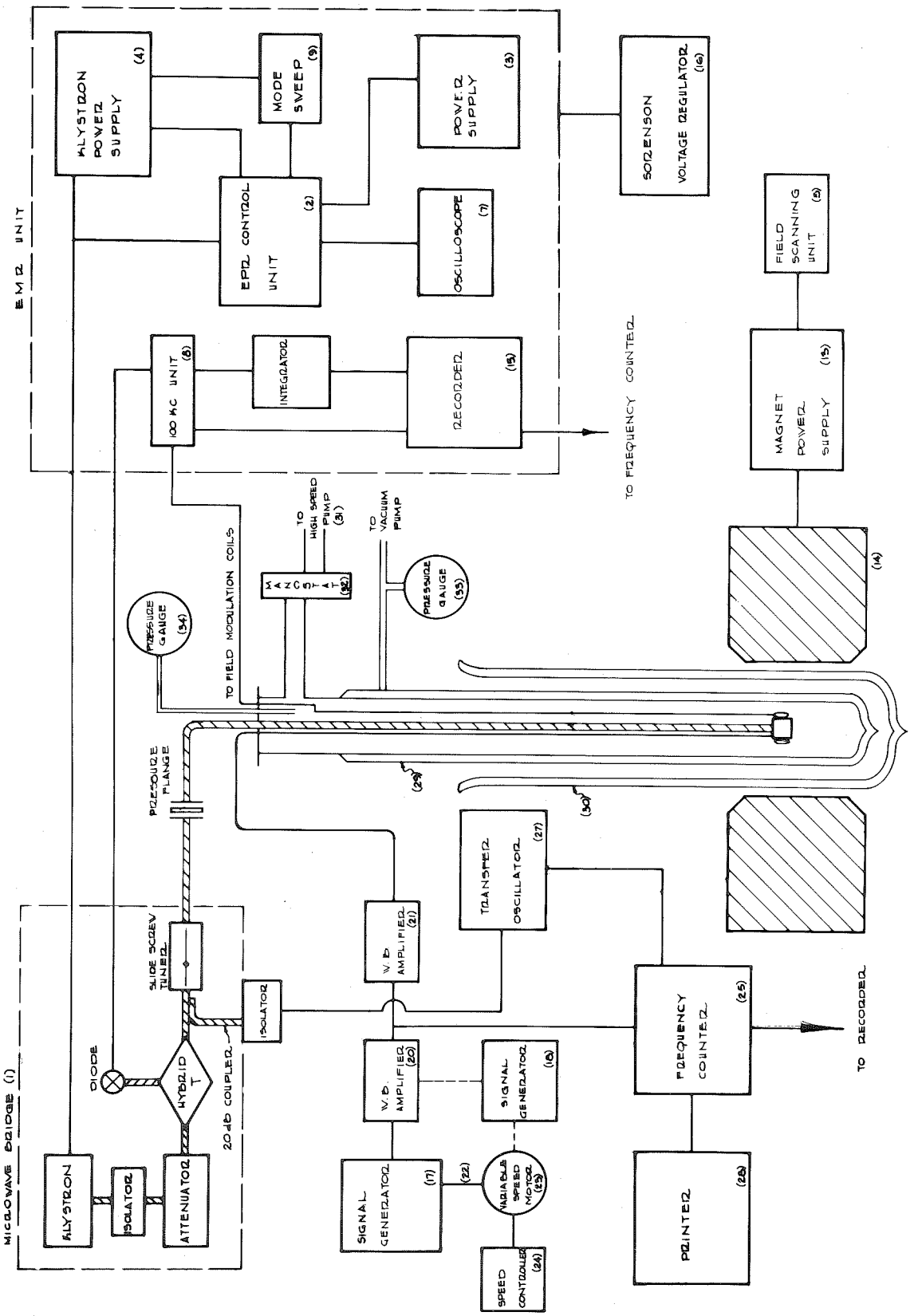

Figure 14. Block diagram

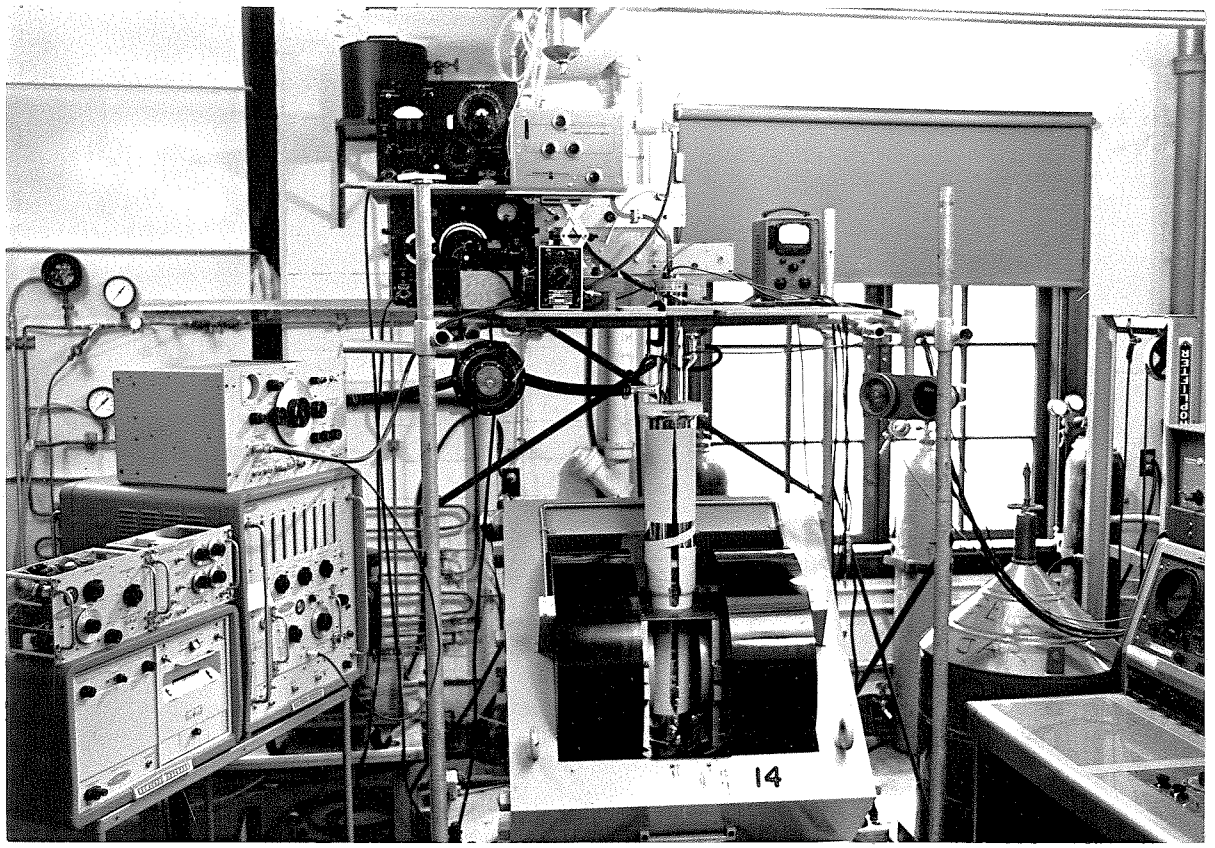

Figure 15

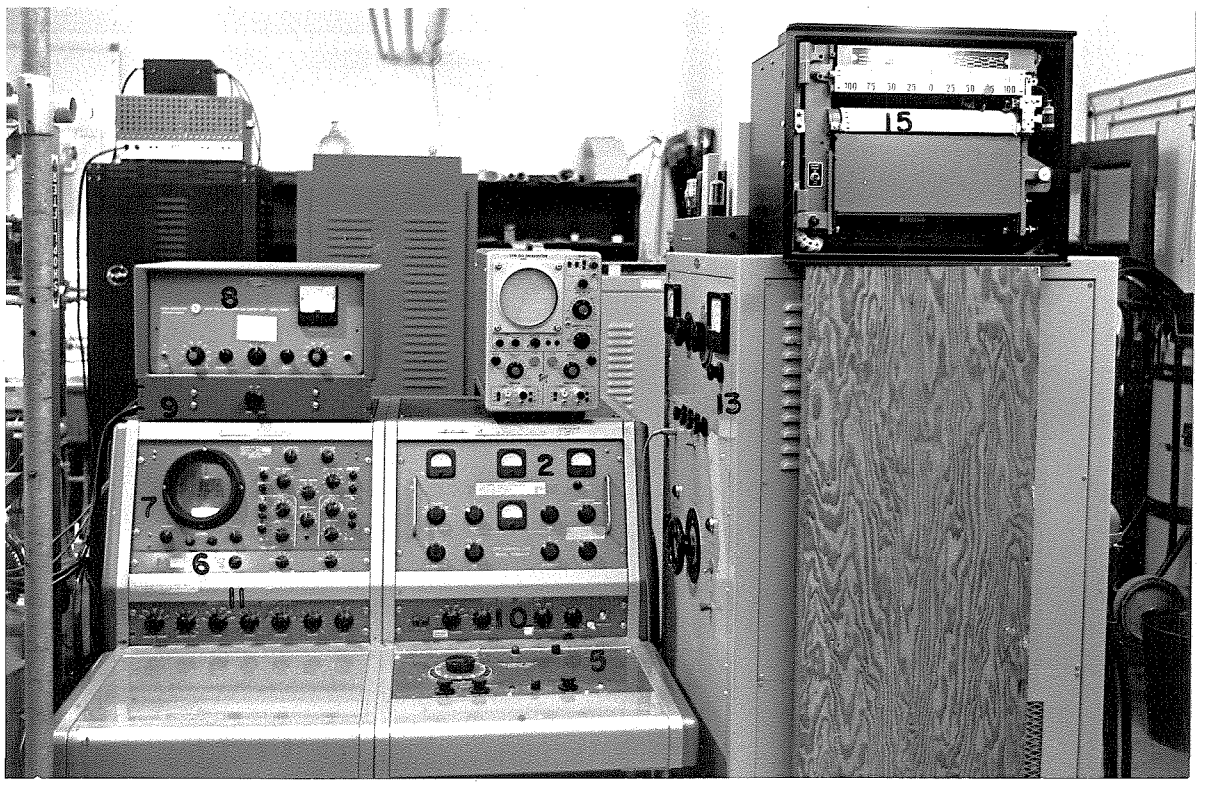

Figure 16

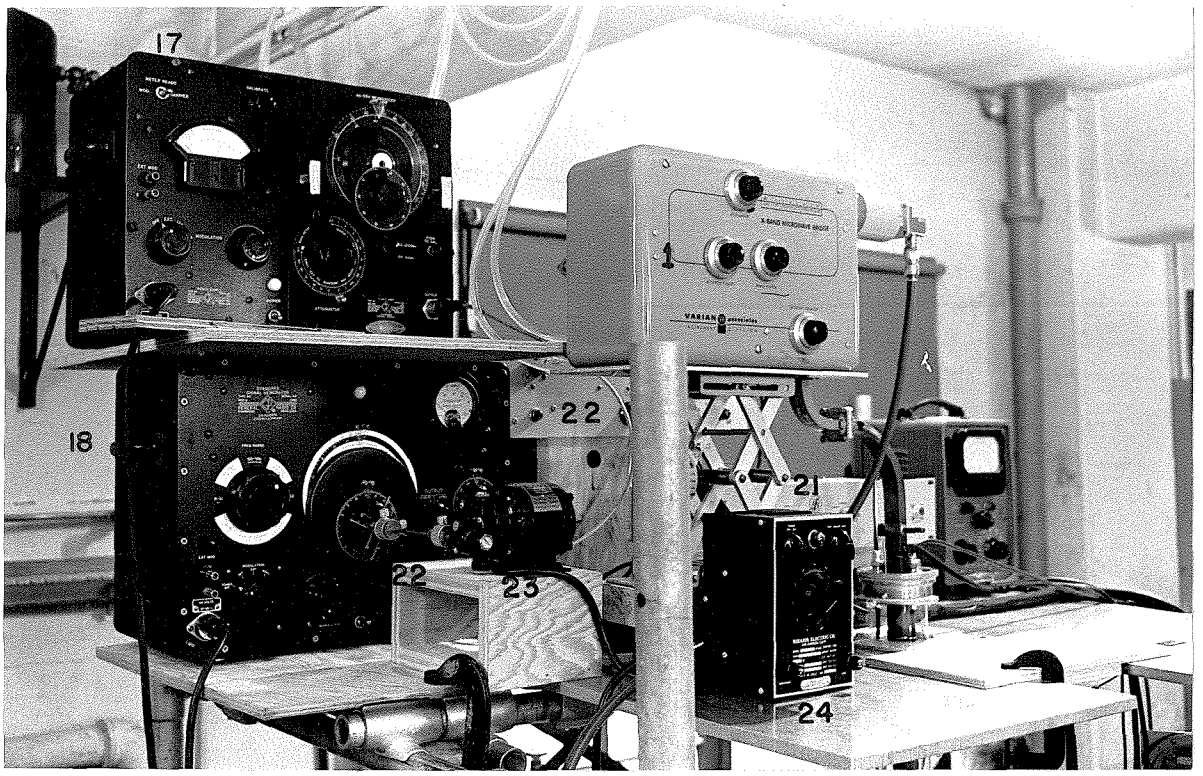

Figure 17

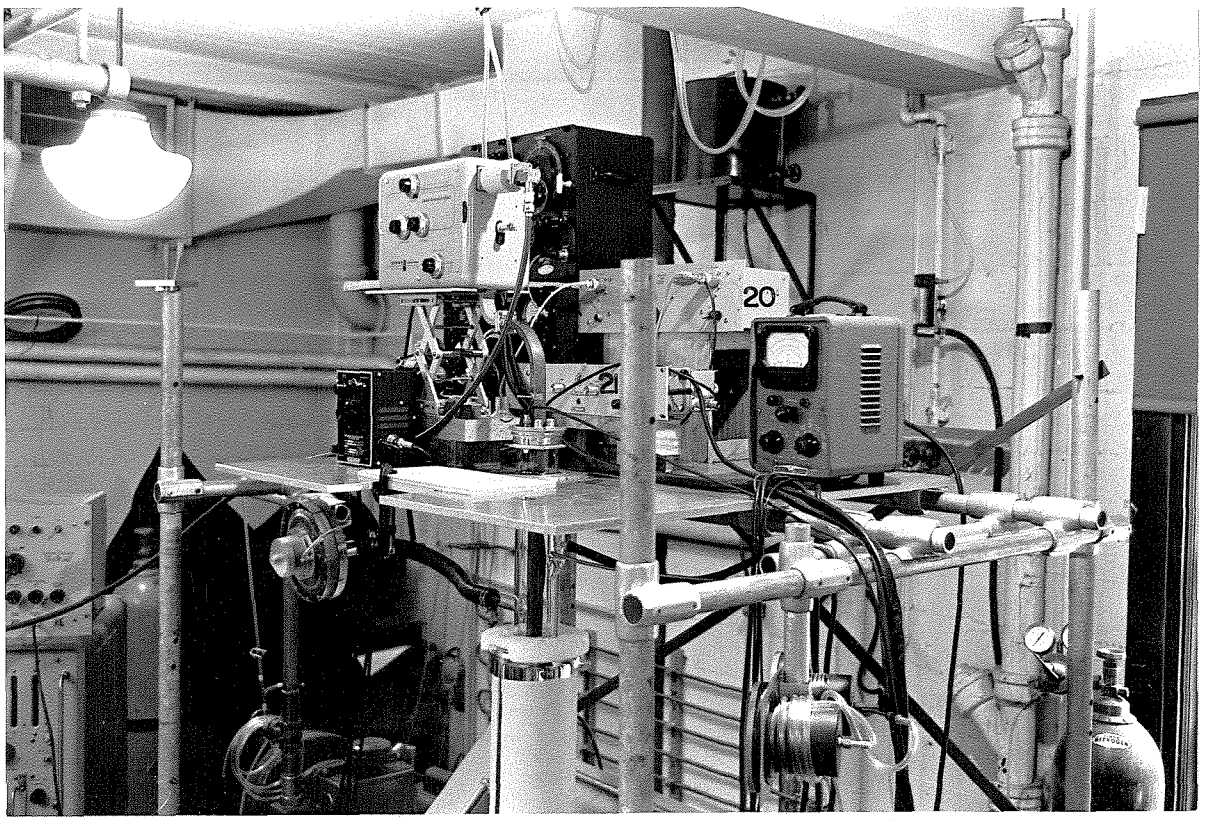

Figure 18

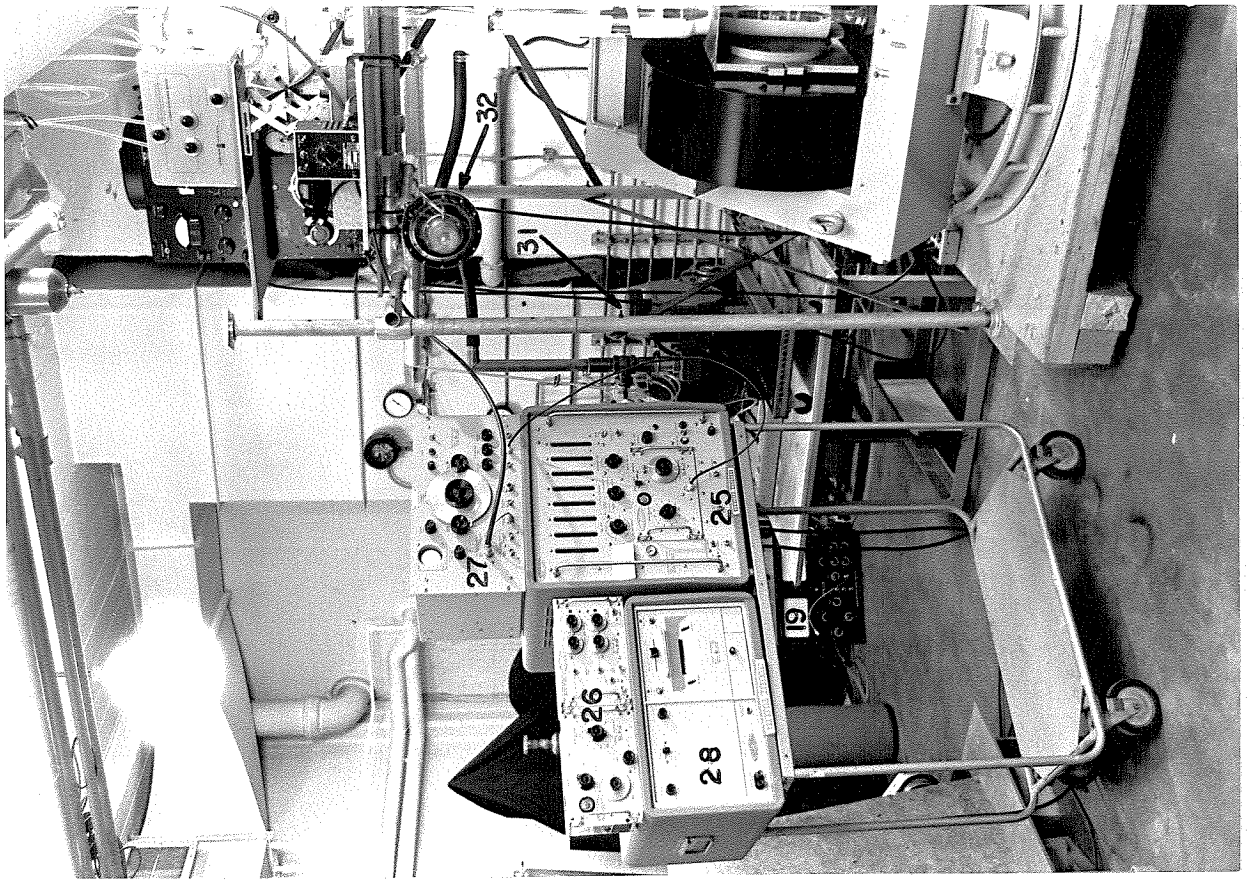

Figure 19

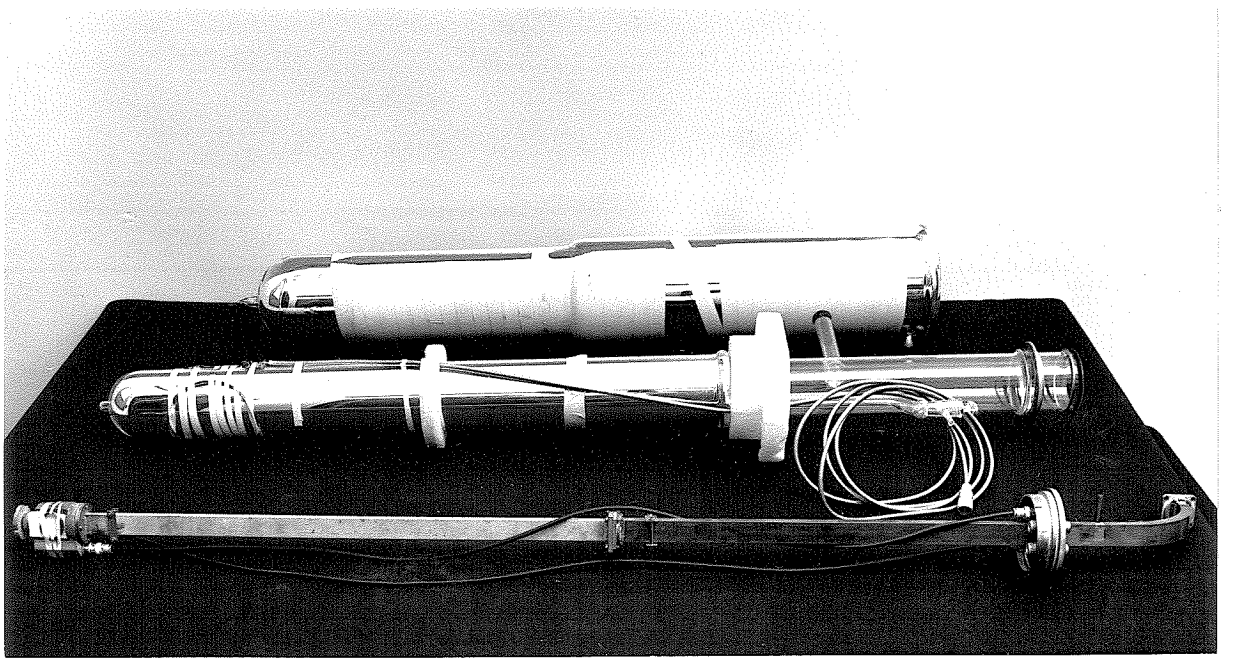

Figure 20

(10) Sweep Unit 4250 A(83)*

(11) Output Control Unit V4270A(75)*

(12) Sweep Amplifier Unit V4240(76)*

(12a) Power Supply Unit V4261B(66)*

We used the 12" magnet system made by Varian Associates. This includes

(13) the Magnet Power Supply V2100-B(292)

and (14) the Rotating 12" Magnet V4012-313(332)

In all the ENDOR experiments both 1.75" pole caps were removed from the magnet leaving a 5.20" gap. This did not seem to cause any additional line broadening in our solid state free-radicals.

The data was recorded with a

(15) Brown Recorder (-5 to + 5mV).

Line voltage for the spectrometer is controlled by a

(16) Sorenson A.C. Voltage Regulator 1000-S.

The ENDOR equipment directly involved in producing the rf in the cavity coil included:

(17) General Radio Signal Generator (40-250 Mc)
(40-250 Mc)1021AV(2023)

(18) General Radio Signal Generator
(5kc-50Mc)1001A(3482)

(19) Simpson TV-FM Signal Generator**
(2-250Mc) 479 (modified)

---

*These items are not used in present ENDOR experiments although they were used in the early experiments.

**We added a "Varicap" to the oscillator for f.m. purposes. We tried using this generator in place of the GR Generators but found numerous spurious signals. This unit was abandoned until further work could be done on shielding the system.

(20) Hewlett Packard (HP) Wide-Band Amplifier
460AR(4066)

(21) Instruments for Industry Wide-Band Amplifier
500 A (110-6003P)

ENDOR components are shown more fully in Figure 17 and Figure 18. The output (about 1 volt) of the GR generators was fed to the HP WB Amplifier which had about 10db gain. The output from this amplifier was then fed through the IFI WB Amplifier (gain = 10db) to the rf coil in the cavity. Both amplifiers are of the distributed type having a 200Mc band-width. However, since the rf coil has fixed inductance, and, furthermore since the feed lines are about 4' long the actual power delivered to the rf coil can vary quite drastically with frequency.

The frequency was varied by driving the GR generators through a

(22) General Radio Coupling Unit (GR part # 1750-301)

with a

(23) Bodine D.C. Motor Type NSE-11R*

whose speed was controlled by a

(24) Minarik Speed Controller SE-11(2810).

The rate (and direction) of sweep could thus quickly be varied by a factor of 1-100.

For the purposes of frequency measurement (both rf and microwave) we used a

(25) Hewlett Packard Frequency Counter**

(26) with plug in units for frequency range 10-250 Mc**

---

*The motor was geared down in the ratio 324:1. Maximum speed of slow shaft was 21 rpm.

**Borrowed from E.E. Department.

(27) HP Transfer Oscillator*

and a (28) HP Printer**

The rf frequencies were recorded directly on the chart paper by manually simultaneously gating the frequency counter and a side pen on the recorder. The instantaneous frequency was recorded by the printer and this gave a point by point plot of the rf frequencies. The system was gated about 30 times per minute.

The importance of high (S/N) in the ENDOR experiment has been emphasized. Therefore, the first step in the experiment is to make a relative maximization of (S/N).

After the spectrometer has warmed up for at least an hour the procedure recommended by Varian Associates is followed. This includes impedance matching of the microwave crystal diode and adjusting the phase of the phase sensitive detector. Both of these quantities are a function of the klystron frequency. It has also been empirically established that for our unit the optimum phase setting is a function of the 100kc modulation amplitude.

For microwave detection a 1N23F crystal diode was used.† These diodes should be rechecked before each major experiment because their characteristics are sometimes greatly affected by the treatment they

---

*Supplied by A. F. Hildebrandt.

**Borrowed from E.E. Department.

†This nomenclature replaces that of Microwave Associates' MA423A. According to Varian Associates the 1N23F gives the best (S/N) with their system. We further selected from several 1N23F crystals that which gave the best (S/N).

receive. For example, it has been found that a sudden increase in the crystal biasing current can considerably reduce (S/N).

Having maximized (S/N) one next makes a measurement of the absolute sensitivity. A special high-Q cavity (see Part II) was used for this measurement. (It should be noted that everything will need to be remaximized when the actual ENDOR cavity is used. However, this procedure will apprise us of the range of sensitivity possible using the ENDOR cavity.) A crystal of ruby weighing 250 micrograms having a concentration of Cr^{+3} of 0.05% was prepared. This is equivalent to about 10^{15} spins (S = 3/2). The ruby spectrum consisted of four lines each about 30 gauss wide. So for (S/N) = 1 the sensitivity was about 10^{13} ΔH spins. ΔH is the half-power line width. (In other words, if one had a sample for which ΔH = 1 gauss = 2.80 Mc one could detect 10^{13} spins.) Actually for our measurements (S/N) $\approx$ 5. Furthermore we were using only a 6 gauss (p to p) modulation amplitude. The maximum sensitivity as given in the Varian specification is $2 \times 10^{11} \Delta H$ spins. The measured sensitivity was within a factor of 10-50 of the rated sensitivity and therefore we felt justified in proceeding with the ENDOR experiment.

An important step that can best be considered here is that of the crystal alignment. The crystal mount (Fig. 11) was prepared to close tolerances so that the crystal was known to be in one plane (the c/2 plane) to within less than 30'. An edge of the crystal was then aligned relative to a mirror mounted on the outside of the cavity by using a microscope mounted on a milling machine. This could be done to a tolerance of about 10'. After the cavity had been mounted on the silvered stainless steel wave guide and inserted into (see Fig. 20)

(29) the helium dewar

and (30) the nitrogen dewar

within the magnet gap, a sighting was made on the mirror using an auto-collimator. The mirror orientation was thus related to the orientation of the pole faces of the magnet. This entire procedure allowed one to determine the crystal orientation to within about $\frac{1}{2}^{\circ}$.

The cool-down procedure follows. Liquid nitrogen is first added to the outer dewar and a pressure of about 1 atmosphere is maintained in the jacket of the helium dewar.*

After the contents of the inner dewar have cooled down over a two hour period the helium dewar jacket is evacuated and the stop-cock closed. Finally liquid helium is transferred.

We were able to cut our helium consumption by a factor of three (to three liters per experiment) after going consecutively through five defective transfer tubes. Two of these were new commercial units so poorly constructed that a minimum of 2 cm^2 contact area existed via dielectric spacers between the inner and outer tubes.

Once the helium transfer was completed we either proceeded directly to the EMR experiment or in several cases we pumped on the helium using

a (31) Cenco 13 cu. fpm pump**

and controlled the pressure with

a (32) manostat (see Part II).

---

* It is very important to flush the helium dewar jacket with nitrogen gas several times before each experiment because of the rather high rate of diffusion of helium through glass.

**Loaned to us by P. V. Mason.

We normally took about 30 minutes to get below the lambda point of helium. This gave the cold helium gas a chance to cool the components in the dewar.

Having attained the helium temperature range one looks for the EMR signal at low power to avoid saturation. It is wise to take a good EMR spectrum to compare with the room temperature spectrum for that orientation. (See Fig. 9.)

Typical operating conditions for ENDOR were

Klystron frequency	9017 Mc
Microwave power (incident or cavity)	60mW
100kc modulation amplitude	5G(p to p)
Time constant	0.3-1.0 sec
Signal voltage gain	80-90 db
Recorder chart speed	2 inches per minute
rf scan rate	5-500kc sec^{-1}
rf power	3 watts (1G rf field in coil)

The experimental set up allowed the observation of X" only. The LLMT model indicates that this is a poor way to do the experiment. Furthermore, field modulation is not the best way to observe the ENDOR signal. However, at <u>that</u> time this was the only feasible way for us to do the experiment.

We therefore proceeded to set the magnetic field at either peak of the <u>derivative</u> of the absorption curve. Clearly, it is important that the magnetic field remain at this value over a prolonged period of time. For this reason the magnet system was allowed to stabilize for about three hours and was then cycled in a modified way. This eliminated drift problems--at least as far as the magnet was concerned.

The distant ENDOR line, when observable, is much more intense than the local ENDOR lines. Therefore we always first looked for the

distant ENDOR line. For protons this falls at 13.5Mc in a field of 3175 gauss. One can usually see a rather strong signal at this frequency. At elevated rf powers the line is quite broad due to its inherent nature and one is particularly interested in splittings found on the wings since these represent the long-range dipolar interactions.

We therefore scanned the range 0 Mc $\leq \frac{\omega}{2\pi} \leq$ 13.5 Mc. About 25 lines were observed! See Figure 21. It soon became evident that these obeyed the relationship

$$n \frac{\omega_i}{2\pi} = 13.5 \text{ Mc} \qquad \text{where} \quad n = 1,2,3 \cdots 25.$$

Due to the high rf powers used and the intensity of the distant ENDOR line the transition of the distant ENDOR line was induced each time the generator moved through a sub-harmonic of 13.5Mc. It was not obvious whether the harmonics were generated in the glutaric acid crystal itself or whether they were due to signal distortion. Although the wave form appeared as a "pure" sine wave on an oscilloscope the latter is most reasonable. Furthermore, a reduction of rf power by a factor of 100 causes the harmonic lines to disappear and then the distant ENDOR line for n = 1 takes on the width and shape which the n > 1 lines had.

In one sense the harmonic lines were convenient since they allow one to measure ν_p without the necessity of reducing the rf power at 13.5Mc. However, in general the presence of these lines can obscure any local ENDOR line whose frequency is less than 13.5Mc. Therefore, in future experiments this problem will have to be resolved.

In ruby we had observed symmetrical ENDOR lines. (See Fig. 13.) However in glutaric acid the ENDOR line shape had the same shape as discussed in Section B (Fig. 3). The center frequency of the line was

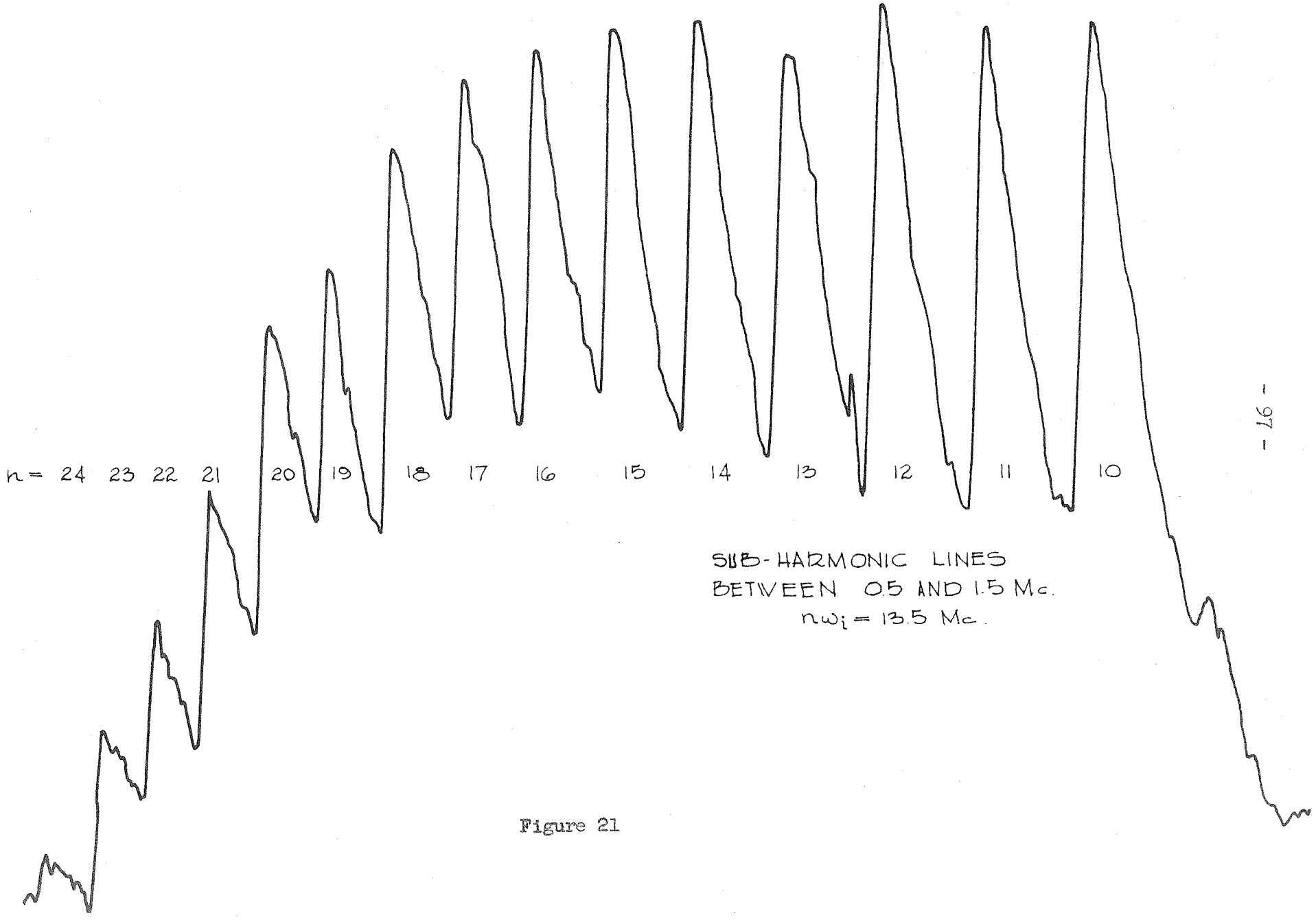
n = 24 23 22 21 20 19 18 17 16 15 14 13 12 11 10
SUB-HARMONIC LINES
BETWEEN 0.5 AND 1.5 Mc.
$n\omega_i = 13.5$ Mc.

Figure 21

determined by scanning through the line several times in both directions. Then the normalized signal intensity was plotted versus frequency for all these spectra and the average of the cross-over points for each pair of scans was taken as the center frequency. The whole procedure is rather tedious!

Finally it should be mentioned that the existence of the distant ENDOR line is very convenient since ν_p has to be known accurately in order to calculate $\underset{\sim}{A}$ from the measured ENDOR frequencies. The presence of the distant ENDOR line eliminates the need for accurate field measurements. This concludes the remarks on the ENDOR experiment.

G. ENDOR DATA, SUMMARY AND CONCLUSIONS

ENDOR Data

The lines observed in obtaining the ENDOR data in glutaric acid can be divided into two broad groups.

1. Lines which correspond to predicted ENDOR lines.
   a. In crystal X. This crystal had been been x-irradiated for 6 hours and u.v.-irradiated for about 4 hours.
   b. In crystals Y and Z. These crystals had been x-irradiated for about 6 hours and u.v.-irradiated for about 8 hours.
2. Lines which do not correspond to predicted ENDOR lines.
   a. "Sub-harmonics" of the distant ENDOR line.
   b. Electronic pick-up signals.
   c. Unexplained lines.
   d. Lines near 13.5Mc.

In Figure 22 the glutaric acid data is presented in such a way as to illustrate these various groups. For $\vec{H}_o \parallel \vec{a}, \vec{b}$ crystals X and Y were used. For $\vec{H}_o \parallel \vec{c}^*$ crystal Z was used. The results are plotted so as to bear out the spectrum obtained for each crystal for the appropriate orientations. Above each spectrum for the three orientations are indicated the frequencies calculated from the room temperature hyperfine tensors. These calculated frequencies are marked with an arrow labeled with the proton that gives rise to those transitions.

Although a wide range of intensities were found in the measurements we do not in general show relative intensities. The reason is

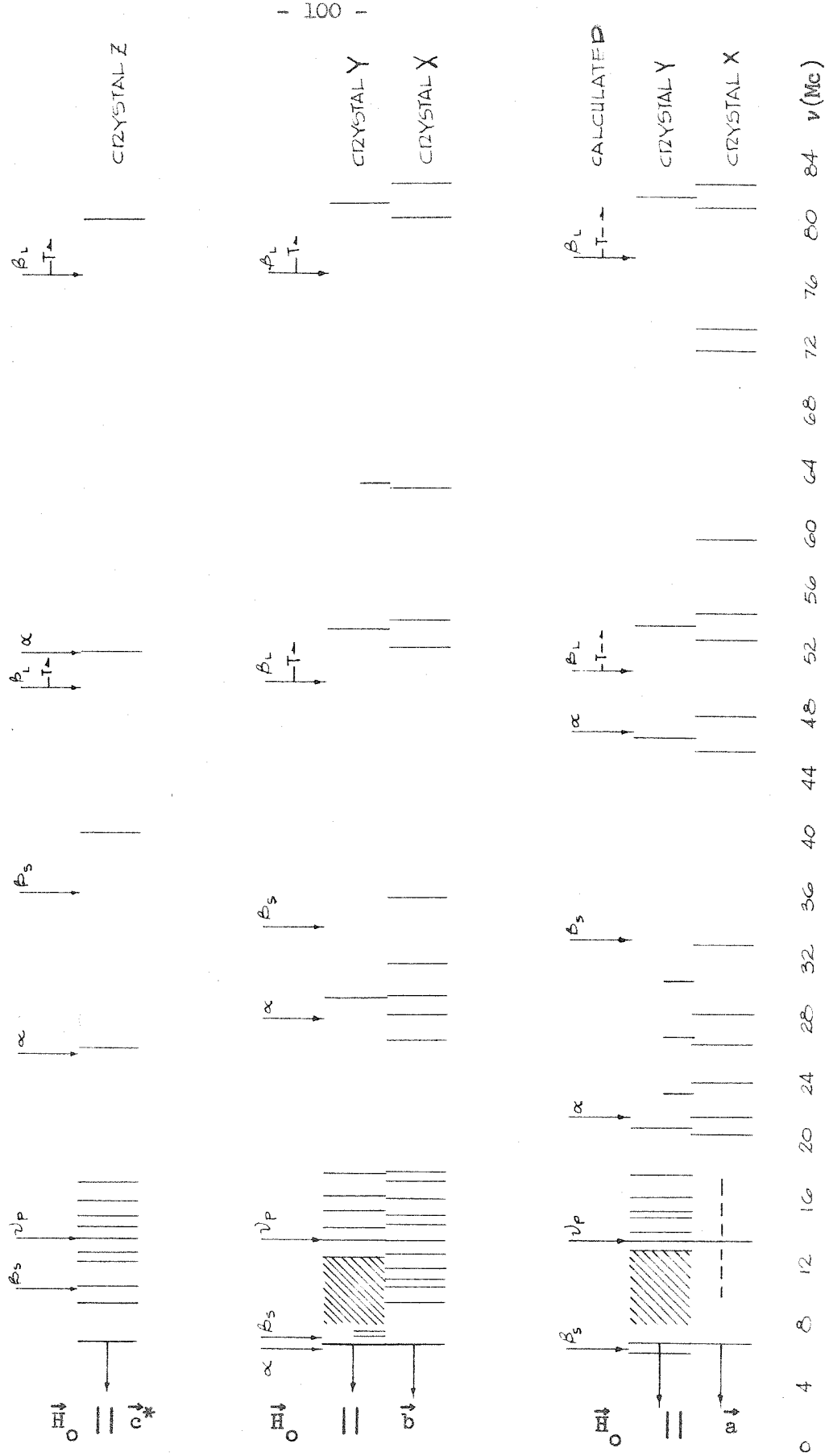
CRYSTAL Z
CRYSTAL Y
CRYSTAL X
CALCULATED
CRYSTAL Y
CRYSTAL X
β_L
T
α
β_s
ν_p
H_o
c*
b
a
0 4 8 12 16 20 24 28 32 36 40 44 48 52 56 60 64 68 72 76 80 84 ν(Mc)

Figure 22

that it is not known whether the various intensities are due to changes in the rf level or due to differences in transition probabilities. Short lines indicate transitions which are very doubtful because $S/N \approx 1$.

For the sake of clarity any indication of the line-widths is omitted. Usually these were between 0.1 and 0.5 Mc. In the case of crystals Y and Z the "coalesced" lines (80 Mc for example) were as wide as 1.0-1.5 Mc.

Diagonal lines designate those regions of the spectrum in which we were unable to make measurements because of serious pick-up problems. An arrow pointing toward 0 Mc from the 6.75 Mc line indicates that true ENDOR lines—if they fell in this region—would in all probability be masked by the sub-harmonic lines.

For $\vec{H}_o \parallel \vec{a}$ we show with dashed lines the fact that we did not look for lines around 13.5 Mc. Finally we imply by —T— that the calculated values for the ENDOR transitions must almost certainly be low because of the change in splittings that occurs in going to low temperatures. Careful measurements on this were made for only one orientation and there the change was found to be about 10 Mc. Rough checks for the other orientations also indicated an increased splitting.

The first task was always that of finding the distant ENDOR line at 13.5 Mc. One could then use this rather intense line to maximize S/N. Invariably S/N increased with

1. increased field modulation
2. increased rf power
3. increased microwave power

and 4. with the precision with which one could sit at the point of maximum slope on the EMR absorption line.

The same seemed to hold true for the local ENDOR lines. Figure 23 shows a typical distant ENDOR line observed at low rf powers. Both the forward and reverse scan are given. The relaxation times are such that at least 30 seconds must elapse between such scans or one will not see a signal on the reverse scan. Figure 23 also shows the decay rate of a distant ENDOR line. The rf was turned off when the scan reached the maximum peak of the line. This spectrum would indicate a nuclear relaxation time of the order of 10 seconds.

The second task was of course to find the local ENDOR lines. Figure 24 indicates our success. These lines are always considerably less intense than the distant ENDOR line and some of the lines were presumably not observable at all with the available sensitivity. This then is a major objective of future experiments--to increase sensitivity.

The fact that the ENDOR lines are only about ten times narrower than the EMR lines is somewhat disappointing. There are two obvious factors which might contribute to this line width.

1. Field inhomogeneity (Cole, et al. also used a 5" magnet gap).
2. Orientational disorder of the radicals.

The fact that the latter might make a measurable contribution seems to be borne out by the difference in the results for crystals X and Y. The doublets in crystal X seem to indicate two orientations differing so little that it would not be detected in the usual EMR measurements. The measurements on crystal Y seem to point to the fact that extended u.v.-treatment caused a spread in orientation about some average value. The coalesced lines in crystal Y are always broader than the individual lines in crystal X. See Figure 25. There are almost certainly other contributions to the line width which are related to our reference in Section B

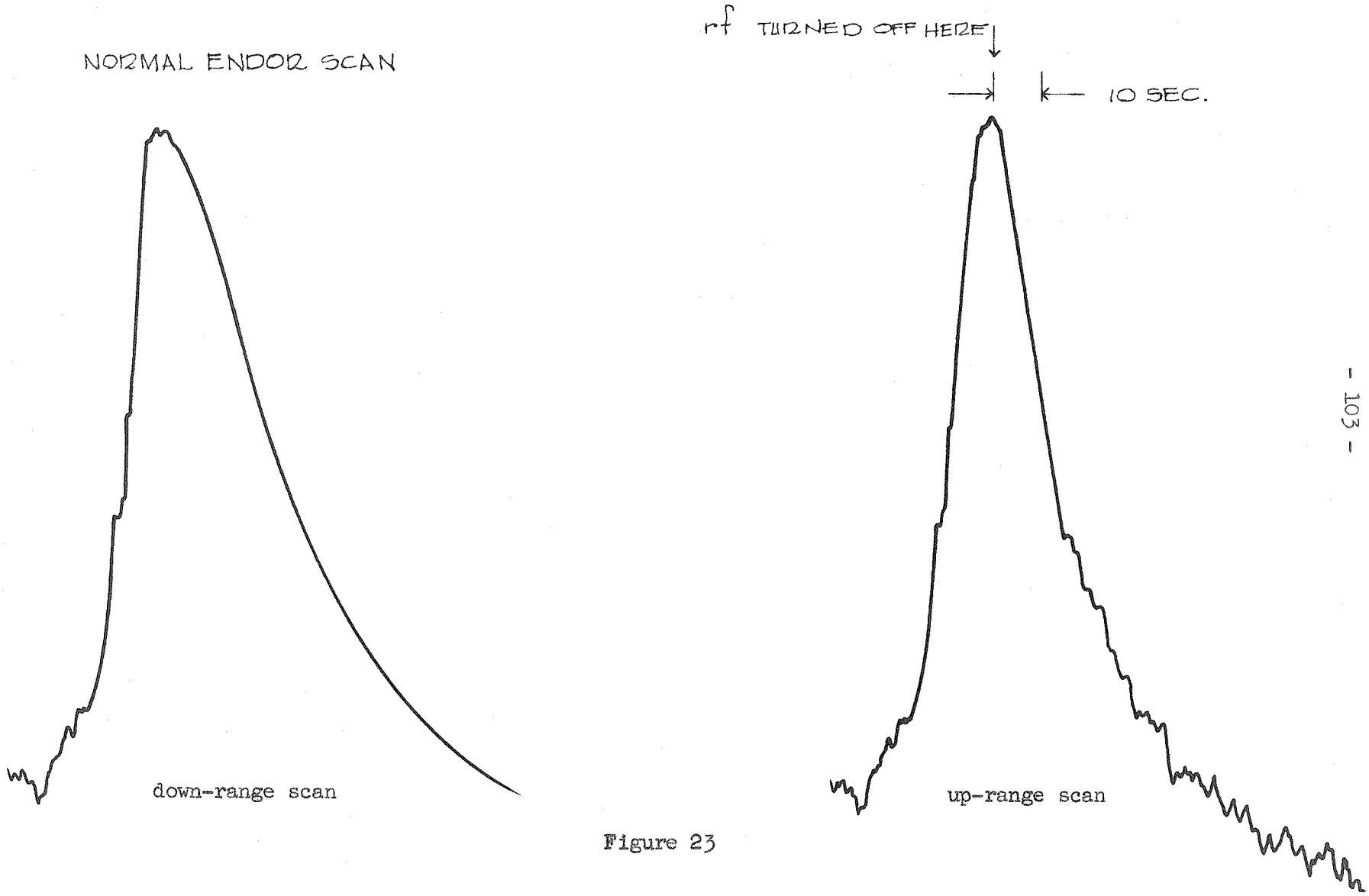
NORMAL ENDOR SCAN
down-range scan
rf TURNED OFF HERE
10 SEC.
up-range scan

Figure 23

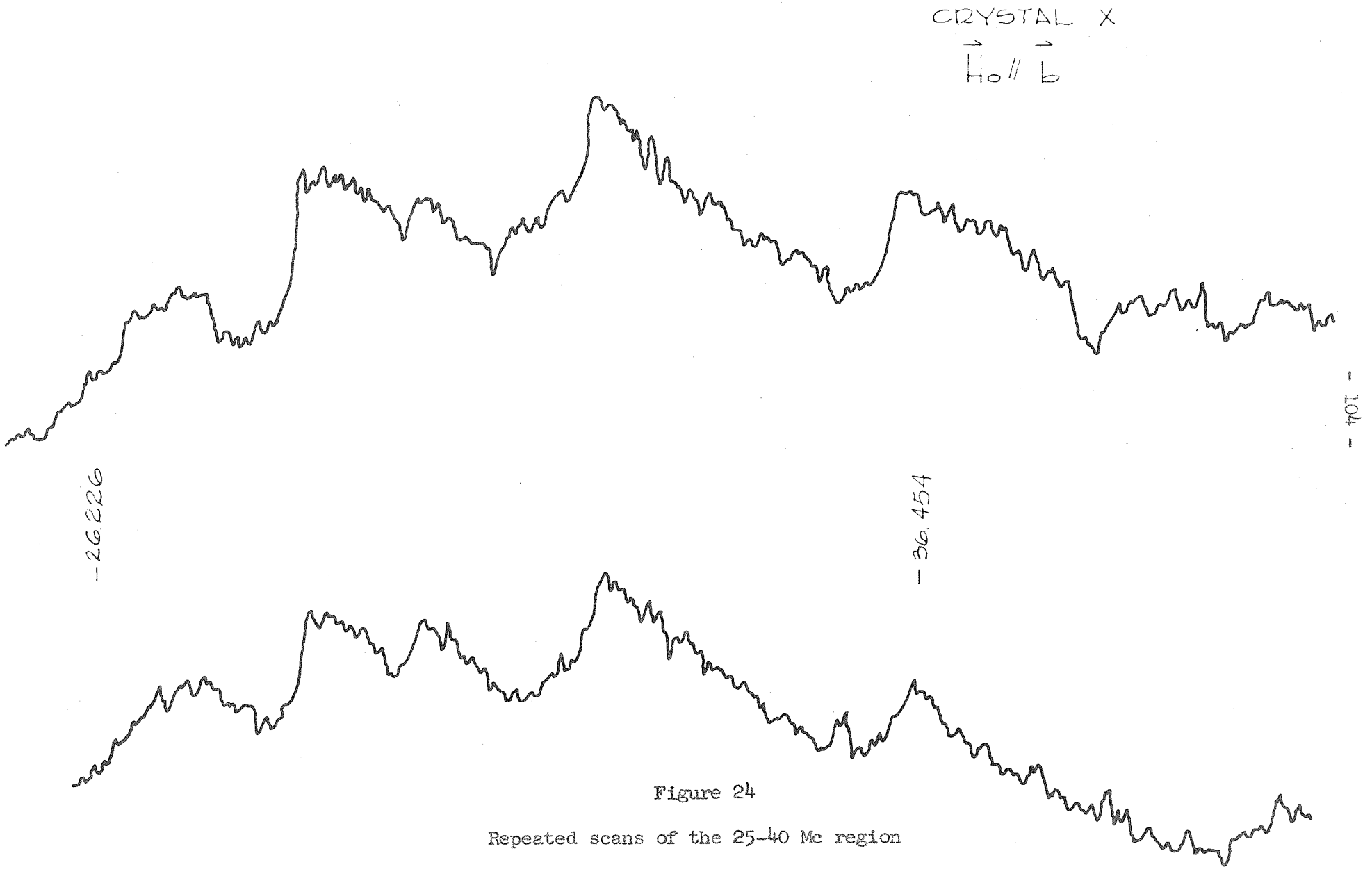

Figure 24

Repeated scans of the 25-40 Mc region

DOUBLET COLLAPSE
$\vec{H}_o \perp \vec{a}$
41.944
43.093
44.268
45.633
46.956
48.441
43.788
45.397
46.543
47.839
49.094
(Mc)

Figure 25

to the line broadening processes for the EMR lines. ENDOR thus provides a means whereby such effects can be studied.

Another feature which is somewhat disturbing is the variation with temperature of the proton splittings. We indicated that for $\vec{H}_o \parallel \vec{c}^*$ the splitting for the β_L-proton becomes about 10 Mc greater at low temperatures than it is at room temperatures. Therefore the ENDOR frequencies will be about 5 Mc higher than calculated from the room temperature data.* (The α and β_S-proton splittings remained constant to within the accuracy of EMR measurements for $\vec{H}_o \parallel \vec{c}^*$.) This is borne out by our results. Note that for all three orientations the α-proton splittings seem not to be affected by the temperature change.

Why the ENDOR lines for the β_S-proton are so elusive is not known. The low frequency transitions of each pair may well have been masked by other signals. However, the high frequency lines should have been observed. For $\vec{H}_o \parallel \vec{b}$ the low frequency transition for the α-proton, $\nu_-^{(\alpha)}$, was probably also masked by the unwanted signals. It is conceivable that either the 7.3 or the 7.6 Mc line (shown as short lines) may be the $\nu_-^{(\alpha)}$ line.

In practice we were usually able to measure the lines with a precision of 1:10^4** as compared with EMR where the precision is less than 1:10^2. So by ENDOR one gains a factor of about 100--if one neglects the difficulties mentioned above. Those difficulties--

---

*ENDOR frequencies are given approximately by $\nu_\pm \approx \frac{\mathscr{A}}{2} \pm \nu_p$.

**Not true for lines near 13.5 Mc.

orientational disorder, temperature dependent splittings, and absence of several lines--vitiate the significance of an accurately calculated hyperfine tensor. (It is trivial to calculate such a tensor from the data using the procedure given in Section B.) Furthermore, a rather significant point arises when one looks at the cases where both ν_+ and ν_- have been observed for one orientation. The calculated values for $\delta' = \nu_+ - \nu_-$ are different than the measured values. The difference is probably greater than experimental error and indicates that the problem needs to be treated in higher order.

The origin of many of the observed lines which have the characteristics of real ENDOR lines is unexplained. Several of these occur in crystal X but not in Y. The sub-harmonic lines have been explained and they are primarily a nuisance. Some lines are strictly electronic in origin and their characteristics differ from those of the ENDOR lines. We always made a dry run in which $\vec{H}_o$ was set to a point far removed from the EMR lines. In this way the lines which were unrelated to the glutaric acid spectrum could be identified.

Finally there are the lines near 13.5 Mc, which we had hoped could be designated as γ-proton lines. See Figure 26. However it would seem that there are more lines than would arise from just the γ-protons.* This is not unreasonable since one might expect that the ω_α-proton could interact about as strongly with the unpaired electron as the γ-protons do. What other contributions one might have from nearby nuclei is unknown. It would therefore be presumptuous to

---

*The precision with which these lines can be measured is rather poor primarily because of the poor S/N. This may partially explain the differences between crystals X and Y for $\vec{H}_o \parallel \vec{b}$.

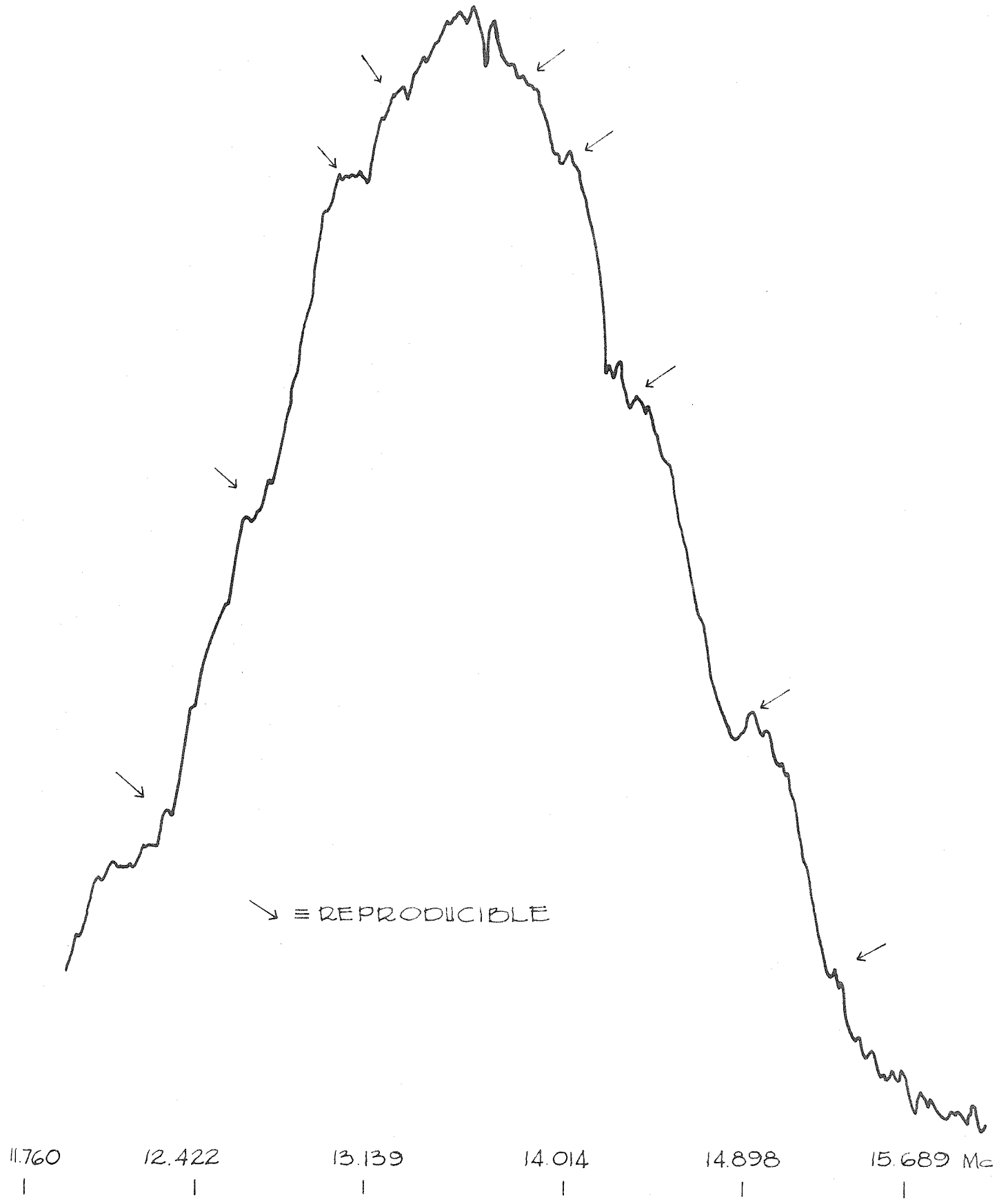

Figure 26

arbitrarily assign any of these lines to the γ-protons. More detailed study (isotopic, for example) is in order. The need for increased sensitivity is here again emphasized.

Summary and Conclusions

The initial purpose of this research was to observe ENDOR in an organic free-radical. This has been successfully accomplished. The complete ENDOR system has been described in detail. Although these experiments have yielded much information the need for improved sensitivity has been emphasized repeatedly. There are at least four ways in which such an improvement can be made. In Section B it was pointed out that the LLMT model predicts a much more intense ENDOR signal for dispersion than for absorption measurements. Since we have been able to observe the distant ENDOR line this model may have some applicability in this system. If it does then one can increase S/N

1. by looking at the dispersion effect. We are not set up to do this at present.

Furthermore, detection via straight field modulation does not result in the best S/N. This can be improved

2. by pulse modulating the rf for detection purposes.

From what has been said earlier S/N can also be increased

3. by increasing rf power

and 4. by increasing microwave power.

In spite of the temperature dependent problems already discussed low temperatures are still necessary to maintain a high S/N. Needless to say, a fuller understanding of the ENDOR mechanism in organic systems would also help in sensitivity optimization.

During the course of preliminary investigations of free-radicals suitable for the ENDOR experiment a rather pronounced effect was observed to take place in glutaric acid. When single crystals of x-irradiated glutaric acid containing the radicals A and B are u.v.-irradiated radical B essentially disappears. The complete hyperfine tensors for the A radical were calculated from the room temperature EMR data. Procedures were described for

1. Calculating hyperfine and g-factor tensors from EMR data
2. Calculating hyperfine tensors from ENDOR data.

From the ENDOR data on glutaric acid we had also hoped to obtain more precise values for the hyperfine tensors and to determine the γ-proton coupling constant. As was pointed out, however, the calculation of the hyperfine tensors from the ENDOR data is not particularly meaningful because of uncertainties relating to temperature dependent line shifts and orientational disorder. The latter effect, essentially not observable by EMR is well resolved by the ENDOR technique. Furthermore, although the magnitude of the γ-proton coupling constant cannot be given, we can state that the interactions of the electron with other "nearby" nuclei must be taken into account. The value of the coupling constants for many of these nuclei can in principle be determined by the ENDOR technique.

The above effects---temperature dependent splittings, orientational disorder, and interactions with "nearby" nuclei---certainly make important contributions to the EMR line width. ENDOR thus provides a means whereby such EMR line-broadening effects can be studied.

Finally, it should be noted that the work is yet in its infancy. The only two organic systems studied to date are the two saturated dicarboxylic acids. There are a large number of different organic systems amenable to such study--radical ions (CO_2^-, for example), metal complexes, unsaturated systems, etc. Even our preliminary results seem to indicate that the energy level problem needs to be treated in higher order. I predict that in the next few years the ENDOR method will be applied to many organic systems and will yield a great deal of new information on the electron-nuclear interaction. This in turn will encourage further refinement of the theoretical calculations of hyperfine interactions in these systems.

PART II

AUXILIARY EQUIPMENT

A LOW TEMPERATURE EMR SYSTEM

The detection by electron magnetic resonance (EMR) of triplet excitations in conjugated organic molecules like naphthalene requires that one irradiate the sample inside the cavity with ultraviolet (u.v.) light at reduced temperatures. There are a large number of other EMR experiments which require low temperatures, quite often liquid helium temperatures (1°-4.2°K). Therefore, it was desirable to design a low temperature EMR system which would be flexible and convenient to use.

Several types of low temperature EMR systems that allow in situ u.v.-irradiation are described in the literature (60,61). The particular features that are incorporated in the design discussed below include

1. The system employs a high Q cylindrical TE_{011} cavity
2. The microwave cavity and its coupling mechanism are at room temperature
3. The sample is known to be at a fixed low temperature
4. The sample and/or external field can be rotated for anisotropic studies

and 5. The sample can easily be changed during the course of an experiment.

In the discussion that follows this system is briefly described and detailed drawings of the components are given. We will omit the word "Part" in what follows wherever its meaning is clear. For example, when X is written it can be read Part X.

The low temperature EMR system consists basically of a helium cold finger inserted into a high Q cylindrical TE_{011} mode cavity. This

is shown in Figure 27. Figure 28 gives a cross sectional view of the dewar proper and Figures 30-35 are detailed drawings of the individual components. Figure 29 serves as an assembly guide. These components are now considered in order.

A, B, C, and D form the bottom end of the dewar proper. This dewar is of conventional design* employing 304 (nonmagnetic) stainless steel (304SS) with welded joints throughout. A is the o-ring-containing room temperature flange. B forms the bottom of the liquid nitrogen dewar or can and C the bottom of the liquid helium can.** D is an adaptor flange which matches C to the particular helium cold finger one wishes to use. As far as the dewar is concerned the inside diameter of C and D can be enlarged.

I bolted to J serves to maintain F and K coaxial. This is rather important since there is some warpage of the individual dewar sections(or cans) as they are cooled and rewarmed. This is particularly true of the helium can because of the way it is suspended. I is made of 304SS to cut down its thermal conductivity, since at this point such a contact is a potential heat leak. Typical thermal conductivities (62) are given below (in units of mW $deg^{-1}cm^{-1}$).

	4°K	300°K
Copper: hand drawn	3500	4000
annealed	17000	4000
Brass	30	1000
Stainless steel	2.5	400
Pyrex	0.9	10

*The design was obtained from Professor G. Wilse Robinson.

**The cans can clearly be filled with any refrigerant. We will use nitrogen and helium in the discussion only for convenience.

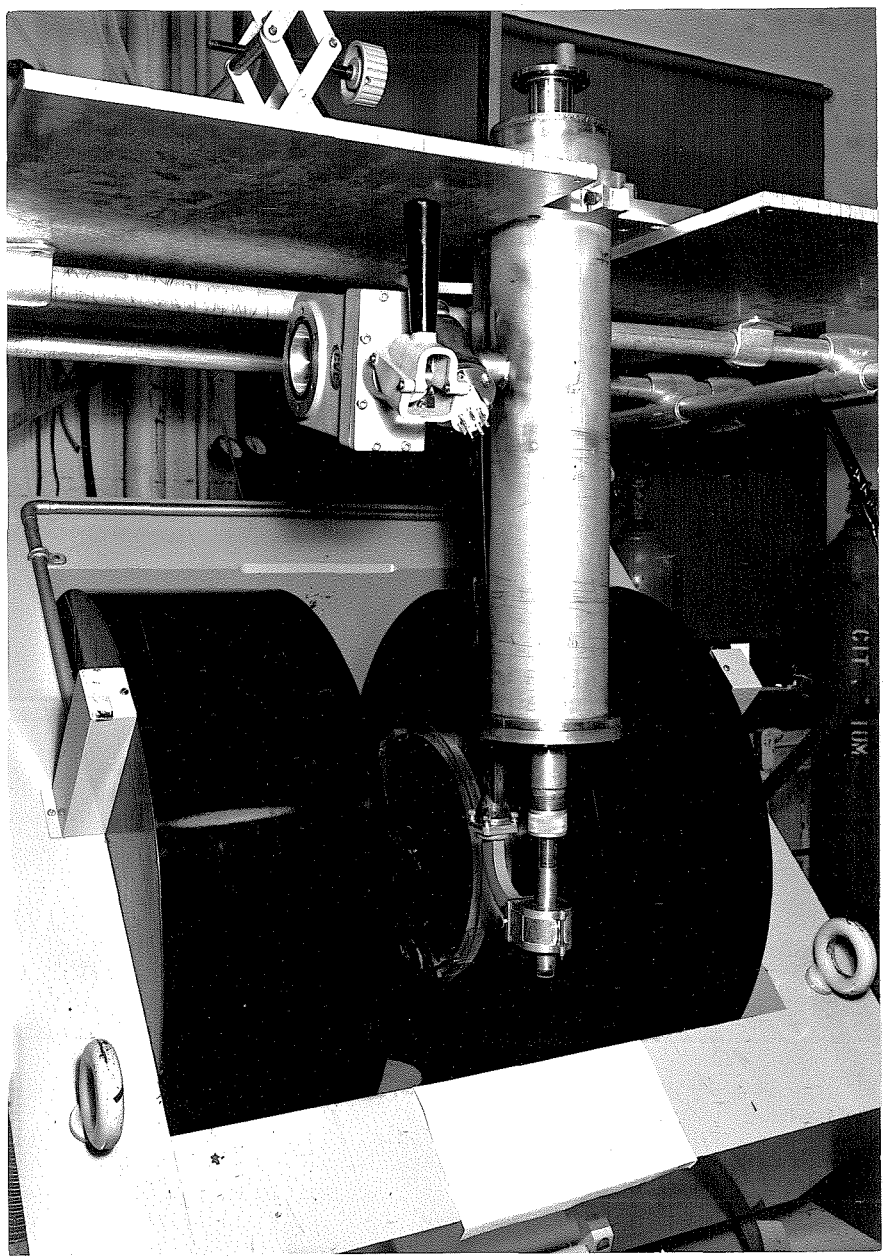

Figure 27. Low temperature EMR system

DEWAR : CROSS-SECTIONAL VIEW

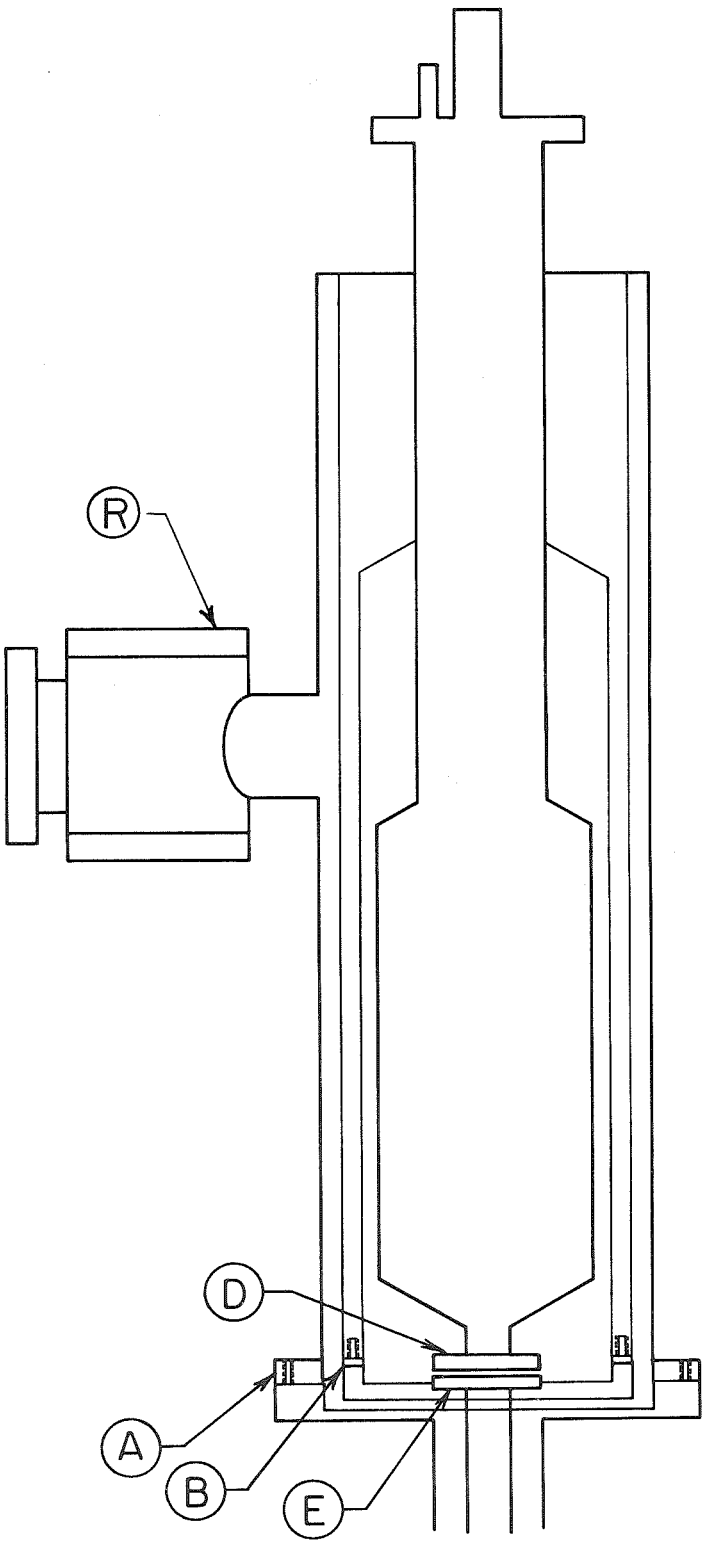

Figure 28

ASSEMBLY DIAGRAM FOR LOW TEMPERATURE EMR SYSTEM K-II

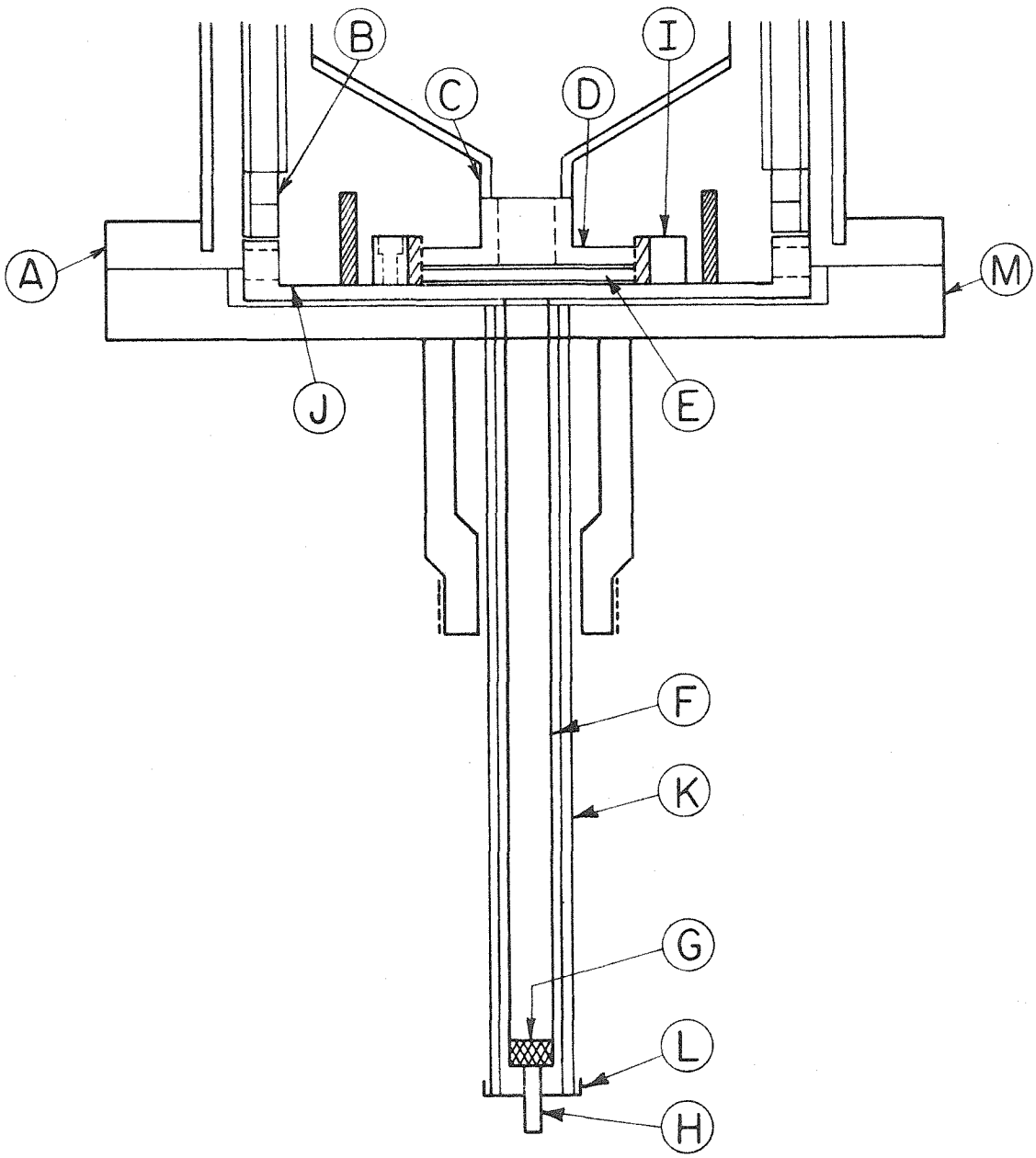

Figure 29

ADAPTOR FLANGE

(TO BE WELDED ON TO HELIUM DEWAR)

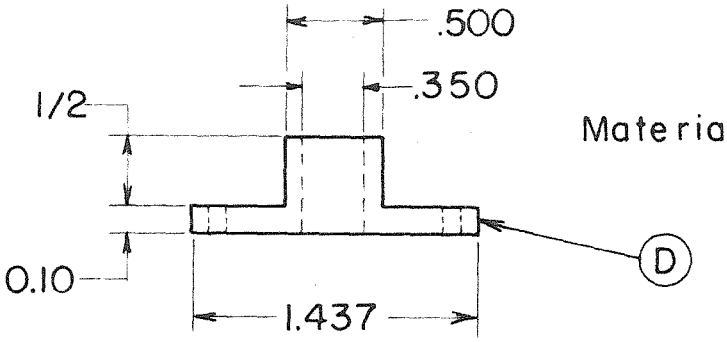

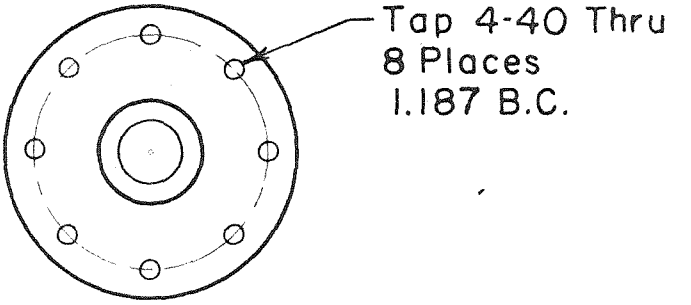

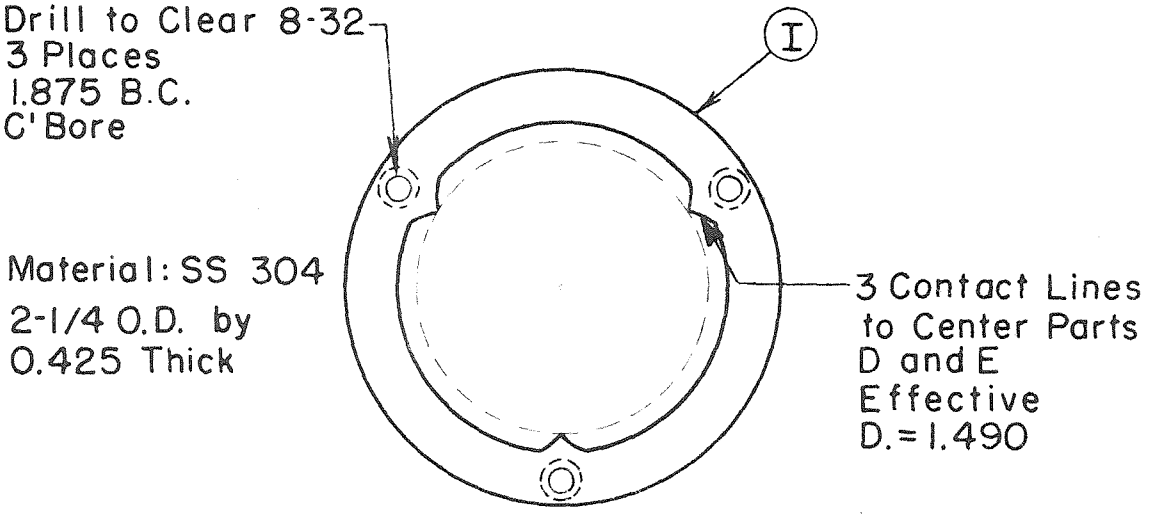

CENTERING COLLAR

Figure 30

HELIUM FINGER

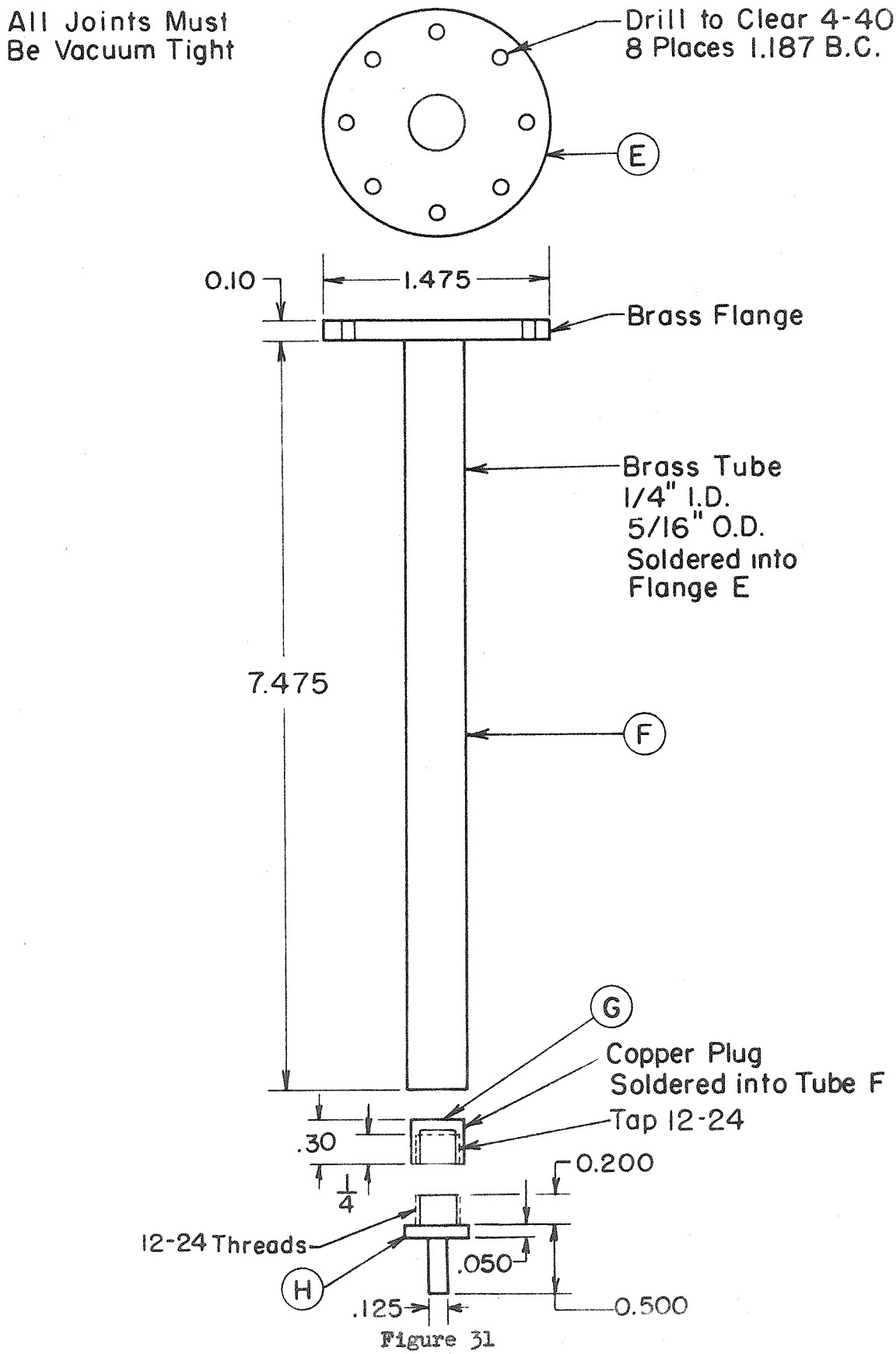

Figure 31

NITROGEN SHIELD

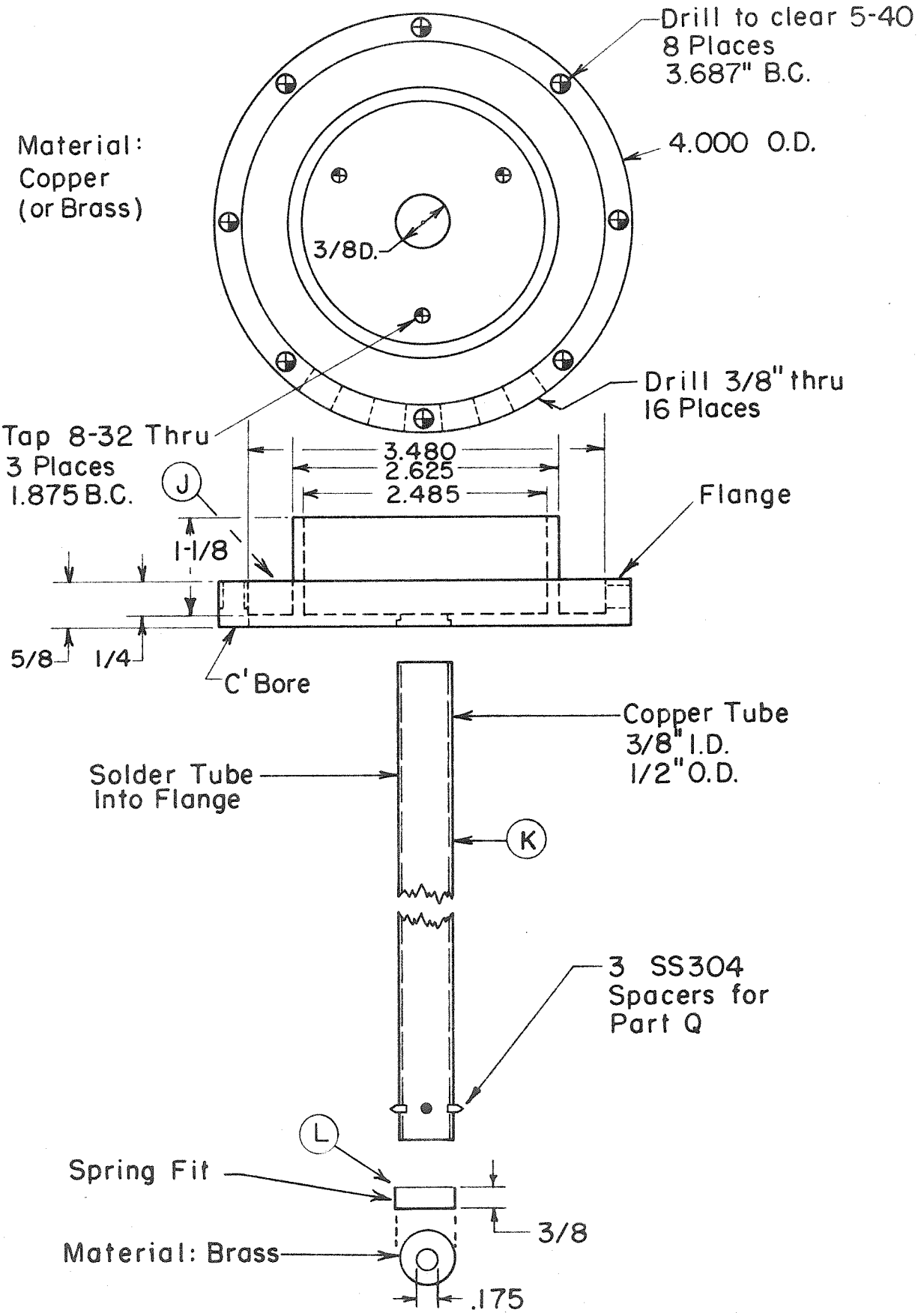

Figure 32

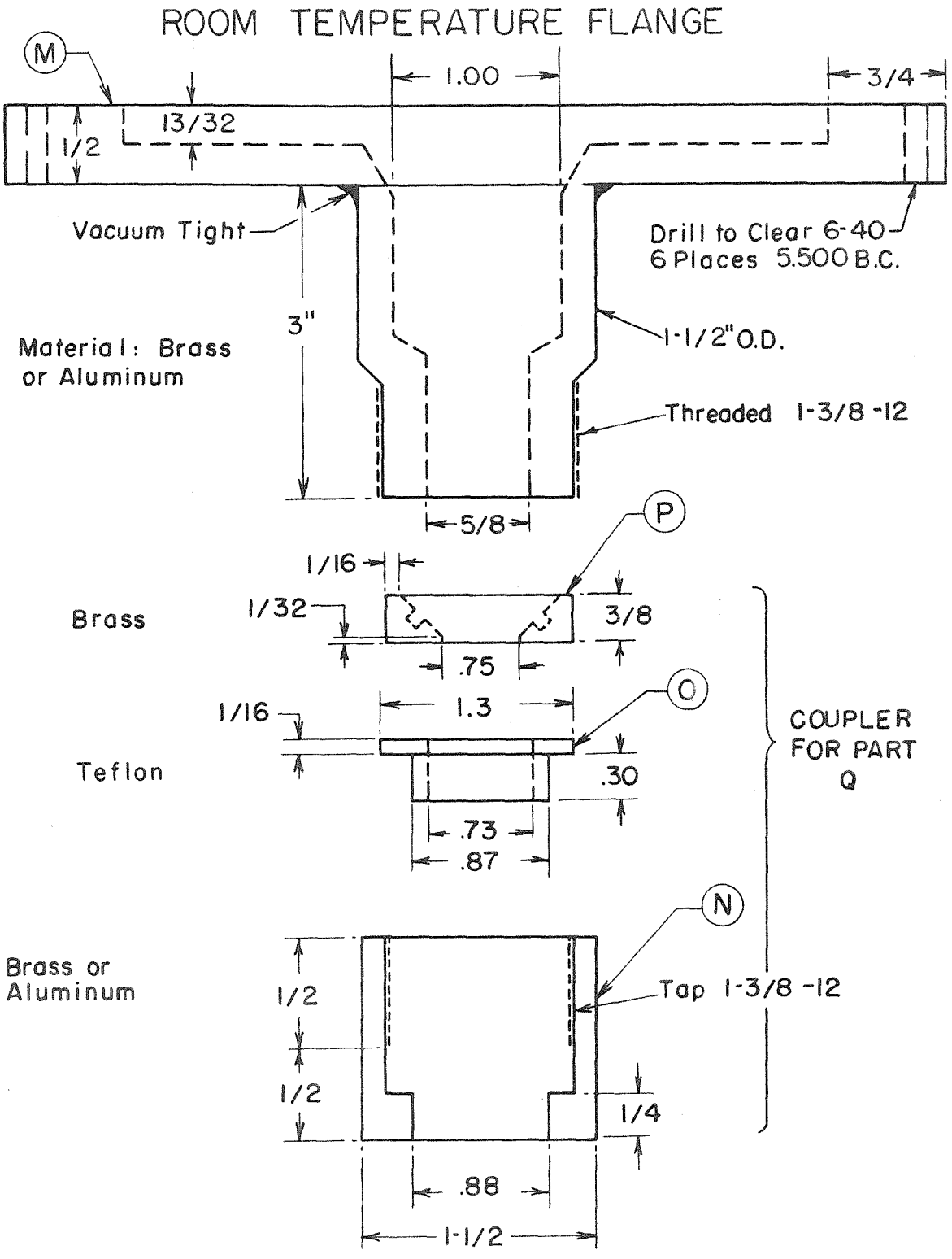
ROOM TEMPERATURE FLANGE
M
1.00
3/4
13/32
1/2
Vacuum Tight
Drill to Clear 6-40
6 Places 5.500 B.C.
3"
Material: Brass
or Aluminum
1-1/2" O.D.
Threaded 1-3/8 -12
5/8
P
1/16
1/32
Brass
3/8
.75
1.3
O
1/16
Teflon
.30
.73
.87
COUPLER
FOR PART
Q
N
Brass or
Aluminum
1/2
Tap 1-3/8 -12
1/2
1/4
.88
1-1/2

Figure 33

QUARTZ VACUUM JACKET

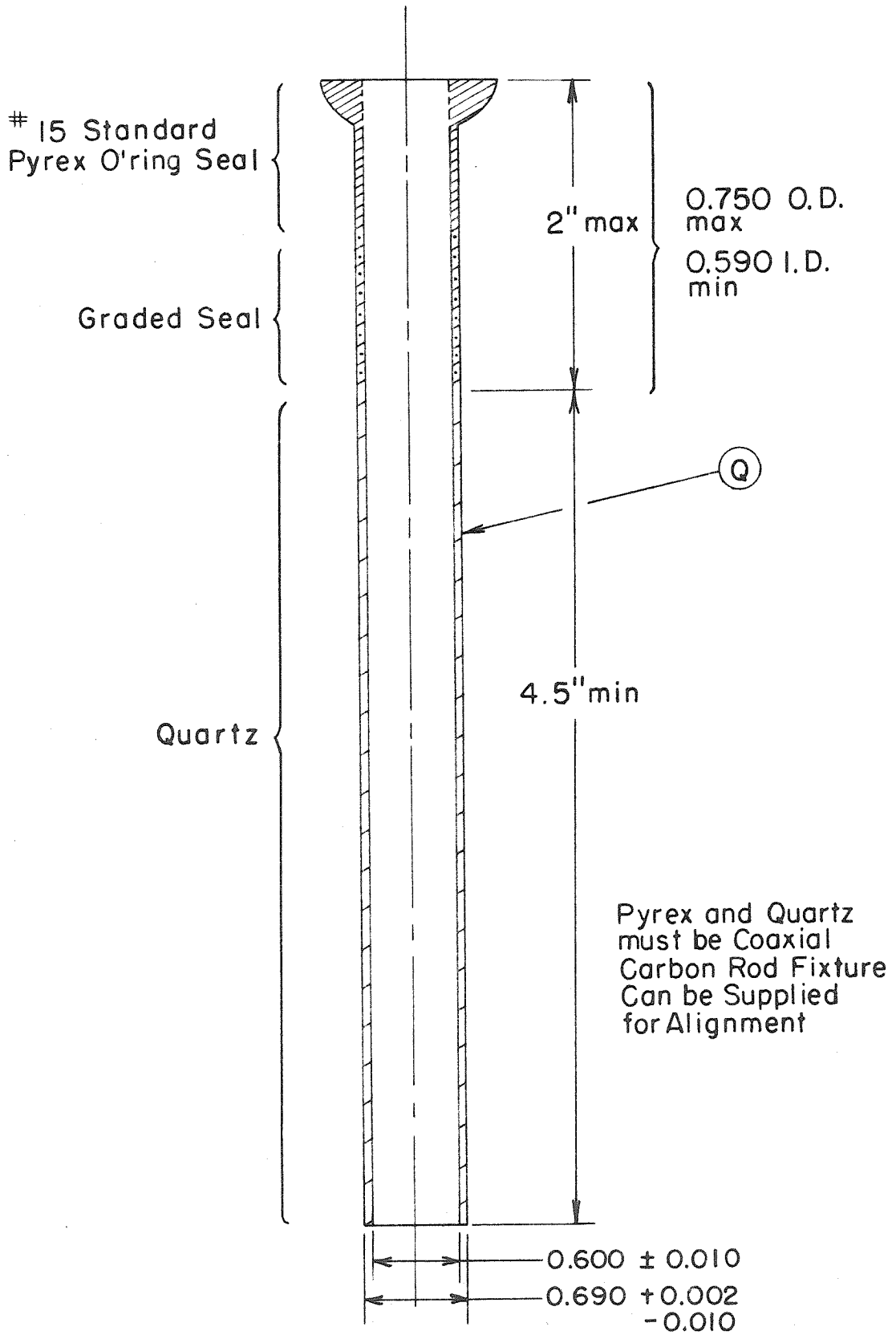

Figure 34

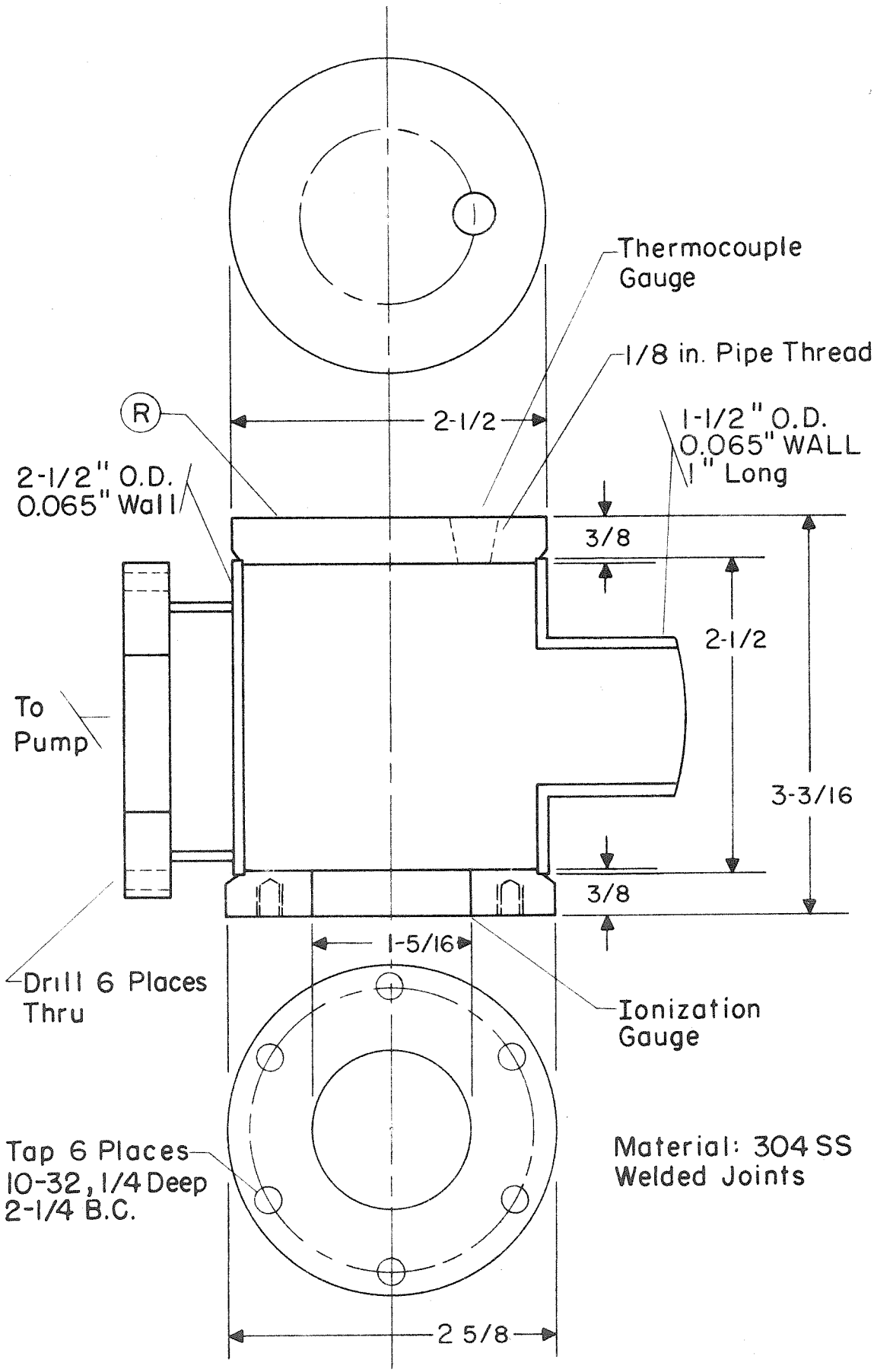
Thermocouple Gauge
1/8 in. Pipe Thread
R
2-1/2
1-1/2" O.D.
0.065" WALL
1" Long
2-1/2" O.D.
0.065" Wall
3/8
2-1/2
To Pump
3-3/16
3/8
1-5/16
Drill 6 Places Thru
Ionization Gauge
Tap 6 Places
10-32, 1/4 Deep
2-1/4 B.C.
Material: 304 SS
Welded Joints
2 5/8

Figure 35

The helium cold finger itself (which forms a helium tight seal with D using an indium wire "o-ring"), comprised of E, F, G and H, is shown as a metal tube having a small metallic sample mount* on the end. This was the finger first built for prototype purposes although it was ultimately to be replaced by a quartz finger.** G and H are made of high purity annealed copper or aluminum so as to maintain good thermal contact between refrigerant and sample.

E as shown in the detailed figure is represented as a symmetric unit. In practice the welding process introduces strains and asymmetries in the dewar proper. Therefore the helium finger must always be custom fitted to the individual dewar in order that F and K can be maintained coaxial.

J, K, and L form the nitrogen shield. L simply makes the interior of the cavity look a little less discontinuous to the microwaves. The design is such that at 80°K or below the bottom of L is approximately in the plane of the "ceiling" of the cavity. The sample mount H protrudes through L into the region of maximum magnetic field.

The 3/8" holes in J are to increase the pumping speed for the volume immediately surrounding the helium can. One notices that except for these holes the path for a gas molecule from the vicinity of the helium can to the pump has a very low cross section. Therefore, if the 3/8" holes were absent the gas in the volume around the helium can would

---

*It should be remembered that the metal distorts H_1 somewhat and small samples must be mounted accordingly.

**Such a finger has subsequently been made by O. Hayes Griffith, and works very satisfactorily.

appear effectively as a "virtual" leak (63). In order to prevent room temperature radiation through these holes from falling directly on the helium can the 2.485 i.d. ring has been included.

M is the room temperature flange to which the quartz vacuum jacket Q is coupled by coupler N, O, P. An o-ring is used between P and Q to reduce rigidity and prevent glass-to-metal fracture.

The upper end of Q is a standard pyrex o-ring joint which forms a simple quick-coupling vacuum seal with M. The lower part of Q is fused quartz. The reason for this is discussed below in connection with the microwave cavity.

R is made to receive a thermocouple gauge and an ionization gauge. Flexible stainless steel tubing* from the diffusion pump is coupled to R. A switching system has been built which allows the vacuum to the dewar to be broken without requiring that the diffusion pump be shut off.

This completes the description of the dewar. The rate of helium loss using the metal finger is about 400 cc per hour. When the quartz finger is used the rate is about 600 cc per hour. This slight disadvantage is compensated by the convenient features of the system.

The design of the cold finger described above is essentially determined by the properties of the microwave cavity to be used. We used a TE_{011} cavity (see Fig. 10 for mode distribution), because

---

*When using such tubing one end should attach to a floating coupling ring so that any angular orientations can be accommodated. This tubing cannot be twisted about its axis.

1. Such cavities can have a very high Q

2. It has a very good filling factor for the kind of samples normally used

3. The microwave magnetic field is axially symmetric

and 4. Its symmetry matches that of the cold finger.

The cavity is shown in Figure 36 and its component parts in Figures 37-39. It has not been designed for maximum Q. In spite of this its unloaded Q with poorly conducting walls is about 15000. (Q reduction due to design* is about 20%.) The cavity was designed to require as short a length as is reasonable for both the metal cold finger (particularly for the metal sample mount) and for the quartz cold finger. One essentially compromises between Q maximization and rate of helium loss.

The cavity body (which is not shown in the dimensioned drawings) consists of a glass (pyrex or quartz) cylinder having a 2.020" outside diameter which is cut to a length of about 1.025". A hole is then drilled through the glass. It is symmetrically located and should be about 1/4"-5/16" in size. This is for the purpose of coupling microwaves into the cavity. The bakelite piece shown in Figure 37 is cut along the plane marked ℄ in the upper view. One of the resulting pieces is glued** to the glass cylinder so that the 1/4" hole in the glass is placed symmetrically with respect to the thinnest part of the bakelite. After the bond has cured, this surface (near the coupling hole)

---

*For the important considerations involved in the design of such cavities see Propositions 3 and 4.

**Eastman 910 Adhesive is quite satisfactory. (Made by Eastman Kodak Co.)

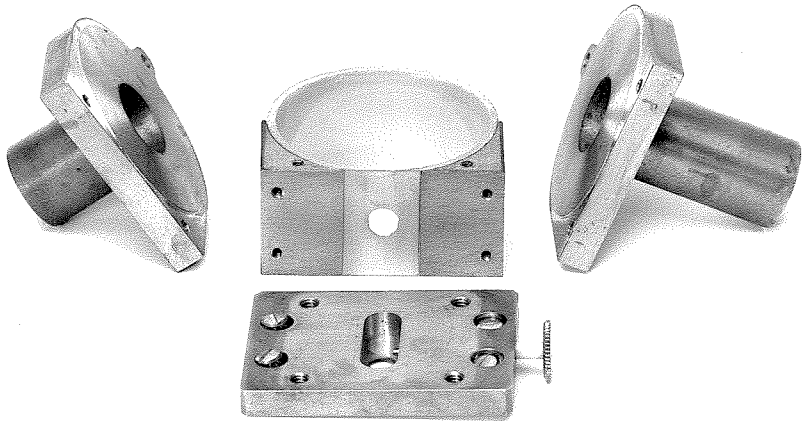

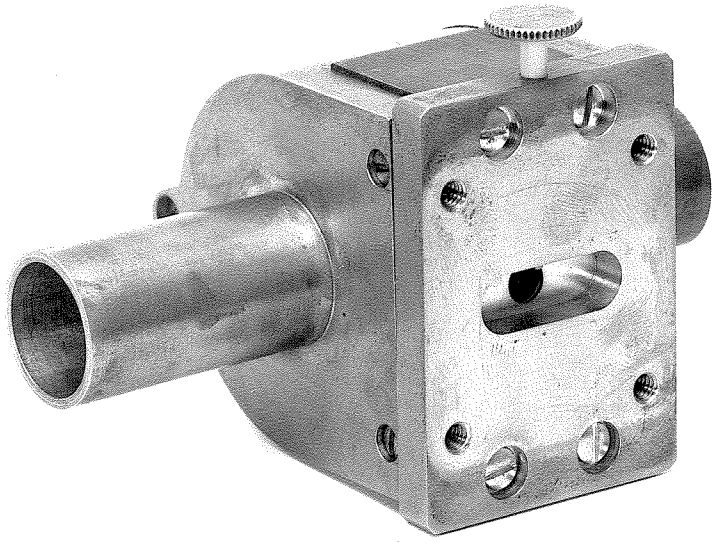

Figure 36. TE_{011} cavity

CAVITY COMPONENTS SUPPORT

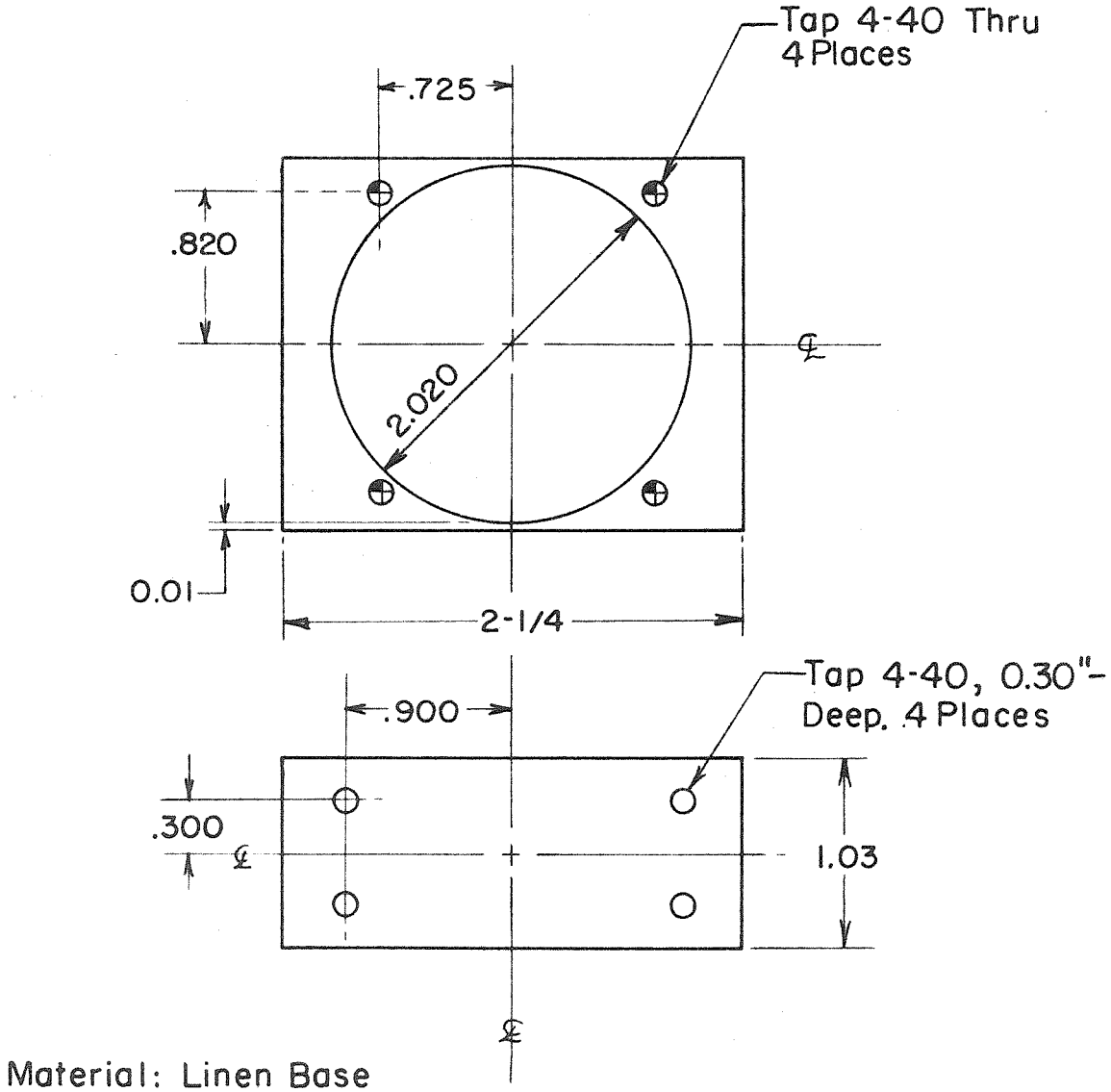

Material: Linen Base
Bakelite

Figure 37

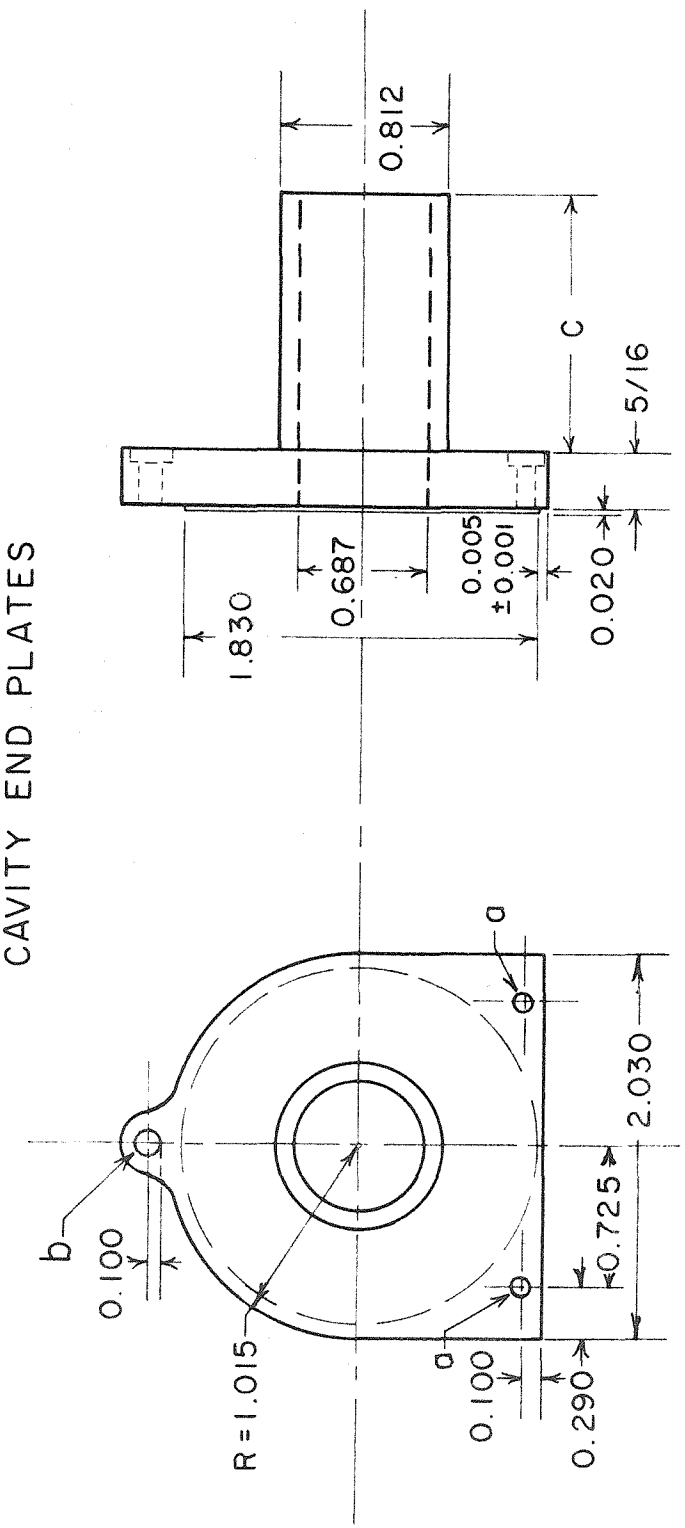
CAVITY END PLATES
0.812
C
5/16
0.020
0.005
±0.001
0.687
1.830
a
2.030
0.725
b
0.100
R=1.015
a
0.100
0.290

Figure 38

COUPLING PLATE

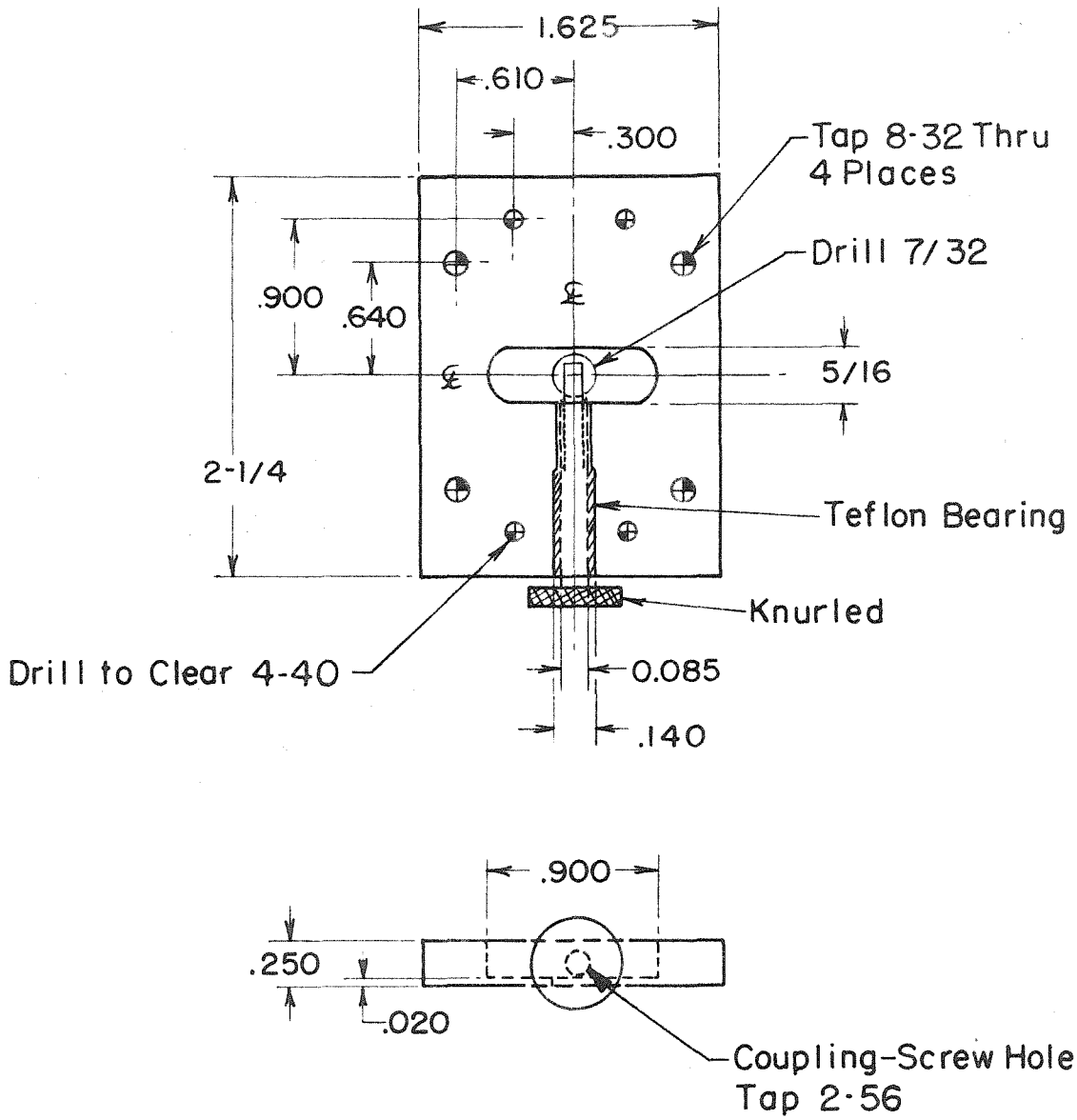

Figure 39

is lapped evenly until eventually the thinnest part of the glass is about 0.015"-0.020" thick. This part is silver plated (and should be flashed with gold) and the cavity is completed by adding the end pieces shown in Figures 36 and 38. The coupling plate with tuning screw is then attached. (This plate has been made so that standard X-band waveguide can be coupled directly to it.) The teflon bearing around the coupling (or tuning) screw holds it snugly and eliminates any microphonics due to the screw. Such microphonics are often a source of noise in EMR experiments.

Such cavities have good EMR characteristics and are very convenient to use for most room temperature EMR experiments. (This is the high Q cavity with which sensitivity was checked in Part I, Section E.) Although they are quite easy to construct they should be handled with care.

The cylinders (or arms) protruding from the ends of the microwave cavity prevent microwaves from leaking out of the cavity. In general, the attenuation, α, of rf power down a tube of length ℓ having a diameter d which is beyond cut-off for that frequency is given by

$$\alpha = 30\text{db} \ \frac{\ell}{d} \ .$$

These cylinders with d = 11/16" are beyond cut-off for the dominant TE_{11} mode at 9 Gc. The microwave are thus attenuated about 60db and leakage is negligible.

These cylinders must also be kept small enough (in d) so that they can be considered as a small perturbation on the TE_{01} mode in the cavity. If d is increased much beyond 11/16" the arms will not be beyond cut-off for the TE_{11} mode and microwaves could be coupled out of

the cavity. These arms with d = 11/16" can be considered as a minor perturbation on the system. The resonant frequencies of the cavity with and without the arms differ* by about 2%.

A rather more important frequency shifting mechanism that must be taken into account in the design is that due to dielectric and/or metal insertions. Adding a quartz tube of 17 mm o.d. with a 1 mm wall lowers the frequency by about 6%. The addition of the shield and metal cold finger raises the frequency about 1%. (This is reasonable since one is essentially eliminating one of the two arms which caused a 2% lowering in the frequency.)

It was stated above that the TE_{01} mode is a very high Q mode. To maintain this high Q a quartz vacuum jacket was used. The loss caused by dielectric materials inserted into an rf field is roughly proportional to the product of a quantity designated as the loss tangent, tan δ, with the electric field density over the volume of the dielectric. This loss is directly reflected in the Q of the cavity and thus in the sensitivity of the system.

Quartz has a very low loss tangent;** tan δ = 0.0001 at 10 Gc. Compare this with water for which tan $\delta \approx 1$ at these frequencies. (However, for ice at -12°C tan $\delta \approx 0.001$.) If the entire cavity were filled with quartz then the maximum Q would be

$$Q_{max} \approx \frac{1}{\tan \delta} \approx 10^4.$$

---

*The frequency is clearly lower for the cavity with the arms. They may actually improve the filling factor by effectively making the cavity longer.

**See reference 51 for tan δ values.

Clearly the quartz tube has a negligible effect on the cavity Q. (For pyrex $Q_{max} \approx 100$.)

Since one normally uses roughly cylindrical or cubical samples the TE_{01} mode provides a good filling factor. The microwave magnetic field is axially (x-axis) symmetric and H_x drops off proportional to J_o, the zero order Bessel function (see Fig. 10).

Again, because of the axial symmetry of H_x the effective microwave field which induces transitions is unaffected by a rotation of the external field about the cavity's x-axis. Therefore, if one attaches the 100 kc coils to the magnet a convenient system for angular studies results.

The field distribution of the TE_{01} mode is further convenient since coupling to a metal rod along the x-axis is negligible. Such coupling would be disastrous because the metal rod inside a conducting cylinder forms a coaxial line. Coaxial lines have no cut-off frequency and microwaves would be coupled out of the cavity. Even if such coupling out of the cavity did exist to a very minor degree it could be a source of microphonics. To prevent this the coaxial line was designed to be a very poor AC conductor.

The attenuation α along a coaxial line is given by

$$\alpha \sim \frac{1}{\ln \frac{b}{a}}$$

where $\frac{b}{a}$ is the ratio of the diameters of the outer and inner conductors respectively. When $\frac{b}{a} \to 1$, $\alpha \to \infty$. Therefore by making the two "conductors" almost the same diameter we can eliminate coupling out of the cavity.

However, α represents an I^2R loss. Since the Q is not affected by the nitrogen shield and/or the helium finger we can conclude that coupling to them is negligible.

For either the metal or quartz cold finger, the u.v. light can be introduced through the quartz plate forming the bottom of the quartz vacuum jacket, Q. When the metal finger is used it is difficult to determine the sample temperature, and this is particularly so when u.v. light is incident on the sample. Whenever small changes in temperature are important it is desirable for u.v.-irradiation experiments that the quartz finger be used (here the sample is immersed in liquid helium).

Unless special precautions are taken this can present some difficulties due to the ice which settles to the bottom of the tube. Cavities basically the same as the one described in which, however, the u.v. light is introduced through an aperture(s) in the side of the cylindrical cavity have been built* and used. This is another reason for using a quartz vacuum jacket and a quartz finger. The path length of the light through these quartz pieces is less than 3 mm. This is negligible compared to the path length when light pipes are used.

The size of sample that can be used in the quartz cold finger is limited to $d' \approx 0.22''$ where d' is the inside diameter of the finger. (This of course is ultimately determined by the permissible size of the cavity arms.) The metal finger can accommodate considerably larger samples. However, in that case the sample cannot be changed during the

---

*One used most recently was designed by M. W. Hanna and the author and was constructed by H. Sternlicht.

course of an experiment. Furthermore, sample rotation over any appreciable angle requires that the whole dewar be rotated. (The magnet can only be rotated about 90°.) For this reason and for the others discussed above the quartz finger is usually used.

This system, then, incorporates all the features that were listed at the outset of the discussion. To conclude we shall explicitly mention the two major disadvantages which this system has.

1. The useable sample size is seriously restricted.
2. The temperature cannot (in the present modification) be varied uniformly and controllably over certain ranges. (It can be controlled accurately from 1°-4.2°K and from about 60°-77°K.)

In spite of these limitations the system has been used extensively in these laboratories and in several cases has even yielded significant results.

REMOTE-TUNED HIGH-POWER F.M. SIGNAL GENERATOR

The signal generator shown in Figure 40 was discussed in Part I Section E. Its unique feature is the employment of a remote resonant (tank) circuit which is composed of L_o, L_o' and C_o. A remote tank is particularly convenient for ENDOR experiments when one would like the ENDOR coil to act as the inductor in a tank. Using the ENDOR coil as a tank coil essentially increases the rf field by a factor of Q, the quality factor of the tank. (The Q can easily be made greater than 10.)

Values for L_o, L_o' and C_o will of course vary with each system. Usually the system will be designed around L_o, and L_o' and C_o are then determined by feedback requirements and the desired frequency range. L_o' effectively provides the feedback voltage.

It is quite reasonable that using a remote tank in the megacycle region will introduce unwanted resonances. Such resonances are more numerous the longer the feed lines between the oscillator tube and the tank become. For this reason a filter and a trap are associated with the grid circuit. L_1 and C_2 form a low pass filter and L_2-C_3-R_2 forms a narrow pass series resonant circuit (trap). These values too will depend on the particular system used.

At the end of this discussion typical values for the components are given. This list includes the values for the above named elements for the case where the feed lines were about four feet long and where the oscillator tuned over the region from 2-18 Mc.*

---

*The unit (modified) has also been operated between 10 and 60 Mc.

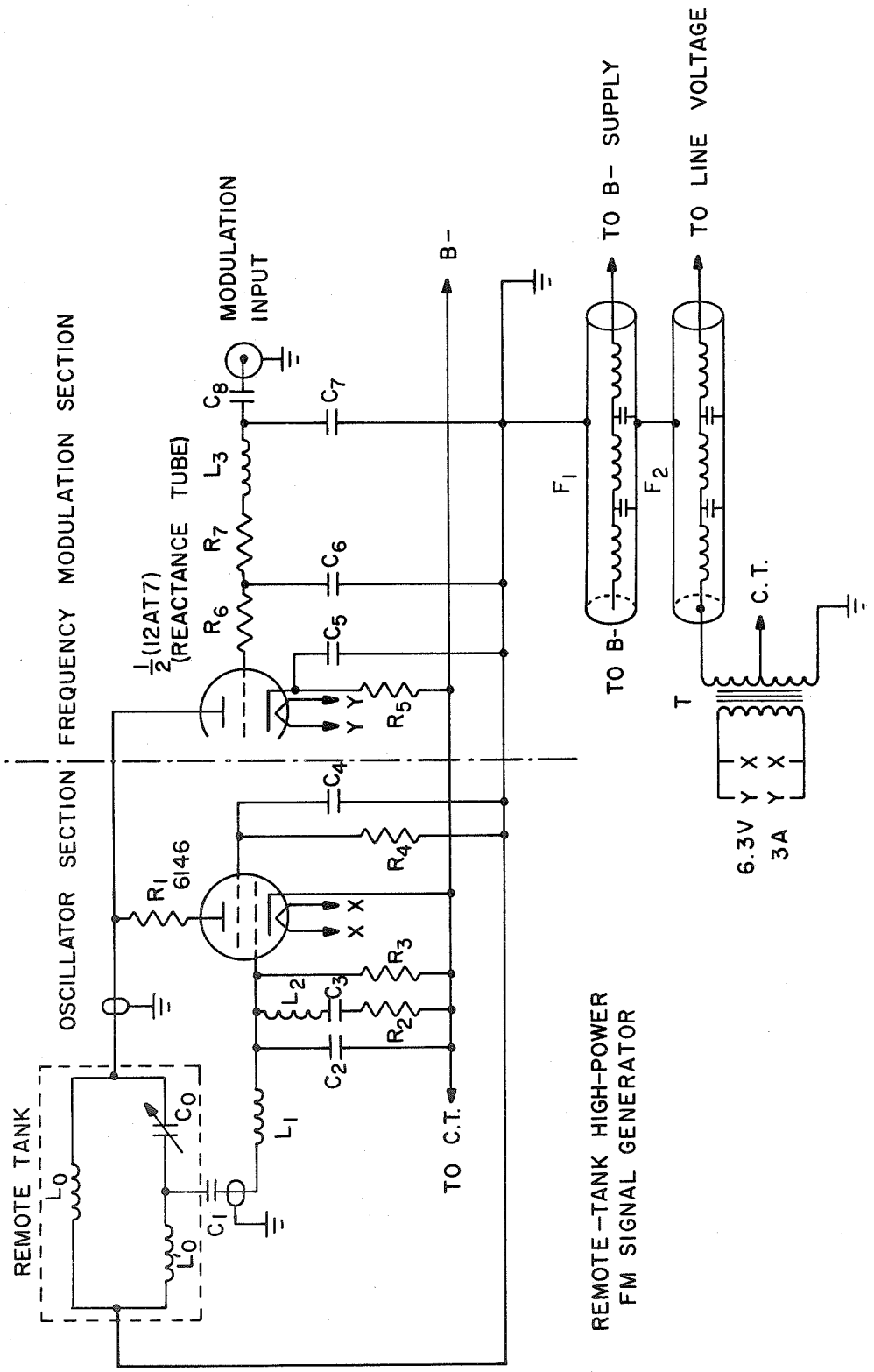
REMOTE TANK
OSCILLATOR SECTION
FREQUENCY MODULATION SECTION
REMOTE-TANK HIGH-POWER FM SIGNAL GENERATOR
MODULATION INPUT
½(12AT7) (REACTANCE TUBE)
6146
TO C.T.
B-
TO B- SUPPLY
TO B-
TO LINE VOLTAGE
C.T.
6.3V 3A

Figure 40

For those values, L_1-C_2 presents zero admittance Y ($Y \equiv \frac{1}{Z}$ where Z is the impedance) beyond 25 Mc. This eliminates a spurious resonance in the 30-40 Mc region which varies in frequency as C_o is tuned. Because of this the filter is more applicable than a trap. L_2-C_3-R_2 acts as a fixed trap tuned to 23 Mc. This shunts the spurious 23 Mc resonance to ground.

R_1 is used to destroy parasitic oscillations* in the plate circuit. C_1 and R_3 are adjusted to prevent intermittent oscillation.*

In order to run the ENDOR coil at ground potential the generator is supplied with B^-. Both B^- and the filament voltage are fed through filters** F_1 and F_2 which are constructed so as to completely eliminate rf leakage. For the same reason the chassis is made of 1/4" aluminum with 1/8" ventilation holes. (Recall that α = 30db $(\frac{\ell}{d})$.)

With B^- = -325V the magnetic field produced in L_o was about 7 gauss. The 6146 tube can be operated with a plate voltage as high as 600V. Such a value would substantially increase the magnetic field strength.

---

*For a good discussion of parasitic and intermittent oscillations see reference 53.

**Made according to a design supplied by A. F. Hildebrandt.

Typical values for the components

L_o = 0.55 μh

L'_o = 0.75 μh

C_o = 70-280 pf

C_1 = 50 pf — Silver Mica

C_2 = 1.5-7 pf — Variable mica disc capacitor

C_3 = 7-15 pf — Variable mica disc capacitor

C_4 = 1000 pf — Silver Mica

C_5 = 4μf — 450 VDC Dry Electrolytic

C_6 = 100 pf — Silver Mica

C_7 = 0.001 μf — Disc

C_8 = 0.1 μf — 600 VDC

L_1 = About 5-15 μh--variable inductor

L_2 = About 7-20 μh--variable inductor

L_3 = ~ 0.2 mh — rf choke

R_1 = 22Ω - 5W — Carbon

R_2 = 150Ω - $\frac{1}{2}$W — Carbon

R_3 = 10K - 1W — Carbon

R_4 = 25K - 5W — Wire-wound

R_5 = 2.7K - $\frac{1}{2}$W — Carbon

R_6 = 150Ω - $\frac{1}{2}$W — Carbon

R_7 = 10K - $\frac{1}{2}$W — Carbon

MANOSTAT

A pressure regulator, or manostat, for controlling the pressure above liquified gases was built according to a design given in reference 64. A point not very explicit in that design is the need for a stopping device which limits the range of travel of the bellows when they are under reduced pressure. In Figure 2 of reference 64 the faint horizontal lines going just above the first fold of the bellows represents this need. Provision must somehow definitely be made for this. The manostat shown in Figure 41 has a diameter of 8".

CRYSTAL STRUCTURE BASES

It is usually desirable when studying single crystals of compounds by EMR to make a model of the crystal structure. A particularly convenient base for such models is often used by the crystallographers in these laboratories. However the cost per base is about $30. The design was modified so as to bring the cost into a range which would allow one to make and keep such models. This modification is shown in Figure 42. Apart from the perforated sheets aluminum is used throughout. This base can be built for $5. The crystal structure shown is that of glutaric acid.

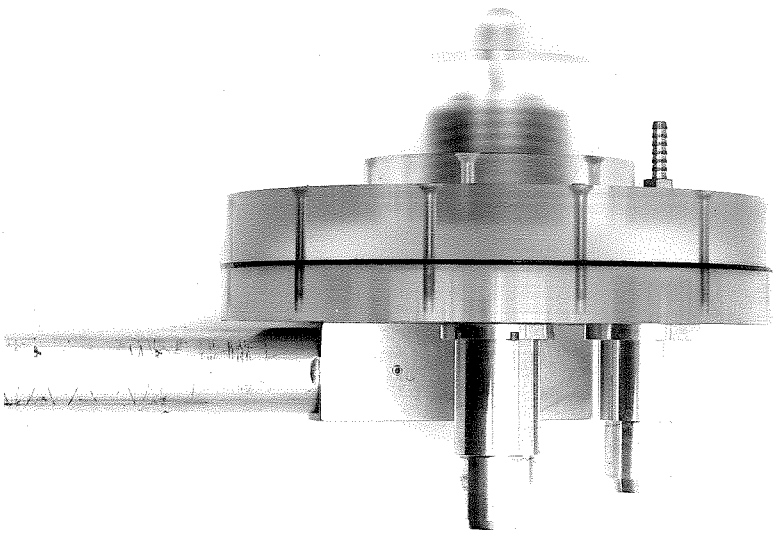

Figure 41. Manostat

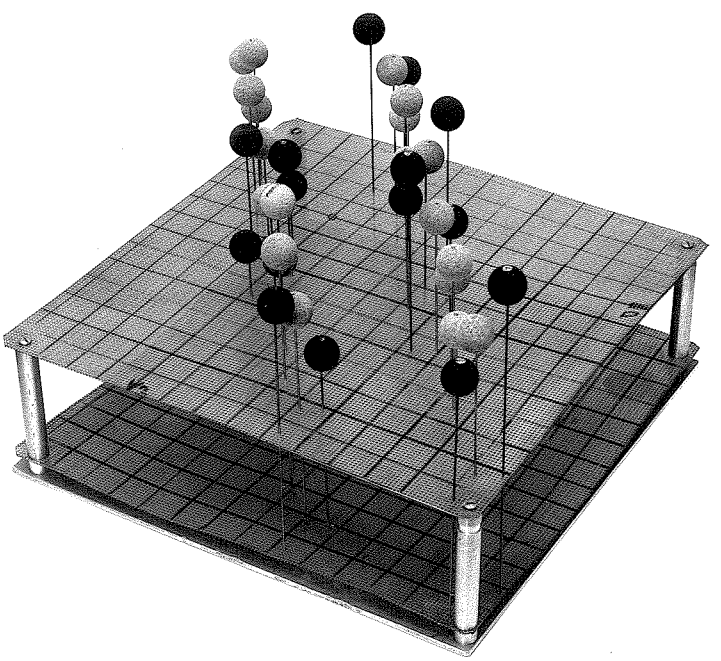

Figure 42. Crystal structure base

BIBLIOGRAPHY

1. Debye, P. Ann. d. Phys., 81 (1926), 1154-1160.
2. Giauque, W. F. J. Am. Chem. Soc., 49 (1927), 1864-1877.
3. Giauque, W. F. and McDougall, D. P. Phys. Rev., 43 (1933), 768.
4. Kurti, N. and Simon, F. Nature, 133 (1934), 907.
5. de Haas, W. F., Wiersma, E. C. and Kramers, H. A. Physica, 1 (1933-1934), 1-13.
6. Gorter, C. J. Phys. Z., 35 (1934), 923-938.
7. Kurti, N. and Simon, F. Proc. Roy Soc., A149 (1935), 152-176.
8. Gorter, C. J. Physica, 14 (1948), 504.
9. Rose, M. E. Phys. Rev., 75 (1949), 213-214.
10. Bleaney, B. Proc. Phys. Soc. London, A64 (1951), 315-316.
11. Pound, R. V. Phys. Rev., 76 (1949), 1410-1411.
12. Kastler, A. J. Phys. et Radium, 11 (1950), 255.
13. Kastler, A. Compt. Rend., 233 (1951), 1444-1446.
14. Overhauser, A. W. Phys. Rev., 92 (1953), 411-415.
15. Carver, T. R. and Slichter, C. P. Phys. Rev., 92 (1953), 212-213.
16. Abragam, A. Phys. Rev., 98 (1955), 1729-1735.
17. Abragam, A. and Combrisson, J. Compt. Rend., 245 (1957), 157-160.
18. Abragam, A. and Proctor, W. G. Compt. Rend., 246 (1958), 2253-2255.
19. Jeffries, C. D. Phys. Rev., 117 (1960), 1056-1069.
20. Jeffries, C. D. Progress in Cryogenics, 3 (1961), 130-173.
21. Webb, R. H. Am. J. Phys., 29 (1961), 428-444.
22. Barker, W. A. Revs. Mod. Phys., 34 (1962), 173-185.
23. Feher, G. Phys. Rev., 103 (1956), 500-501.
24. Feher, G. and Gere, E. A. Phys. Rev., 103 (1956), 501-503.

25. Bloch, F. Phys. Rev., 70 (1946), 460.

26. Feher, G. Phys. Rev., 103 (1956), 834-835.

27. Feher, G. Phys. Rev., 105 (1957), 1122.

28. Feher, G. Phys. Rev., 114 (1959), 1219-1244.

29. Holton, W. C. and Blum, H. Phys. Rev., 125 (1962), 89-103.

30. Portis, A. M. Phys. Rev., 91 (1953), 1071-1078.

31. Cowen, J. A., Schafer, W. R. and Spence, R. D. Phys. Rev. Letters 3 (1959), 13-14.

32. Abraham, M., McCausland, M. A. H. and Robinson, F. N. H. Phys. Rev. Letters 2 (1959), 449-451.

33. Terhune, R. W., Lambe, J., Makhov, G. and Cross, L. G. Phys. Rev. Letters 4 (1960), 234-236.

34. Lambe, J., Laurence, N., McIrvine, E. C. and Terhune, R. W. Phys. Rev., 122 (1961), 1161-1170.

35. Cole, T. Private Communication.

36. McConnell, H. M., Heller, C., Cole, T. and Fessenden, R. W. J. Am. Chem. Soc., 82 (1960), 766-775.

37. Heller, C. and McConnell, H. M. J. Chem. Phys., 32 (1960), 1535.

38. Ghosh, D. K. and Whiffen, D. H. Mol. Phys., 2 (1959), 285.

39. Miyagowa, I. and Gordy, W. J. Chem. Phys., 30 (1959), 1590-1595.

40. Pooley, D. and Whiffen, D. H. Mol. Phys., 4 (1961), 81-86.

41. Horsfield, A., Morton, J. R., Rowlands, J. R., and Whiffen, D. H. Mol. Phys., 5 (1962), 241-250.

42. McConnell, H. M. and Robertson, R. E. J. Phys. Chem., 61 (1957), 1618.

43. McConnell, H. M. Unpublished Lecture Notes available at C.I.T. Book Store.

44. Pooley, D. Thesis, University of Birmingham (1961).

45. Margenau, H. and Murphy, G. M. The Mathematics of Physics and Chemistry (D. Van Nostrand, New York, 1956), 301-332.

46. Horsfield, A., Morton, J. R. and Whiffen, D. H. Mol. Phys., 4 (1961), 169-175.

47. Booth, F. B. Thesis, C.I.T. (1963).

48. Morrison, J. D. and Robertson, J. M. J. Chem. Soc. (1949), 1001-1008.

49. Goldstein, H. Classical Mechanics (Addison-Wesley Publishing Company London, 1959), 93-109.

50. Griffith, O. H. and McConnell, H. M. Submitted to Proc. Nat. Acad. Sci. U.S.A.

51. Moreno, T. Microwave Transmission Design Data (Dover Publications, 1958).

52. Ginzton, E. L. Microwave Measurements (McGraw-Hill Book Company, New York, 1957).

53. Terman, F. E. Electronics and Radio Engineering (McGraw-Hill Book Company, New York, 1955).

54. Kronig, R. de L. Physica, 6 (1939), 33.

55. Webb, R. H. Rev. Sci. Instr., 33 (1962), 732-737.

56. Chester, P. F., et al. Rev. Sci. Instr., 30 (1959), 1127-1128.

57. Cole, T., Heller, C. and Lambe, J. J. Chem. Phys., 34 (1961), 1447-1448.

58. Seidel, H. and Wolf, H. C. Naturw., 46 (1959), 597-

59. Wheatley, J. C., Griffing, D. F., Estle, T. L., Rev. Sci. Instr., 27 (1956), 1070-1077.

60. Hutchison, C. A. and Mangum, B. W. J. Chem. Phys., 34 (1961), 908-922.

61. Varian Associates Technical Bulletin #1353.

62. Croft, A. J. Experimental Cryophysics (Eds. Hoare, F. E., Jackson, L. C., and Kurti, N.), p. 123. (Butterworths, London, 1961.)

63. Dushman, S. Scientific Foundations of Vacuum Technique (John Wiley and Sons, Inc., New York, 1962).

64. Sommers Jr., H. S. Rev. Sci. Instr., 25 (1954), 793-798.

PROPOSITION 1

This proposition deals with the radiation damage of small unsaturated molecules as studied by EMR. In 1960 I proposed that the effect of room temperature x-irradiation on such molecules be investigated. Prior to that time several publications (1 - 3) had appeared dealing with the free-radicals formed in this way in saturated systems. However, essentially no work had been done on the unsaturated systems. It was suspected that the radicals formed in the latter case might be basically different than those formed in the former case. In particular it was hoped that σ-radicals might be detected. The term σ-radical implies that the unpaired electron resides in a σ-orbital.

With this object in mind the following compounds have been investigated (in most cases as single crystals) using the EMR technique.

2-furancarboxylic acid (furoic acid)

3-furancarboxylic acid

3,4-diphenyl 2-furancarboxylic acid

3,4-diphenyl 2,5-furandicarboxylic acid

2-thiophenecarboxylic acid (thiophenic acid)

3-thiophenecarboxylic acid

2-pyrrolecarboxylic acid

2-furaldoxime

2-furamide

2-potassium furoate

maleic acid

maleic anhydride

potassium acid maleate*

fumaric acid

2,3-dihydroxy fumaric acid

potassium acid fumarate

trans-2-methyl 2-butenoic acid (tiglic acid)

cis 2-methyl 2-butenoic acid (angelic acid)

trans 2-butenoic acid (crotonic acid)

cis-methylbutenedioic acid (citraconic acid or methyl maleic acid)

trans-methylbutenedioic acid (mesaconic or methyl furmaric acid)

methylenebutanedioic acid (itaconic or methylene succinic acid)

1,4-butadienecarboxylic acid (trans-trans-muconic acid)

propenedioic acid (glutaconic acid)**

dipotassium nitroacetate

diphenyl mercury

X-irradiation of any of the above (except angelic acid) gives a long-lived free-radical. Many of these show a spectral spread (EMR) of 150 Mc and more and yet essentially none of the parent molecules possess a potential β-proton (on β-protons see p. 43 of this thesis or reference 2). It is well known that α-protons give a maximum spectral spread of about 90 Mc (excepting cases where negative spin densities exist). Therefore either the radical

---

*Independently investigated by Heller and Cole (4).

**Independently investigated by Heller and Cole (5). They have studied extensively the allyl type radical formed in this system.

1. may have been formed by adding a H atom*

or else 2. it may be a σ-radical.

Although none of the above named systems have been worked out in detail (Part I of this thesis prevented that) the results of some preliminary investigations are given in the reprinted article included at the end of this proposition. There it is indicated that hydrogen addition, or H-aufbau, is the radical forming process. Although hydrogen addition had been previously observed at low temperatures ((6), see also (7)) this is seemingly the first known case of such a process resulting in a stable long-lived free-radical at room temperatures.

More recently, investigations** in this laboratory have definitely established the initial suggestion that H-aufbau is also the damage mechanism in maleic and fumaric acids. Several of these systems will shortly be investigated in more detail, particularly diphenyl mercury. It is quite possible that of the two stable free-radicals formed one may be the phenyl radical.

---

*This suggestion is due to H. M. McConnell.

**O. Hayes Griffith and A. L. Kwiram.

Reprinted from the Proceedings of the National Academy of Sciences
Vol. 48, No. 4, pp. 499–500. April, 1962.

*RADIATION DAMAGE IN ORGANIC CRYSTALS: AUFBAU PROCESSES**

By Alvin L. Kwiram and Harden M. McConnell†

GATES AND CRELLIN LABORATORIES OF CHEMISTRY,‡ CALIFORNIA INSTITUTE OF TECHNOLOGY

Communicated by John D. Roberts, February 26, 1962

A great variety of long-lived oriented free radicals have been produced in organic single crystals by high energy radiation.[1–9] Practically all of the many examples studied thus far have involved *abbau processes;* that is, the long-lived oriented free radical is derived from the parent (undamaged) molecule by loss of a hydrogen atom, a carboxyl group, etc. The purpose of this note is to point out that in some systems long-lived oriented free radicals can be formed by *aufbau* processes, in particular by H-atom addition. Thus, for example, the spin resonance of X-irradiated tiglic acid ($CH_3CH{=}C(CH_3)COOH$) suggests a single stable long-lived π-radical

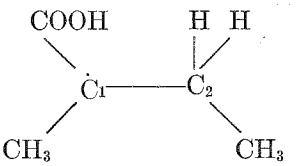

(I)

The π-spin density on C_1 is one half, and the two aliphatic (π) H-atoms attached to C_2 are equivalent with nearly isotropic splittings of ~35 Mc. The protons of the CH_3 group attached to C_1 have similar hyperfine interactions.

A similar H-aufbau is definitely involved in furoic acid where X-irradiation gives a predominant radical species whose paramagnetic resonance is *best interpreted* by the structural formula II with equivalent π hydrogen atoms on C_3 and

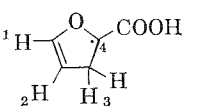

(II)

with π-spin densities ρ_i on carbon atoms C_i of $\rho_4 \sim 1/2$, $\rho_2 \sim 1/3$, $\rho_1 \sim -1/6$. The large spin density on C_2 can presumably be attributed to the resonance structure,

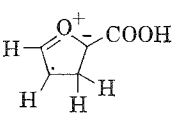

Evidently the spin transmission through the oxygen linkage is quite efficient.

A detailed analysis of these spectra, as well as similar spectra obtained in the radiation damage of other unsaturated acids is in progress.

* Supported by the National Science Foundation.

† Alfred P. Sloan Fellow.

‡ Contribution No. 2821.

[1] McConnell, H. M., C. Heller, T. Cole, and R. W. Fessenden, *J. Am. Chem. Soc.*, **82**, 766 (1960).

[2] Heller, C., and H. M. McConnell, *J. Chem. Phys.*, **32**, 1535 (1960).

[3] Pooley, D., and D. H. Whiffen, *Mol. Phys.*, **4**, 81 (1961).

[4] Cole, T., and C. Heller, *J. Chem. Phys.*, **34**, 1085 (1961).

[5] McConnell, H. M., and R. W. Fessenden, *J. Chem. Phys.*, **31**, 1688 (1959).

[6] Atherton, N. M., and D. H. Whiffen, *Mol. Phys.*, **3**, 1 (1960).

[7] Ghosh, D. K., and D. H. Whiffen, *Mol. Phys.*, **2**, 285 (1959).

[8] Miyagawa, I., and W. Gordy, *J. Chem. Phys.*, **32**, 255 (1960).

[9] Kurita, Y., and W. Gordy, *J. Chem. Phys.*, **34**, 282 (1961).

PROPOSITION 2

Most of the efforts to determine the effects of x- and γ-irradiation on biological materials have been concerned with changes induced in the metabolic processes (8). In spite of the complexity of such systems much valuable information has been obtained (9).

The EMR technique although not well suited for the investigation of the processes themselves is valuable in principle whenever a metabolic process results in a product having an unpaired electron(s). (It is of some use in the study of transient radicals.) It was quickly recognized, however, that due to the many damage sites in these large molecules and the resulting line broadening, the amount of information obtainable was quite limited. For this reason most of the EMR investigations have been concerned with the damage occurring in simple constituents such as amino acids (10) and sugars (11).

Significant advances have recently been made (and are being made) in understanding the properties of DNA and its role as the "code-carrier" of genetics (12). It would therefore be of interest to study the effect that x- and γ-irradiation might have on its replicating functions. Damage would almost certainly occur in the phosphate and sugar groups which form the backbone of the DNA molecule. Again, the effects on the DNA molecule itself are very complex (13). If one were most interested in the direct genetic effects of radiation on the replicating process then one might consider the first order problem to be that of changes induced in the code words themselves.

With this in mind R. F. Stewart, acting on a suggestion made by Professor N. Davidson, provided me with 1-methyl thymine, a derivative of one of the DNA code words. (This is a derivative of one of the four code words in DNA, thymine, adenine, guanine, and cytosine). In DNA itself the 1-methyl group of 1-methyl thymine is "replaced" by the DNA molecule.

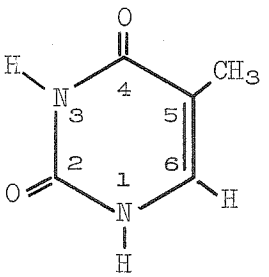

thymine

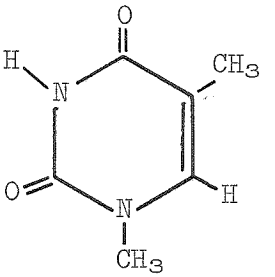

1-methyl thymine

It is proposed that the long-lived free-radical formed upon x-irradiation of 1-methyl thymine at room temperature is

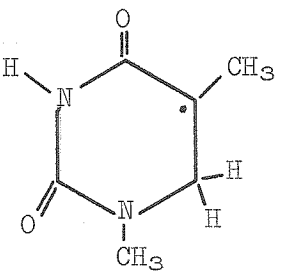

The initially colorless single crystal of thymine after irradiation for about 8 hours has a distinct reddish color. A typical EMR spectrum exhibits the following hyperfine structure--

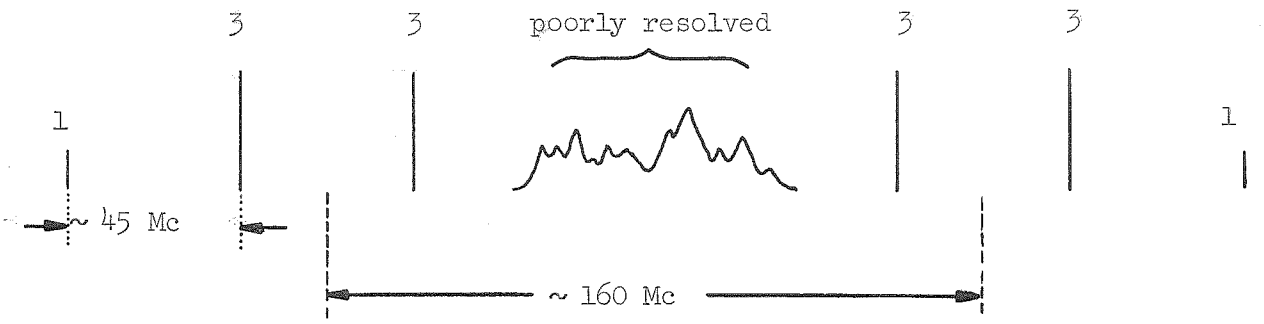

The presence of two radicals is immediately suspected

1. because of the asymmetry existing only in the central region

and 2. because of the relative line shifts in that region as $\vec{H}_o$ is varied.

We will consider only the radical giving rise to the outer lines. It is reasonable to assume then that there are two sets of lines, the lines in each set having relative intensities of 1:3:3:1 and a splitting of about 45 Mc. The two sets are probably due to a rotating methyl group since the splittings within each set are identical and essentially isotropic.

The large splitting which separates the two 1:3:3:1 sets indicates an interaction with a single nucleus of spin $I = \frac{1}{2}$. This eliminates the nitrogen nucleus (N^{15}:I = 1) from the picture. The fact that this splitting is large and quite isotropic suggests a β-proton interaction.

If one assumes that a hydrogen atom has added across the double bond (14) (as shown above) and that an appreciable twist exists in the molecule then one can satisfy the above conditions. If one of the two resulting protons (bonded to the 6-position) approximately "eclipses" the unpaired electron distribution (in a p orbital, say, centered on the 5-position) then the other proton can be approximately in the nodal plane

of the p orbital. Therefore, the interaction of the former will be large--of the latter small. That the above assumptions are reasonable is further borne out by the fact that over a very limited range of orientations each of the lines in the 1:3:3:1 sets are split again by about 5 Mc.

If the above interpretation is correct then one is faced with two minor questions:

1. Why the methyl group interaction is not larger (one would expect it to be about 70 Mc),

and 2. Why the large twist of the β-protons exists.

Although 1-methyl thymine undergoes a reversible photochemical dimerization (15) across the double bond it is unlikely that the radical arises from such a system.

It would be interesting to try to substitute a damaged 1-methyl thymine molecule on the DNA chain to determine what effect it might have on the replicating process. Other DNA constituents should also be investigated in an effort to understand the damage products that might occur in DNA itself.

The word <u>might</u> should be emphasized. A single crystal of 1:1 hydrogen bonded complex of 1-methyl thymine with 9-methyl adenine gives essentially no damage. The hydrogen bonding scheme in this complex is not the same as that in DNA.

PROPOSITION 3

A low temperature EMR system has been described in Part II. We propose

1. A rather novel modification of that system which retains all of its important features but has the advantage that large samples can be used

and 2. A highly flexible ENDOR system based thereon.

The sample size requirement in the low temperature system discussed in Part II arises from the limitation on the size of the (end) arms on the cavity. However, if the entire cavity were evacuated, then the quartz vacuum jacket and (to a point) the nitrogen shield could be eliminated. Thus the helium finger could be enlarged essentially to the size of the arms, if desired.

The major obstacle to cavity evacuation* is the coupling hole through which the microwaves are introduced into the cavity. However, we have demonstrated that coupling into the cavity through a thin section of dielectric has no deleterious effect on cavity Q or (S/N).

Therefore, taking a silvered quartz cylinder one can remove the silver at the point of coupling so as to form the equivalent of a dielectric-filled coupling hole. The cavity walls then function also as the vacuum jacket. This system now allows much greater flexibility for purposes of sample and/or coil insertion for either rf introduction or for temperature control.

---

*One can, of course, use an o-ring system.

As stated repeatedly in Part I of this thesis one of the major problems in the ENDOR experiment is the introduction of a high rf field inside the cavity. If the rf coil could form the inductance of the tank circuit of a signal generator then, for example, the high power oscillator of Part II could be used and relatively high fields obtained. This could be done if the silver in the TE_{011} cavity could be appropriately cut so as to essentially form a coil.

The field components for the TE_{01} cavity are (16) as follows:

$$H_z \sim J_0(kr)\sin(k'z)$$
$$H_r \sim J_1(kr)\cos(k'z)$$
$$E_\theta \sim J_1(kr)\sin(k'z)$$
$$H_\theta = E_z = E_r = 0$$

where (r,θ,z) are the cylindrical coordinates, J_n the nth order Bessel function and the k's are constants. Since $H_\theta = 0$ and since the current through any surface is given by

$$I = \oint_c \vec{H}\cdot\vec{d\ell}$$

there can be no z component for the current in the cavity walls. Furthermore, there need be no current path between the end plates and the cylinder walls. This would allow one to use the center cylindrical section as a coil if the silver were cut appropriately.

One might argue that cutting the silver in a helical manner essentially leaves the current paths unaltered in first order. However, the most important AC consideration is that of capacitive coupling. The capacitive reactance goes like

$$\sqrt{-1}\ X_c = \frac{1}{\omega C}\ .$$

X-band frequencies are $\sim 10^{10}$ cps and as a result the capacitance between "turns" of our helix will effectively function as a short for the microwaves.

An important factor that must be taken into account is that of the currents induced in the end plates of the cavity by the rf current flowing in the helix. In order to reduce this effect to negligible size one must use a silver plated dielectric for the end plates. The skin depth δ is given by

$$\delta = \frac{1}{2\pi}\sqrt{\frac{\lambda\rho}{30\mu}}$$

where λ is the wavelength of the rf, ρ is the conductivity of the metal and μ is its permeability. The skin depth is a measure of the penetration of a magnetic field into a metal; the field drops by $\frac{1}{e}$ in a distance δ. At x-band for a fairly good silver coating $\delta \approx 10^{-4}$ cm, and for 100 Mc $\delta \approx 10^{-3}$ cm. Therefore, if the plating is about 10^{-3} cm thick the eddy currents for most of the rf frequencies we will use can be neglected.

The major advantages of this system which are pertinent to the ENDOR experiment can now be summarized.

1. The microwave cavity and the coupling adjustment (for microwaves) are at room temperature.
2. The cavity can be designed to fit into a two inch magnet gap. (This could help reduce ENDOR line widths.)
3. Samples can be easily inserted and rotated.
4. The rf coil (the helix) does not add to the microphonic noise of the system.

5. Straightforward adaptation to high-power rf circuitry is possible.
6. A second rf coil can be introduced into the helium cold finger to be used either as a secondary rf excitation frequency source or as a receiver coil for NMR experiments.
7. In situ irradiation (primarily u.v.) can be carried out.

PROPOSITION 4

In this proposal a design for doing Overhauser experiments is described. In the typical Overhauser experiment with which the organic chemist is concerned three main considerations are involved (17);

1. A paramagnetic species is introduced into a solvent along with the compound one desires to investigate by NMR.
2. Sufficient microwave power is applied to saturate the electronic transition of the paramagnetic species.

and 3. The NMR transitions of interest are observed.

From the NMR standpoint it is desirable to keep the field fixed. As a result the microwave frequency must be varied in order to find the electronic transition. Since the band pass of resonant cavities is usually extremely narrow one can use a broad band device such as the slow-wave structures (17) (helices) employed in travelling wave tubes. At x-band frequencies ($\approx 10^{10}$ cps) the helix structure is still useable but at higher frequencies it becomes inconveniently small (< 3mm i.d. if one wants to avoid higher order modes). In the system proposed here this limitation on the frequency is removed.

If the cavity-helix system described in proposition 3 is used the helix on the cavity walls can function as the NMR transmitter coil. If it is also to function as the receiver coil then the diameter of the cavity should be reduced as much as possible in order to increase the filling factor. However, there is a lower limit on the diameter for a given frequency. A plot of the radius, a, of a TE_{01} cavity as

a function of its length, 2z, for a given wavelength λ_o, has an asymptote for 2a = 36 mm at x-band. (These quantities are related through the equation

$$\lambda_o = \sqrt{\frac{4}{\frac{1}{z_o^2} + \left(\frac{2u'_{mn}}{\pi a}\right)^2}}$$

where u'_{mn} is the nth root of the first derivative of the mth order Bessel function.) This then is the <u>minimum</u> diameter for the TE_{01} cavity at x-band. At higher microwave frequencies this diameter is conveniently reduced.

As far as the EMR part of the Overhauser system is concerned one one is left with three requirements;

1) The microwave cavity must be tunable

2) The microwave source must be simultaneously tunable and have a high output power

and 3) There must be a simple EMR detection system.

The first requirement is easily fulfilled. The TE_{011} cavity is the standard wave-meter cavity. (In practice it may be more convenient to use a metallic insertion tuning technique.)

The second requirement has in the past been difficult to fulfill. Most high power microwave sources operated at x-band or <u>below</u> in frequency and had very limited tuning ranges. However, very recently (1962) a high power backward wave oscillator (BWO) has become commercially available.* The BWO is one of the products of the recent developments in microwave tube design. Its important features for our purposes are

---

*Watkins-Johnson Company, Palo Alto, California.

its wide electronic tuning range and its high-power output. The unit of interest to us can be electronically tuned over the range from 14-20 Gc with an average CW output of 100 W.* This BWO could be locked to the tuneable cavity using standard circuits and would then track the cavity over the desired range.

The third requirement involves only the straightforward adaptation of any standard detection system. The Varian 100kc unit would serve very nicely as the basic element in such a system.

The main advantages embodied in this design are

1) High power and wide range tuneability are provided in a simple, reliable manner--electronically speaking. This should be compared with high power pulsed magnetron circuitry and with matching problems involved in the slow wave structures.

2) Operation over a wide range of frequencies, and especially in the k-band region is permitted. This is particularly important from the standpoint of the increased chemical shifts obtaining in higher fields.

---

*Watkins-Johnson model number WJ-205.

PROPOSITION 5

Several ENDOR experiments are proposed.

1.

An effort should be made to observe ENDOR in x-irradiated sodium formate. The EMR of the resulting CO_2^- radical ion reveals the spectrum (18) shown below

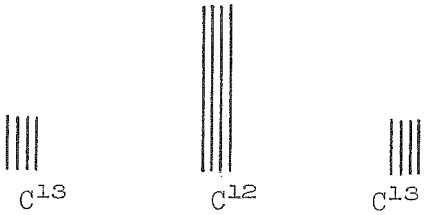

(Relative intensities not to scale)

The intense middle component split into four lines represents the unpaired electron on $C^{12}O_2^-$ interacting with the Na^{23} nucleus. Similarly the outer pair of lines represent the interaction between $C^{13}O_2^-$ and Na^{23}. An obvious reason for the measurement of ENDOR frequencies in this system would be to obtain more accurate values for the various coupling constants. It might also be possible to measure the quadrupole interaction due to Na^{23}. The measurement of the C^{13} splittings would certainly be of theoretical interest. However, of greater interest would be the investigation of the ENDOR mechanism in this system. There is essentially only one atom of each of the three magnetic nuclei Na^{23}, C^{13} and H^1 in the molecule and furthermore C^{13} is already in a dilute form (natural abundance is 1%). As a result a considerable amount of information could in principle be obtained:*

---

*Some preliminary work we have already done (actually we proposed in 1959 that this x-irradiated compound be investigated by EMR) indicates that $NaHCO_2$ crystals do not shatter at low temperature! Recently T. Cole has indicated that he is also planning to look for the ENDOR transitions in this system.

a. Observation of distant ENDOR lines for H^1, C^{13}, and Na^{23}

b. ENDOR line widths

c. ENDOR line decay time

d. Rate and nature of spectral diffusion.

On the last point in particular it is of interest to determine the nature of spectral diffusion under conditions in which either the $C^{12}O_2^-$ or the $C^{13}O_2^-$ resonances are saturated.

A slightly more complex but related system would be the $\cdot CH(SO_3)_2^=$ and $\cdot N(SO_3)_2^=$ radical ions (19).

2.

Again, an effort should be made to observe ENDOR in x-irradiated malonic acid. This is in a sense the "classic" solid state free radical and theories of the interactions of the unpaired electron with the proton--i.e., the C_2CH fragment--are usually based on malonic acid as a model. Not only is this experiment important from the standpoint of understanding the mechanism for ENDOR in these systems but more important the data obtained would be valuable in the refinement of the theoretical calculations.

This is particularly true for the C^{13} interactions in these systems. To date no extensive EMR measurements have been made on the C^{13} coupling tensors in solid state free-radicals.* The ENDOR measurements could provide accurate data for configuration interaction calculations and for the anistropic contribution to the coupling constant.

---

*See however the work of C. Giuliano on C^{13} in malonic acid in references 20 and 21.

Furthermore, the coupling of the α-C^{13} atoms 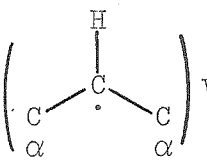 with the

unpaired electron could be accurately measured. To date there is no reliable data on this interaction. Since such an interaction would be small it is unlikely that it is measurable by EMR. However, its value is of importance in the calculation of the hyperfine interaction of the unpaired electron with the C^{13} nucleus on which that electron is centered (22).

If ENDOR cannot be observed in malonic acid then these experiments should be performed on a comparable system. Similar measurements on $\cdot CH_3$ would be of significance. Using the ENDOR technique it might be possible to detect an isotope effect on the hyperfine interaction (21).

ADDITIONAL RESEARCH PROPOSALS

6. As indicated in the text of this thesis, measurements definitely need to be made of the electronic relaxation times in solid state free-radicals.

7. Recent development in semiconducting parametric amplifiers have made it possible to operate several of such diodes (gallium arsenide, for example) at low temperatures. As a means of increasing EMR spectrometer sensitivity, a detection system employing a parametric amplifier should be designed and built.

8. It could be of some benefit to use two adjacent crystal harmonics of the Hewlett Packard Phase-Locking Synchronizer in the control of the source and local oscillator klystrons in superheterodyne spectrometers. The fundamental frequency would be used as the frequency of the if strip.

9. In 1960 I proposed that direct verification be made of the nature of the Kolbe synthesis using the EMR technique. Subsequently some preliminary work done with C. D. Russell definitely revealed the steady state presence of an unpaired spin with a lifetime of less than 1 minute. The paramagnetic species was not identified.

10. In 1961 I proposed that the cyclopentadienyl free-radical could probably be formed by x-irradiation of C_5H_5Tl at reduced temperatures.

REFERENCES FOR PROPOSITIONS

1. McConnell, H. M., Heller, C., Cole, T. and Fessenden, R. W. J. Am. Chem. Soc., 82 (1960), 766-775.

2. Heller, C. and McConnell, H. M. J. Chem. Phys., 32 (1960), 1535.

3. Ghosh, D. K. and Whiffen, D. H. Mol. Phys., 2 (1959), 285.

4. Heller, C., and Cole, T. To be published.

5. Heller, C. and Cole, T. J. Chem. Phys., 37 (1962), 243-250.

6. Geib, K. H., and Harteck, P. Ber., 66 (1933), 1815-1825.

7. Fischer, H. J. Chem. Phys., 37 (1962), 1094-1096.

8. Latha, L. G. The Nucleic Acids, V. 3 (Eds. Chargoff, E. and Davidson, J. N., Academic Press, New York, 1960), 527-546.

9. Effects of Ionizing Radiations on Immune Processes, Ed. C. A. Leone (Science Publishers, New York, 1962).

10. Miyagawa, I. and Gordy, W. Bull. Am. Phys. Soc., 5 (1960), 227.

11. Ueda, H., Kuri, Z., and Shida, S. J. Chem. Phys., 35 (1961), 2145-2147.

12. Martin, R. G., Matthei, J. H., Jones, O. W., and Nirenberg, M. W. Biochem. Biophys. Res. Comm., 6 (1961-1962), 410-414.

13. Shields, H. and Gordy, W. Proc. Nat. Acad. Sci., 45 (1959), 269-281.

14. Kwiram, A. L. and McConnell, H. M. Proc. Nat. Acad. Sci., 48 (1962), 499-500.

15. Beukers, R., Ijlstra, J., and Berends, W. Rec. trav. chim., 77 (1958), 729.

16. Wilson, I. G., Schramm, P. W., and Kinzer, J. P. Radar Systems and Components (by Bell Laboratories Staff, D. Van Nostrand, New York, 1949), p. 912.

17. Richards, R. E. and White, J. W. To be published.

18. Ovenall, D. W., and Whiffen, D. H. Mol. Phys. 4 (1961), 135-144.

19. Horsfield, A., Morton, J. R., Rowlands, J. R., and Whiffen, D. H. Mol. Phys., 6 (1962), 241-250.

20. Giuliano, C. R. Thesis, California Institute of Technology, 1961.

21. McConnell, H. M. and Giuliani, C. R. J. Chem. Phys., 35 (1961), 1910-1911.

22. Karplus, M., and Fraenkel, G. K. J. Chem. Phys., 35 (1961), 1312-1323.

GLOSSARY

a isotropic hyperfine coupling constant, see $\underset{\sim}{A}$

$\underset{\sim}{a}, \underset{\sim}{b}$ see $\underset{\sim}{A}$

$(\vec{a},\vec{b},\vec{c})$ crystallographic unit cell triple

$\vec{c}^*$ unit vector chosen so that $\vec{a}\cdot\vec{c}^* = \vec{b}\cdot\vec{c}^* = 0$ and $\vec{c}\cdot\vec{c}^* \geq 0$

db decibel

$\vec{e}_i$ unit vector related to $(\vec{i},\vec{j},\vec{k})$
$\vec{e}_1 \equiv \vec{i}, \quad \vec{e}_2 \equiv \vec{j}, \quad \vec{e}_3 \equiv \vec{k}$

f farad

$\underset{\sim}{g} \equiv g_o \underset{\sim}{1} + \underset{\sim}{g}'$ where $\underset{\sim}{g}$ is the electron g-factor tensor

g_N nuclear g-factor

h henry

$h = 6.62517 \times 10^{-27}$ erg sec Planck's constant

if intermediate frequency

$(\vec{i},\vec{j},\vec{k})$ orthogonal cartesian triple

$k = 1.38044 \times 10^{-16}$ erg $^\circ K^{-1}$ Boltzmann's constant

k-band approximately 15-35 Gc

$m_S \equiv S_z \qquad m_I \equiv I_z$

$n_{\pm}$ number of nuclei having $I = \pm \frac{1}{2}$

p (prefix) pica (10^{-12})

rf radio frequency

t time

u_i direction cosine $u_i \equiv \vec{u}_H \cdot \vec{e}_i$

$\vec{u}_H$ unit vector in external field direction

u.v. ultra-violet

x-band 8.2-12.4 Gc

$\underset{\sim}{A}^{i}$ is the hyperfine coupling tensor for nucleus i

$$\underset{\sim}{A} \equiv \underset{\sim}{a} + \underset{\sim}{b} = a\,\underset{\sim}{1} + \underset{\sim}{b} \qquad a = \tfrac{1}{3}\,\text{trace}\,\underset{\sim}{A} \equiv \tfrac{1}{3}\,\text{tr}\,\underset{\sim}{A}$$

AC alternating current

DC direct current

$E, (\vec{E})$ energy or electric field (vector)

G gauss

G (prefix) giga (10^9)

$H, (\vec{H})$ magnetic field (vector)

$\vec{H}_o$ external (DC) field vector

I current or nuclear spin quantum number

$\vec{I}^{i}$ spin angular momentum vector for nucleus i

I^{i}_{j} refers to component of $\vec{I}^{i}$ in j direction

L inductance

$N_{\pm}$ number of electrons having $S_z = \pm \frac{1}{2}$

Q quality factor for a resonant circuit

$$Q \equiv \frac{1}{2\pi} \frac{\text{energy stored}}{\text{energy lost (per cycle)}}$$

R resistance

$\vec{S}$ spin angular momentum vector for the electron

S_i refers to component of $\vec{S}$ in i direction

S electron spin quantum number

(S/N) signal to noise ratio

I_{T_1} nuclear spin-lattice relaxation time

S_{T_1} electronic spin-lattic relaxation time

TE_{lmn} refers to microwave cavities (see reference 51)

T temperature in degrees Kelvin

V volts

W watts

W transition probability for forbidden electronic transitions

($\Delta m_S = \pm 1$, $\Delta m_I = \pm 1$) also W(+-) → (-+) etc.

W_o allowed electronic transition probability ($\Delta m_S = \pm 1$, $\Delta m_I = 0$)

X_c capacitive reactance

Y admittance $Y \equiv 1/Z$

Z impedance

$\mathcal{g}$ measured (EMR) g-values

$\mathcal{s}$ measured (EMR) splittings

$\mathcal{s}(\vec{e}_i \vec{e}_j)$ designates plane in which $\mathcal{s}$ is measured

$\mathcal{H}$ spin Hamiltonian

α attenuation; for rf propagating in a tube beyond cut-off,

α = 30db for every length equal to diameter

α-,β-,$\cdots\omega$-proton see p. 43 of thesis

$|\beta| = 0.9273 \times 10^{-20}$ erg G^{-1} Bohr magneton

$\beta_N = 0.50504 \times 10^{-23}$ erg G^{-1} nuclear magneton

$\gamma_S \equiv \frac{\omega_S}{H_o}$ $\gamma_I \equiv \frac{\omega_I}{H_o}$

$\delta = \frac{g_N \beta_N H_o}{kT}$; $e^{-\delta}$ is the nuclear Boltzmann factor

$\delta' \equiv |\nu_+ - \nu_-|$

$\vec{\mu}_e = - |\beta| \vec{S} \cdot \underset{\sim}{g}$ electron magnetic moment

$\vec{\mu}_N^i = g_N \beta_N \vec{I}^i$ magnetic moment of ith nucleus

$|\nu_e| \equiv h^{-1} g_o |\beta| H_o$

$\nu_p \equiv h^{-1} g_N \beta_N H_o$

$\nu_{\pm}$ ENDOR frequencies for $S = \pm \frac{1}{2}$

$$\nu_{\pm} \equiv \nu_p \vec{u}_H \mp \tfrac{1}{2} S_H \vec{u}_H \cdot \underset{\sim}{A}$$

$\omega_S = 2\pi |\nu_e|$ $\omega_I = 2\pi \nu_I$

$\Delta = g_o|\beta|H_o/kT$; $e^{-\Delta}$ is the electronic Boltzmann factor

$$\Delta_{mn} \equiv \begin{cases} 0 \text{ for } m = n \\ 1 \text{ for } m \neq n \end{cases}$$

Ω ohms

(+-) designates the value of S_z and I_z respectively--

i.e. $S_z = +\frac{1}{2}$ $I_z = -\frac{1}{2}$

flip-flop a transition in which the electron and nuclear spins go from (+-) → (-+) or from (-+) → (+-)

flip-flip a transition in which the electron and nuclear spins go from (--) → (++) or from (++) → (--)